UNIVERSITY OF TWENTE.

FACULTY OF ENGINEERING TECHNOLOGY

CIVIL ENGINEERING, WEM-MFS

**BACHELOR THESIS**

# HOW TO DETERMINE THE EFFECTS OF FLOOD WAVES ON THE TEMPORAL DEVELOPMENT OF THE PHREATIC LINE IN EARTH-FILL DIKE BODIES:

A METHOD APPLIED WITH STOCHASTIC NUMERICAL MODELING FOR THE ASSESSMENT OF DIKE STABILITY

**BY**

NICK (P.H.) VAN DE VOORT – UNIVERSITY OF TWENTE

S1721763

**SUPERVISORS**

DR. M.S. KROL – UNIVERSITY OF TWENTE

B.T.M. ERNST MSc – UNIVERSITY OF TWENTE

IR. J. STEENBERGEN-KAJABOVÁ – SWECO NEDERLAND B.V.

JUNE 2019

## PREFACE

This Bachelor Thesis forms the final product in completing the Bachelor Civil Engineering at the University of Twente. The research performed was carried out in the period of April 2019 until June 2019 and is about the determination of the effect of flood waves on the development of the phreatic line in earth dike bodies. Sweco Nederland B.V., main office in De Bilt, supported the development of the research. Within this period I was working at the department Flood Defences.

I would like to thank my bachelor committee for guiding me through the project with their expertise, feedback, and enthusiasm. First of all, I want to thank my supervisor from Sweco, Ir. J. Steenbergen-Kajabová, for her expertise and motivated guidance, which kept me on track during the research. I also want to thank my supervisor of the University of Twente, Dr. M.S. Krol, for his contribution to this research and the challenging conversations we had about the subject and the simulation set-up on how to perform the stochastic analyses. Also B.T.M. Ernst MSc for being the second supervisor.

At last, I want to thank my colleagues of Sweco, for helping me with my questions. It was a pleasant working environment. Finally, my dearest family for their support, especially my sister who offered me a room during the period at Sweco.

Enschede, June 2019

Nick van de Voort

**SUMMARY**

The Netherlands has always been a country threatened by floods. To ensure the flood safety of the dikes, the government prescribes that the totality of the $3700km$ Dutch flood defense system is periodically assessed. In 2017 new flood safety standards were enacted in the Netherlands, including new assessment methods in alegal assessment framework called WBI2017 for the 2017-2023 assessment round. The WBI contains regulations that the administrator must use to perform a safety assessment. The manual also contains instructions for the amount of research, and the type of research that is required, in order to achieve good schematizations of the subsoil and piezometric lines (water pressure lines per soil layer) and how (field) data can be converted to correct calculation parameters. The manual must provide directions for soil calculations on how uncertainties of the soils (strenght) characteristics are represented by making conservative choices in schematization and parameter choices.

At this moment, there are no unambiguous guidelines for composing a soil investigation into a representative image of the soil layer structure in the underground and the geohydrological coherence. Studying available information often results in multiple interpretations. Because of this, uncertainties play an important role when choosing the schematization of both underground and hydraulic conditions (e.g. seepage characteristics).

To that end, this study considered the soil uncertainties in the analyses of transient seepage through earth dikes and investigated their effect on the temporal development of the phreatic line and determined the effect of flood waves on the pore-water pressure in the aquifer and cover layers. It was found that the development of the phreatic line can be addressed by the hydraulic conductivity parameter in seepage analyses.

Therefore, a case-location at the Waal river (between Tiel and Waardenburg) is investigated considering the uncertainty of hydraulic conductivity parameters for unsaturated flow modeling. A random number generation algorithm producing random values for the hydraulic conductivity of dike core materials is coupled with a finite element software, SEEP/W, to analyze the temporal development of the phreatic line.

Monte Carlo Simulation is adopted for stochastic seepage analyses at which the variability effects of the hydraulic conductivity are investigated conducting sensitivity analyses. The variation effect of hydraulic conductivity of fine-grained materials is found to have a significant effect on the location of the phreatic line, whereas the hydraulic conductivity variation of course-grained materials is found to be less significant. This may cause deviations from the position of the phreatic line when assuming homogeneous materials with average material properties. The deviations of the phreatic line become greater on the long-term.

The deviations of the phreatic line show no significant differences between a short-term flood wave and a long-term flood wave. However, on the long-term, the absolute location of the phreatic line can differ significantly as the duration of the flood wave increases.

The pressure head built up in the dike core is significantly higher as the duration of the flood wave increases. As soon as the flood wave is dropping, the phreatic head in the aquifer and cover layer is dropping. Also, the phreatic line follows, resulting in a relative flat phreatic line regardless of the hydraulic conductivity tested in this study. However, residual pressure in the dike core remains at the outer slope side which is caused by the height and duration of the flood wave. An underpressure occurs in the surrounding soil layers. Due to this residual pressure, the effective stress decreases, causing a

decrease in shear strength, which lead to deformations and eventually sliding of the soil. Therefore, the residual pressure can cause dike instability.

Considering the residual pressure, the statistical and probabilistic properties of the phreatic line are assessed for outward macro stability for different flood wave types in the software D-Geo Stability. Hereby, the schematizations of piezometric lines are compared with the conservative method of WBI. It is found that for the case dike, the schematization of the phreatic line at a more realistic level and adressing a piezometic line for the residual pressure above the phreatic line, the dike is assessed to be more instable than wihout dealing with the residual pressure. Also, this alternative schematization showed significant differences with the WBI method for safety assessment.

In general, this study showed more insights which piezometric lines are influencing soil layers in dike compositions and how stochastic analysis (i.e. uncertainty quantification) of the phreatic line can be used for schematization of these piezometric lines when assessing macro stability, instead of making conservative choices in schematisation or parameter choices.

## TABLE OF CONTENTS

## LIST OF TABLES

## LIST OF FIGURES

# LIST OF SYMBOLS

| | |
|---|---|
| $A$ | Designation for summation over the area of an element |
| AEV | Air-entry value |
| AHK | AutoHotKey |
| $[B]$ | Gradient matrix |
| $[C]$ | Element hydraulic conductivity matrix |
| CFD | Cumulative distribution function |
| CLR | Common Language Runtime |
| DXF | Drawing eXchange Format |
| COV | Coefficient of variation |
| $E_i$ | Expected frequency |
| E[X] | Mean |
| FEM | Finite element method |
| $FoS$ | Factor of Safety |
| $\{H\}$ | Vector of nodal heads |
| $H$ | Total head |
| $h$ | Pressure head |
| $[K]$ | Characteristic matrix of an element in FE transient seepage analysis |
| $K_x$ | Hydraulic conductivity in $x$-direction |
| $K_y$ | Hydraulic conductivity in $y$-direction |
| $K_r$ | Relative hydraulic conductivity |
| $K_s$ | Saturated hydraulic conductivity |
| $L$ | Designation for summation over the edge of an element |
| LEM | Limit Equilibrium Method |
| $[M]$ | The element mass matrix in FE transient seepage analysis |
| m | A fitting parameter of Van Genuchten method |
| $M_a$ | The driving moment |
| $M_r$ | The maximum resisting moment |
| $m_v$ | Coefficient of volume compressibility |
| $m_w$ | The slope of the water content curve |
| MCS | Monte Carlo Simulation |
| ME | Margin of error |
| $< N >$ | Vector of interpolating function |
| $N$ | Number of Monte Carlo Simulations |
| n | A fitting parameter of Van Genuchten method |
| $n$ | porosity |
| $O_i$ | Observed frequency |
| PDF | Probability density function |
| $\{Q\}$ | The applied flux vector |
| $Q'$ | The boundary flux |
| r | The correlation coefficient |
| $r$ | Radius |
| $r'$ | Normally distributed random variable |
| $S$ | Degree of saturation |
| $S_e$ | Effective saturation |
| $t$ | Time |
| $U_1$ | Independent random variable 1 |
| $U_2$ | Independent random variable 2 |
| $u_a$ | Air pressure |

| | |
|---|---|
| $u_w$ | Water pressure |
| $Var(\mathrm{X})$ | Variance |
| $X^2$ | The Chi-square statistics |
| $z$ | Elevation |
| $\alpha$ | A fitting parameter of the Van Genuchten method |
| $\alpha'$ | A scale parameter of the gamma distribution |
| $\beta$ | A rate parameter of the gamma distribution |
| $\Gamma$ | Gamma distribution |
| $\gamma_w$ | The specific weight of water |
| $\theta$ | The volumetric water content |
| $\theta'$ | Angles of the slip zone in LEM |
| $\theta_r$ | The residual water content |
| $\theta_s$ | The saturated water content |
| $\Theta$ | Dimensionless water content (normalized water content) |
| $\lambda$ | Storage term for transient seepage |
| $\mu$ | Mean |
| $\sigma$ | Standard deviation |
| $\bar{\sigma}$ | Effective stress |
| $\tau$ | The thickness of an element |
| $\tau_m$ | The maximum shear stress |
| $\psi$ | Matric suction |

## CHAPTER 1

## INTRODUCTION

### 1.1 General

Soil mechanical calculations are based on schematizations. Geotechnical site explorations and the schematization of underground and hydraulic conditions is crucial when assessing the strength of flood defenses. Flood defenses made of natural materials are commonly susceptible to seepage through their dike body. Therefore, misleading estimation or underestimation of seepage may result in failure of these types of flood defenses (Foster, et al., 2000).

For the geotechnical consultant, freedom of choice is limited considerably when choosing the soil characteristics, seepage forces, and the calculation model (Calle, et al., 2011). The consultant is supported by regulations and practical guidelines. These regulations and design guidelines must provide directions for soil calculations on how uncertainties of the soils (strength) characteristics are represented by making conservative choices in schematization and parameter choices or/and are discounted by safety factors. At this moment, there are no unambiguous guidelines for composing a soil investigation into a representative image of the soil layer structure in the underground and the geohydrological coherence (ENW, 2012). Studying available information often results in multiple interpretations. Because of this, uncertainties play an important role when choosing the schematization of both underground and hydraulic conditions (e.g. seepage characteristics).

In practical applications, the prediction of seepage quantity is usually handled with deterministic models in which soil properties are used. The variation of both geotechnical and hydraulic properties of soils are disregard in these studies (Çalamak, 2014). However, the properties show variability since soils are heterogeneous (and anisotropic) to some degree. Therefore, unrealistic results may be obtained in predicting seepage characteristics.

Along with the uncertain inherent heterogeneity, caused by the variation of soil properties due to loading histories and various deposition (Elkateb, et al., 2003), there are other reasons which cause uncertainties in soil properties (Husein Malkawi, et al., 2000):

- Insufficient geotechnical site explorations due to high cost of surveying and measurements,
- Errors caused by the measurement equipment or human being,
- Soil properties that are hard to assess are disregarded.

These uncertainties in soil properties strongly affect the seepage through the soil media (Çalamak, 2014). Due to variation, preferred flow paths or high/low seepage fluxes occur that may be unexpected. When determining the realistic properties of the seepage, uncertainties in soil properties should be taken into consideration. Therefore, the Dutch Expertise Netwerk of Water Safety *(ENW)* introduced the schematization factor. The schematization and corresponding choices (and therefore uncertainties) are taken into consideration, explicitly appointed and quantified. The size of the factor depends on the degree of safety that is used when schematizing the soil layer structure and the water pressures occurring therein. So, the schematization factor is not a fixed one.

In case of a dike, the method includes a basic schematization of the cross-section of the ground construction, that is determined based on available information. Besides, this method includes scenarios, for example, possible deviations of the basic schematization of both the underground and hydraulic conditions, processes that have a negative impact on dike stability and whether a lack of information can be excluded or not (Calle, et al., 2011). Thereafter, the stability factor is determined for the concerning scenario and is combined with the probability of occurrence of this scenario. However, this can often not be determined objectively and an expert is required for the probability estimation.

The probability estimation is logically dependent on the available information from, for example, soil site explorations and area knowledge of the geological consultant. This subjectivity cause uncertainty when schematizing the soil layer structure in the underground and the geohydrological systems. In practice, it appears that non-normative processes, which may nevertheless have an effect on pore water pressures, are incorrectly ignored by subjective interpretation of the consultant when schematizing (Barends, et al., 2004). The schematization factor, the basic schematization, and scenarios are currently a practical alternative since for the execution of a fully probabilistic calculation (using stochastic quantities) no software is yet available that could do this somewhat easily (Calle, et al., 2011).

According to Calle et al., consideration of uncertainties in soil parameters can be achieved using stochastic models (2011). Hereby, the input parameters are considered to be random (i.e. non-deterministic). The randomness of input parameters results in random output parameters of the system. This can be defined with statistical analysis and a probability density function (PDF).

For a prediction of the seepage characteristics, the geohydrological properties must be randomized, such as volumetric water content characteristics, porosity, hydraulic conductivity, etc. of the soil. Also, the hydraulic model must regard both saturated and unsaturated flow, because the unsaturated flow is highly nonlinear but may affect the seepage behavior of the system. The seepage results may elucidate how the top flow line i.e. phreatic line or piezometric line behaves due to variation of the hydraulic conditions. This can be performed for steady-state seepage analysis, but Sweco (engineering consultant in North-Europe) is specifically interested in transient seepage analysis in which the boundary conditions of the system change over time due to flood waves and request to examine the effect of flood waves, and corresponding waveform, on the pore water pressure in the aquifer as well as the effect of this in the cover layer of the dike.

## 1.2 The aim and scope of the study

The aim of this study is to consider the soil uncertainties in the analysis of transient seepage through earth dikes and investigate their effects on the temporal development of the phreatic line and determine the effect of a flood wave on the pore-water pressure in the aquifer and cover layers. The insights must provide tools for designers and assessors with which sufficient safe (i.e. robust) schematizations can be made of these piezometric lines for the assessment of outward (and inward) dike stability. In this research, inherent heterogeneity caused by the variation of soil parameters in space is considered as the source of uncertainty. The uncertainty of soils is simulated with a numerical model by generating random variables of hydraulic soil properties.

## 1.3 Research Questions

In order to achieve the uncertainty quantification, this study will try to answer the following research questions:

1. *What is the effect of flood waves on the temporal development of the phreatic line in dike bodies?*
2. *To what extent does the development of the flood wave, and waveform, affect the hydraulic heads in the aquifers and the cover layers and how does this affect the stability of the dike?*

The two main research questions are elaborated in the following sub-questions:

1. How do the geohydrological parameters of core materials influence the course of the phreatic line in earth dike bodies?

2.
   - i. For which geohydrological parameters is the phreatic line sensitive, and on which time scales is this sensitivity relevant?
   - ii. How do developments of the flood waves, and waveform, affect the development of the phreatic line in dike bodies for the prescribed scenarios?
   - iii. How do developments of flood waves, and waveform, affect the hydraulic heads in the aquifer and cover layer and how does it affect the stability of the dike?

3. What are the differences between the Dutch schematization manual for determining the development of the phreatic line, instructed by WBI 2017, and the schematizations as a result of the numerical computer model?

## 1.4 Approach and report structure

Below a short description of the report structure is given. The research is divided into a number of steps and those will be covered by chapters:

Chapter 2 contains a literature study, which presents the necessary theory and background information for this thesis. Chapter 3, provides a framework of the Monte Carlo Simulation used in this study, in which the theory of Chapter 2 is translated to the model set-up. Chapter 4 focused on the case location in this study, the validation of the model for this case and the scenarios considering in the Monte Carlo Simulation. Chapter 5 presents the results of the simulations for the defined scenarios. Chapter 6 is the application in which the result of the simulation is used for further calculations i.e. the safety assessment of dikes. In Chapter 7, the conclusions will be presented and the discussion is given in Chapter 8.

## CHAPTER 2

## THEORETICAL FRAMEWORK

*This Chapter provides theory and background information for the governing model equations used in software of SEEP/W for the transient seepage analyses. Also, a more descriptive relation is explained for the soil property functions with respect to phreatic lines. At last, the concept of macro-stability and phreatic lines is given.*

## 2.1 Soil property functions and phreatic lines

### 2.1.1 Phreatic line in earth dikes

A dike is, in general, an element with low permeability. In the Netherlands, a dike generally is built on an incompressible sandy aquifer (Pleistocene) and is covered with a semi-permeable top-layer (Holocene). The Holocene and Pleistocene together form the Dutch dike profile (see figure 2-1). In general, forces induced by outer water directly change the hydraulic head in the aquifer and gradually change the hydraulic head in the defense itself (phreatic line, hydraulic head in the top-layer of the dike). Sometimes, aquifers also influence the seepage through the dike itself (Barends, et al., 2004).

A dike can store water under the phreatic line. In soft soil layers water can be stored in the extra voids that arise when the soil starts to deformate (consolidation) and sand layers water storage can occur due to (vertical) compaction. Storage means that the effects of groundwater movement are delayed. This is a transient process since the load itself is changing over time (flood waves) or gradually arise (dike reinforcement, subsidence).

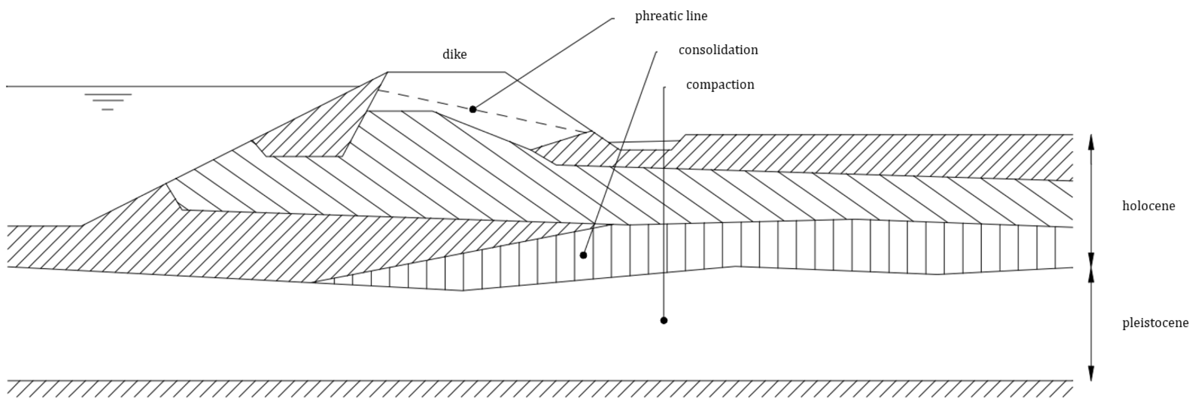


Figure 2-1 Dutch dike profile and storage mechanisms (Barends, et al., 2004)

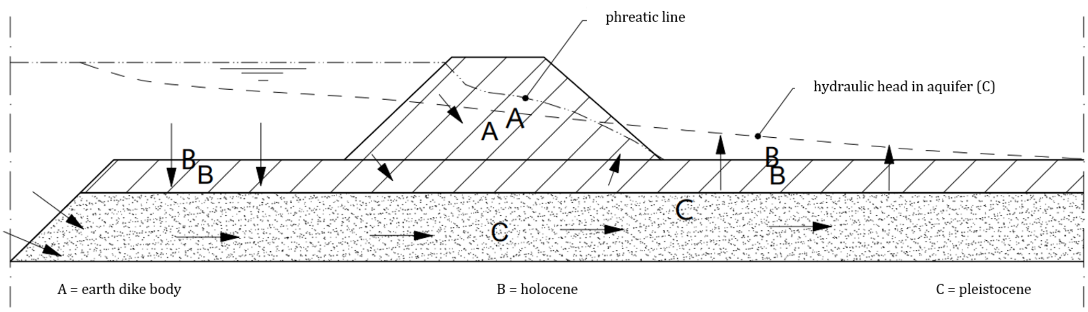


Figure 2-2 seepage in dike body and underground (Barends, et al., 2004)

Figure 2-2 indicates the flow lines and its interaction between layers for seepage under the phreatic line in the Dutch dike. However, seepage is not a confined problem. The phreatic line is only a theoretical top-flow line at which the hydrostatic pressure is zero but the soil above the phreatic line is in partially saturated or unsaturated condition. How this effect is handled in engineering practice will be explained later in this study.

Seepage analysis for unsaturated soils is mathematically characterized by several partial differential equations. These equations are non-linear and also the soil properties considered in seepage equations can be highly non-linear as a function of pressure (Thieu, et al., 2001). For this reason, describing the system itself and deriving the equation that can be applied for modeling saturated-unsaturated systems can be a challenge, especially setting up a numerical computer model. However, in the past decades, the application of computers for solving complex systems has expanded and enabled engineers to use those general partial differential equation solvers.

Two property functions are required for solving transient, unsaturated soil systems: the hydraulic conductivity function and the water storage function (Fredlund & Rahardjo, 1993). These functions can both be written in terms of negative pore-water pressure $u_w$ $[kPa]$ (or pressure head $h$ $[m]$) or matric suction ψ $[kPa]$ (Thieu, et al., 2001). Matric suction can be defined as the difference between the air and water pressure $u_a - u_w$ $[kPa]$ and can be obtained when dry soil exerts pressure on the surrounding soil to equalize the moisture content in the overall soil system. The soil above the phreatic surface is in partially saturated or unsaturated condition. Due to the difference in pressure, pore-water suction exists and therefore mechanical properties of the soil change (Sako & Kitamura, 2006).

The property functions together can be used to dynamically describe soil properties for both saturated and unsaturated soil conditions. These property functions can be assigned to a general partial differential equation for both steady-state and transient seepage problems. Before the general partial differential equations are shown for solving two-dimensional seepage problems for saturated/unsaturated soil systems, the derivation of the two property functions are clarified and some examples of the non-linear relationship between water storage, hydraulic conductivity, and matric suction are given for characteristic soil types.

### 2.1.2 Soil property function: water storage

Soils contain pore spaces that can either be filled with air or water or with a combination of both (difference between saturated and unsaturated soil). Voids are all filled with water when the soil is fully saturated and the volumetric water content of the soil is therefore related to the porosity of the soil:

$$\theta = nS \qquad [2.1]$$

Where $\theta$ $[-]$ is the volumetric water content (between $0 - 1$), $n$ $[-]$ the porosity of the soil, the fraction of the volume of voids over the total volume (between $0 - 1$), and $S$ $[-]$ the degree of saturation (equal to 1.0 in saturated soil).

When soil is unsaturated, the volume of water stored within the voids depends on the matric suction within the pore-water. A function is required to describe the behavior of water content under different pressures in soil because there is no fixed water content in time and space. The relation is visualized in figure 2-3, also known as the soil-water characteristic curve (SWCC).

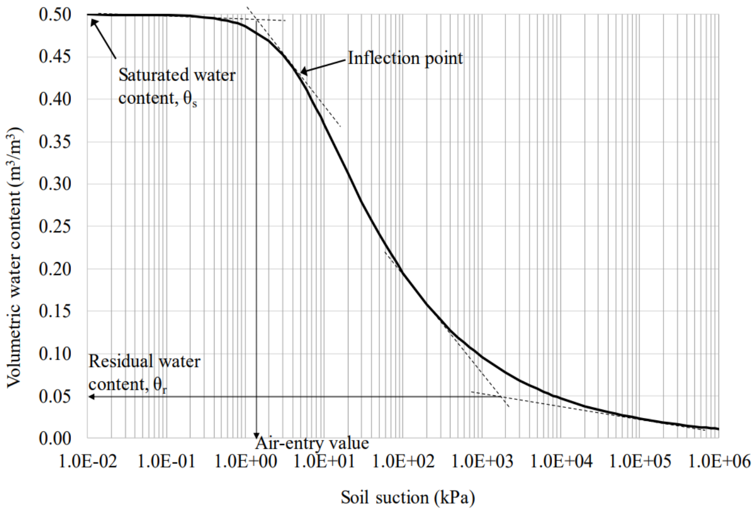


Figure 2-3 Soil-water characteristic curve (Çalamak, 2014)

The volumetric water content is mostly influenced by the distribution and size of particles in the soil and the function describes what portion remains water-filled as the soil drains under stress. The function can be obtained by experimental tests both in laboratory medium or sites, in which data points are plotted on semi-log graphs and a curve is fitted (e.g. figure 2-3). Besides, the function can also be plotted with respect to both positive and negative pore-water pressure (e.g. figure 2-4), in which the zero-line represents the phreatic line. The function is characterized by three main features:

1. Air-entry value (AEV)

When the largest pores or voids begin to drain freely, the water content starts to decrease. This point is called the air-entry value and corresponds to the negative pore-water pressure or in the case of figure 2-3 a relatively low value for soil suction. Soils with uniformly, large shaped pores have relatively low air-entry values (Sako & Kitamura, 2006).

2. The slope of the function $m_w$ $[-]$ for both the positive and negative pore water pressure

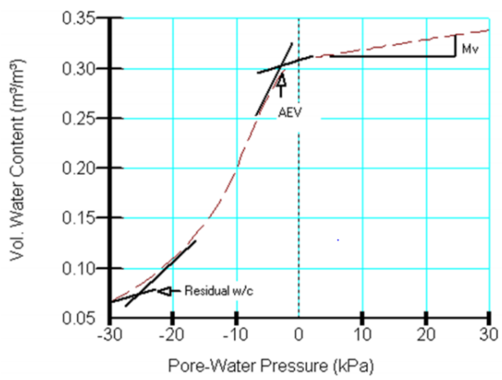


Figure 2-4 Volumetric water content function (Geo-Slope Int Ltd., 2013)

Water can drain in two ways: it can be released by gravitation forces at which the water-filled voids start to desaturate or by compressing the soil skeleton at which the size of the voids reduce and squeeze the water out of the saturated medium. The phenomena can be compared with a water-filled sponge exposed to these different forces. In the saturated system where the pore-water pressure is positive, $m_w$ $[-]$ becomes equivalent to $m_v$ $[-]$, the coefficient of volume compressibility for one-dimensional consolidation (Geo-Slope Int Ltd., 2013), which can be considered as constant. The slope changes in the negative pore-water pressure range. It represents the rate of change for the water content as matric suction occurs. The rate of change is relative high at the point where the largest voids start to drain (AEV) to the residual water content.

3. Saturated water content $\theta_s$ $[-]$ and residual water content $\theta_r$ $[-]$

The third key feature is the residual water content, which is the water content that remains when the negative pore-water pressure further increases. At this point the rate of change is small. The residual water content can also be expressed in the degree of saturation $S$ by dividing the residual water content $\theta_r$ $[-]$ by the porosity $n$ $[-]$ which is almost equal to the saturated water content $\theta_s$ $[-]$.

Figure 2-5 visualizes the differences between the volumetric water content functions typical sample functions in GeoStudio (SEEP/W®).

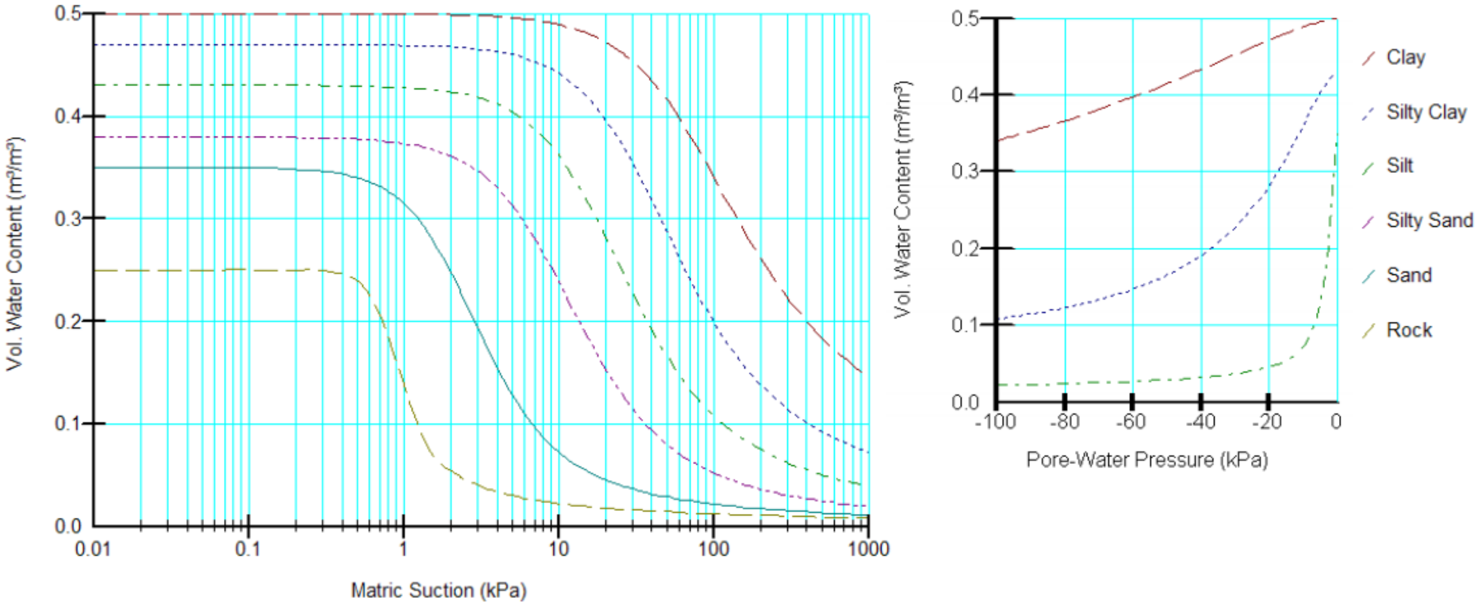


Figure 2-5 volumetric water content function for different soil types. Left: plotted with respect to matric suction; Right: plotted with respect to pore water pressure (Geo-Slope Int Ltd., 2013)

The size of the pores of sand are approximately the same and the particles are large. Therefore, water can easily be released under small negative pore-water pressure. Because of this, the AEV is smaller than other soil types as can be seen in figure 2-5 (left graph). The distribution of sand can be considered as uniform since all pores drain over a small range of pressure, which makes the slope $m_w$ $[-]$ relatively steep.

The widest pores are sometimes filled with small silt particles, which makes the distribution of silt wider and less uniform than sand. The pores become smaller and more negative pore-water pressure must be applied under order to drain the soil mass. Therefore, AEV is higher and the slope is less steep.

As can be seen in figure 2-5 (right graph), it is difficult to identify the AEV for clay since consolidation takes place over a significant range before the air enters the pores. Therefore, the slope is relatively flat on a normal pressure scale. However, due to the compressibility of clay, water and air can be expelled, resulting in volume reduction between particles, which is not immediately recovered when the load is removed. This must be taken into consideration in saturated seepage analysis (Geo-Slope Int Ltd., 2013).

The function of the SWCC can be formulated with saturated and residual values. There are many mathematical equations proposed in the literature for presenting the SWCC. The best fitting methods are those derived by Brooks and Corey (1964), Van Genuchten (1980) and Fredlund and Xing (1994). In this study, Van Genuchten (1980) equation is adopted to estimate unsaturated soil hydraulic properties. Van Genuchten (1980) derived a closed form equation consisting of three curve fitting parameters $\alpha$, n and m for the estimation of the SWCC:

$$\theta = \theta_r + \frac{\theta_s - \theta_r}{[1 + (\alpha h)^{\mathrm{n}}]^{\mathrm{m}}}$$

[2.2]

Where $h$ is the pressure head, which can be taken as $kPa$ and $m$ (SI unit system). Parameter $\alpha$ is related to the inverse of air-entry value and is therefore related to the largest pore size of the soil (Lu & Likos, 2004). It must take as the same unit as the pressure head (i.e. $kPa^{-1}$ or $m^{-1}$). Parameter n is related to the pore size distribution of the soil, and m is related to the assymetry of the model (Matlan, et al., 2014).

The complete derivation of this equation and consideration of fitting models are stated in Appendix A-1 *Water storage function*.

### 2.1.3 Soil property function: hydraulic conductivity

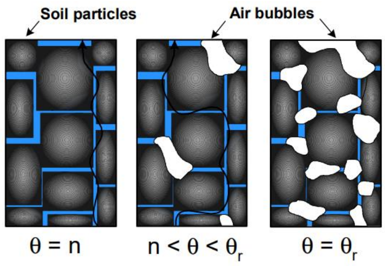


Figure 2-6 water filled flow paths from saturated soil mass to residual (Geo-Slope Int Ltd., 2013)

The hydraulic conductivity reflects the ability of a soil to conduct water under conditions such as saturated and unsaturated. Figure 2-7 illustrates that based on Eq. [2.1] the dimensionless water content can be considered equal to the porosity of the soil when the degree of saturation is equal to 1. In case the air starts to enter, pores become air-filled and become non-conductive, which leads to lower hydraulic conductivity.

In saturated porous media, the quantity of water that is moving through a cross-sectional area depends on the radius of the channels between the particles. Since the radius is raised to the fourth power for calculating the cross-sectional area, the quantity decreases highly non-linear. It would be easier to extract water from sand or gravel samples because of their high transmissivity, compared to clay for instance. See figure 2-7, showing ranges of values of hydraulic conductivity for various geological materials (Freeze & Cherry, 1979):

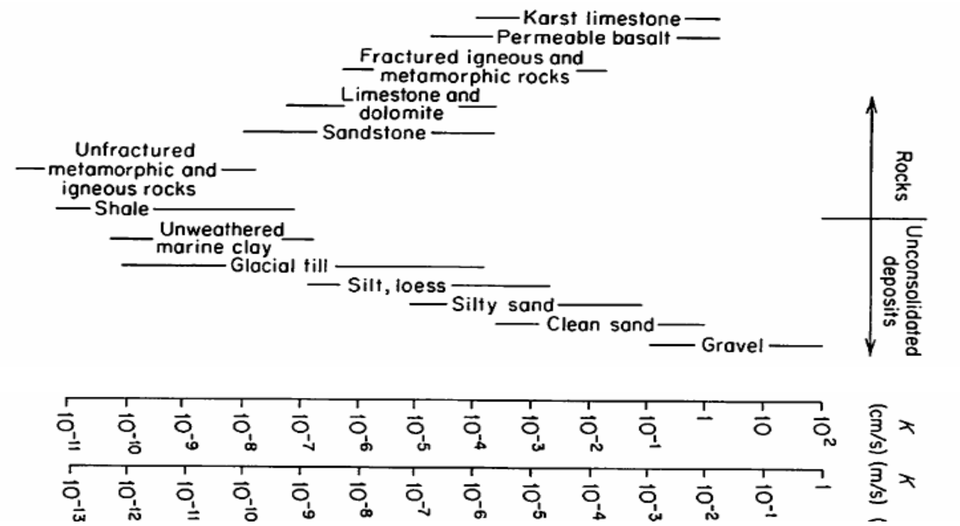


Figure 2-7 Ranges of values of hydraulic conductivity for various geological materials (Freeze & Cherry, 1979)

Table 2-1 gives average parameter values such as the saturated water content $\theta_s$ $[-]$, the residual water content $\theta_r$ $[-]$ and saturated hydraulic conductivity $K_s$ $[cm \cdot d^{-1}]$ for soil textural groups from analysis of a large number of soils estimated by Carsel and Parrish (1988) (Van Genuchten, et al., 1991). These tables serve as guides in several studies for making initial parameter estimates and also gives the fitting parameters $\alpha$ $[cm^{-1}]$ and n of Van Genuchten's (1980) method:

| Texture | $\theta_r$ | $\theta_s$ | $\alpha$ 1/cm | $n$ | $K_s$ cm/d |
|---|---|---|---|---|---|
| Sand | **0.045** | 0.43 | 0.145 | 2.68 | 712.8 |
| Loamy Sand | 0.057 | 0.41 | 0.124 | 2.28 | 350.2 |
| Sandy Loam | 0.065 | 0.41 | 0.075 | 1.89 | 106.1 |
| Loam | 0.078 | 0.43 | 0.036 | 1.56 | 24.96 |
| silt | 0.034 | 0.46 | 0.016 | 1.37 | 6.00 |
| silt Loam | 0.067 | 0.45 | 0.020 | 1.41 | 10.80 |
| Sandy Clay Loam | 0.100 | 0.39 | 0.059 | 1.48 | 31.44 |
| Clay Loam | 0.0% | 0.41 | 0.019 | 1.31 | 6.24 |
| Silty Clay Loam | 0.089 | 0.43 | 0.010 | 1.23 | 1.68 |
| Sandy Clay | 0.100 | 0.38 | 0.027 | 1.23 | 2.88 |
| Silty Clay | 0.070 | 0.36 | 0.005 | 1.09 | 0.48 |
| Clav | 0.068 | 0.38 | 0.008 | 1.09 | 4.80 |

Table 2-1 Average values for selected soil water retention and hydraulic conductivity parameters for 12 major soil textural groups (Carsel & Parrish, 1988).

It becomes clear that the ability to conduct water depends on the amount of water that is available in the soil. This is represented by the volumetric water content, which is a very non-linear relation and makes solving unsaturated flows difficult. As can be seen from the SWCC in figure 2-5, the values range over many orders of magnitude and the distribution is often considered to be lognormal. To illustrate this complexity, the direct measurements of the unsaturated hydraulic conductivity can be seen in figure 2-8. These experiments are difficult and expensive (Gallage, et al., 2013). Therefore, the function is often predicted based on the SWCC. The same three productive methods are visualized below:

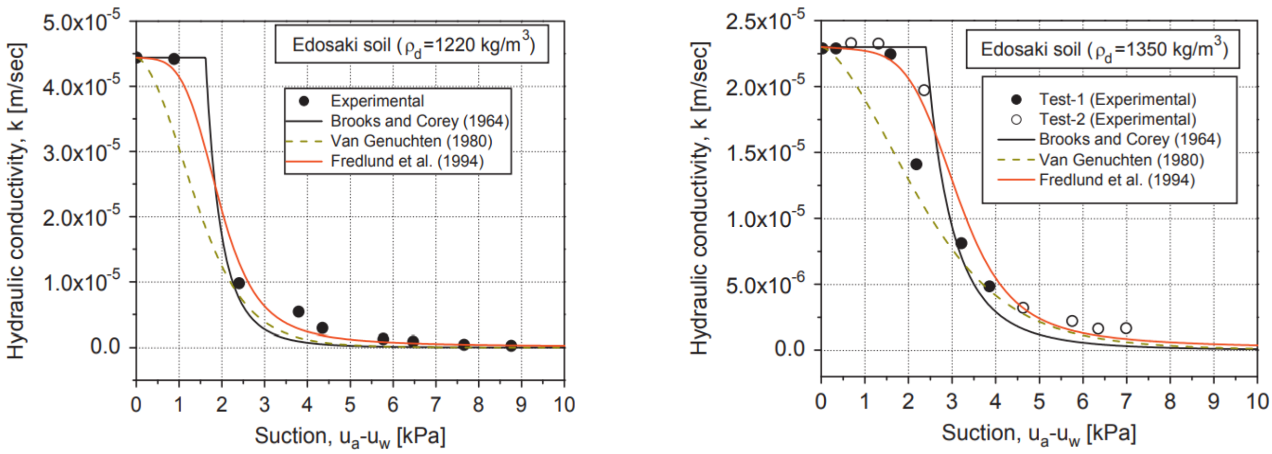


Figure 2-8 Comparison of measured and predicted hydraulic conductivity functions during the drying process for three frequently used methods (Gallage, et al., 2013)

According to Gallage et al., (2013), the best estimation was obtained using both closed-form Van Genuchten's (1980) method for the SWCC (figure 2-6) and Fredlund and Xing (1994) for estimating the hydraulic conductivity function (figure 2-8). The significant difference between the predictive method for the hydraulic conductivity of Van Genuchten (1980) and the measured ones could be attributed to the estimated fit-parameter m: $(m = 1 - 1/n)$ in Eq. [A.4] (Gallage, et al., 2013). This relation reduces the flexibility of the function. Leaving m and n with no fixed relationship could give more accurate results (Fredlund & Xing, 1994).

However, for practical application, in this study, Van Genuchten's (1980) method is used for both estimating the SWCC and hydraulic conductivity with the fixed relationship between n and m. How the hydraulic conductivity function can be predicted from the soil water characteristic curve is explained in Appendix A-2 *Hydraulic conductivity function*.

The equation is as follows (Van Genuchten, 1980):

$$K(h) = \begin{cases} K_s K_r(h) & (h < 0) \\ K_s & (h \geq 0) \end{cases}$$

[2.3]

Herein, $K\ [m \cdot sec^{-1}]$ is the hydraulic conductivity and $K_s\ [m \cdot sec^{-1}]$ is the saturated hydraulic conductivity of a soil. The pressure head is given by $h\ [m]$. $K_r\ [-]$ is the relative hydraulic conductivity, a normalized form, which can be determined with the computed curve fitting parameters of the SWCC:

$$K_r(h) = \frac{\{1 - (\alpha h)^{\mathrm{n}-1}[1 + (\alpha h)^{\mathrm{n}}]^{-\mathrm{m}}\}^2}{[1 + (\alpha h)^{\mathrm{n}}]^{\mathrm{m}/2}}$$

[2.4]

The relation between these hydraulic conductivities in Eq. [2.3] is as follows:

$$K_r = \frac{K}{K_s}$$

[2.5]

### 2.2 Macro stability and phreatic lines

Macro-(in)stability is the failure caused by a loss of stability (balance) of a soil mass along a slip plane. This balance consist of a driving moment, which is caused by the mass of soil at the left side of the center point of a circular slop plane (side of the water), and a resisting moment. This moment is caused by the mass of the soil on the right side of the center point (side of the land). The shear stress along the slip plane is causing resistance. In case the water level rises, the pore-water pressures $u_w$ $[kPa]$ in the soil increase, due to which the effective stresses $\bar{\sigma}$ $[kPa]$ in the soil decrease (figure 2.9). This causes loss of balance and instability of the soil. Hereby, is the water level just an indicator for this failure mechanism. It's not the weight of the water that causes the macro-instability. The actual load is the weight of the soil, which is not changing, but the resistance does which can lead to instability ('t Hart, et al., 2016).

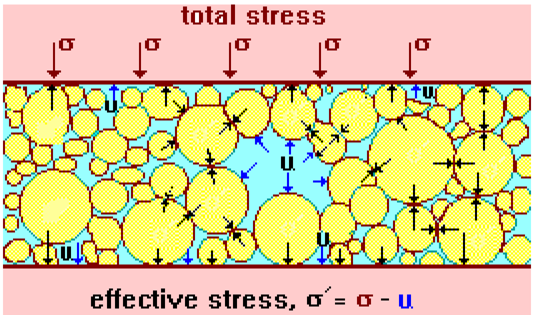

Figure 2-9 Relation between effective stress $\bar{\sigma}$, total stress $\sigma$ and pore-water pressure $u_w$ (Jamal, 2017)

Figure 2.10 visualizes the principle of macro-stability (inner slope), where the highest water level is a critical situation and is causing an increase in pore-water pressure, decrease in effective stress and decrease in shear strength, which leads to deformations and eventually sliding of the soil. For macro-stability (outer slope), the water drop after a peak flow is critical, since the pore-water pressure inside the dike is still relatively high (and also the phreatic surface). The pore-water pressures are lagging inside the dike and subsurface. and the resistance the water was causing has dropped out. Hereby, the is the driving moment at the right

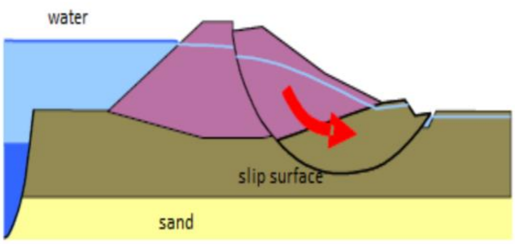

Figure 2-10 Basic principle of macro-instability ('t Hart, et al., 2016).

side of the center point of a circular slope plane (side of the land), and the resisting moment at the right side (side of the water). Macro-stability can also be induced by extreme rainfall. Therefore, the water pressures are increasing whereas the effective stress decreases.

In Chapter 5, the results of the simulations (i.e. representative phreatic lines) are implemented in a calculation model for the assessment of macro-stability (outer slope) and those calculations can be expressed in a factor of safety $FoS$ $[-]$, which must be at least 1.0 or higher in most stability analyses for safety approval (ENW, 2009):

$$FoS = \frac{M_r}{M_a} \tag{2.6}$$

Where $M_r$ $[kNm]$ is the maximum resisting moment and $M_a$ $[kNm]$ the driving moment. How these moments can be calculated is stated in Appendix A-4 *Factor of Safety macro stability*

## CHAPTER 3

## METHODOLOGY

*In this Chapter, the method used for the Monte Carlo Simulation set-up is described including a step-by-step approach. Also, the main code for generating random variables of the hydraulic conductivity and supplementary codes for executing the Monte Carlo Simulation is explained. In order to investigate the effect flood waves have on the phreatic line, a simulation case will be set-up. This will be a non-fictive case since the results of this study could be applied easier to the project Sweco is working on.*

### 3.1The software SEEP/W

In this study, SEEP/W (part of GEO-SLOPE International Ltd. (Canada)) is used at the request of Sweco. SEEP/W can simulate for this purpose two-dimensional stationary flood waves (that change over time) in fully and partially saturated soil on the basis of numerical groundwater flow analysis, based on the Finite Element Method (FEM). Therefore, the software is able to solve the nonlinear governing differential equation of seepage Eq. [A.10], where both property functions (i.e. water storage function Eq. [2.2] and hydraulic conductivity function Eq. [2.3]) are integrated into this partial solution. The solution adopted by FEM is described in Appendix A-3 *Hydraulic model for seepage analysis*.

An advantage of using this software is that SEEP/W allows the use of add-in functions based on Microsoft .NET Common Language Runtime (CLR) including C# (C-sharp) (Geo-Slope Int Ltd., 2013). Add-in functions can define specific soil properties, boundary conditions and for the purpose of this study, generate random soil property values (i.e. a stochastic approach).

### 3.2 Random variable model and uncertainty quantification

The purpose of threating variables in seepage-related problems as random numbers is to treat the uncertainties in the analysis, such as the hydraulic conductivity, porosity, fitting parameters of the soil-water characteristic curve, etc. Also, the boundary and/or conditions may be considered uncertain due to variation of the water table. In this study, flood waves and corresponding waveform are considered to be uncertain. Therefore, typical scenarios of flood waves are created in order to model the effects with respect to the uncertainties of soil properties. These uncertainties can be represented by using random variables. This allows this study to quantify uncertainties in soil properties for transient seepage modeling and analyze the key performance indicators (KPIs).

In the study, the focus is on the development of the phreatic line (i.e. top flow line) as a result of variation in the outer water level. The indicator will be the elevation $z_p$ $[m]$ of the phreatic line for an fixed location on the cross-section of the dike. Additionally, the effect of the variation in the outer water level on the pore-water pressure $u_w$ $[kPa]$ in the aquifer and cover layers will be examined at given locations, since dike stability is affected by the interaction of surface water and pore-water. Pore-water pressure can build up in earth dikes during drawdown conditions. The ability of the soil to release the pore water pressure is slowed if the hydraulic conductivity of the material is low. The excess pore-water pressure can cause slope instability.

The uncertainty is modeled by treating the hydraulic conductivity $K_s\,[m \cdot sec^{-1}]$ and the fitting parameters of Van Genuchten (1980) $\alpha\,[kPa^{-1}]$ and $\mathrm{n}\,[-]$ as random variables. The method of generating random numbers using their probability density functions (PDFs) is introduced herein. But at first the, correlation between the variables $\alpha$ $[kPa^{-1}]$ and n $[-]$ is investigated.

In the study of Çalamak (2014), a statistical analysis is performed based on the fitting parameters for clay and sandy clay soil types gathered from the database of SoilVision (Fredlund, 2005). The database contains over 6000 soils and for the analysis of Çalamak (2014), 100 soils for clay and 103 soils for sandy clay were obtained. The relationship and Pearson product-moment correlation coefficient r (Pearson, 1895) is presented. The coefficient r is in between $-1$ or +1. A correlation of $-1$ indicates that the data points are scattered on a straight descending line. A correlation of 0 indicates that there is no linear relation whatsoever. A correlation of $+1$ means that the two variables are perfectly positively linearly related.

Weak correlation is obtained between the two parameters based on the scatterplots in figure 3-1 and figure 3-2, respectively, the coefficients are 0.24 for clay and 0.34 sandy clay (Çalamak, 2014). The study of Phoon et al. (2010) found also weak correlation but those were negatively correlated. This is inconsistent from a statistical-analyzing point of view.

However, the independence of the two variables is assigned by Van Genuchten (1980) and also in the study of (Li, et al., 2009) are the two variables handled as independently from their probability distributions. The parameter $\alpha$ $[kPa^{-1}]$ is related to the largest pore-size and n $[-]$ is related to the pore-size distribution. Due to the observed inconsistency, the weak correlations are neglected and the variables $\alpha$ $[kPa^{-1}]$ and n $[-]$ are further assumed to be independent.

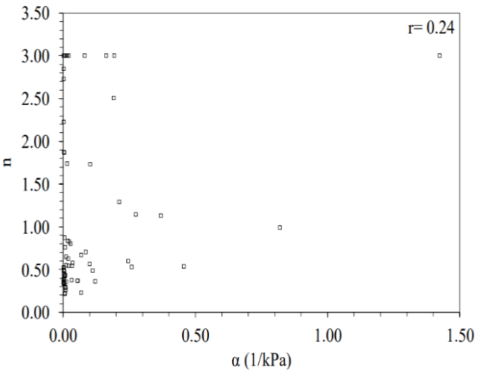


Figure 3-1 relationship $\alpha$ $[kPa^{-1}]$ and n $[-]$ for "clay" (Çalamak, 2014) obtained from SoilVision (Fredlund, 2005)

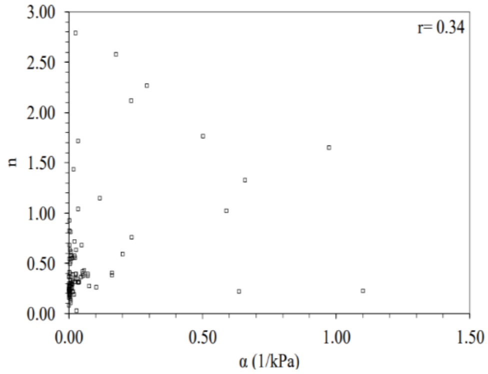


Figure 3-2 relationship $\alpha$ $[kPa^{-1}]$ and n $[-]$ for "sandy clay" (Çalamak, 2014) obtained from SoilVision (Fredlund, 2005)

Since there was no previous study performed with respect to the individual effect of the van Genuchten (1980) parameters, Çalamak (2014) decided to investigate the randomness of the hydraulic conductivity $K$ $[m \cdot sec^{-1}]$ and the van Genuchten (1980) parameters $\alpha$ $[kPa^{-1}]$ and n $[-]$. A sensitivity analysis (MCS's) were conducted for different embankment dam geometries and material types for different transient analysis (rapid drawdown/fill). Çalamak (2014) found that the variation of hydraulic conductivity have a crucial effect on the transient seepage. Similar results were obtained for steady-state seepage.

The variation effects of van Genuchten (1980) parameters resulted in smaller influences on the seepage. The increase in COV values for $\alpha$ $[kPa^{-1}]$ from 0.32 to 1.26 and COV for n $[-]$ from 0.04 to 0.16 did not result in a significant change in the mean seepage rate.

For practical application, it is reasonable to treat $\alpha$ $[kPa^{-1}]$ and n $[-]$ as deterministic values. This may not lead to major errors in seepage analysis. According to the results of Çalamak (2014), the probabilistic behavior of the van Genuchten (1980) parameters are excluded in this study.

The method used to generate random numbers for the variables hydraulic conductivity and the fitting parameters of SWCC consists of two steps:

1. Generation of uniformly random numbers over the interval [0,1] (called a pseudorandom number generator (PRNG), since the random numbers are predictable outcomes)
2. Apply a transformation to the random numbers to generate outcomes from the desired probability distribution. In this study, the Box-Muller method (Box & Muller, 1958) is used. It is a transformation technique, that produces non-uniform, Gaussian-distributed, random numbers. Eventually, random variables can be obtained by defining the probability density functions (PDFs) with a mean and coefficient of variation (COV) (Çalamak, 2014).

As described in the previous sections, hydraulic conductivity and the fitting parameters of Van Genuchten (1980) for the SWCC follow a log-normal distribution. The probability density function of saturated hydraulic conductivity will be as follows:

The mean $\mu_{K_s}$, the expected value of the data set, which is one of the input values. The second moment is the variance ${\sigma^2}_{K_s}$, which shows the variation i.e. how the data is distributed about the mean. The coefficient of variation (COV) is the ratio of the standard deviation to the mean $\sigma_{K_s}/\mu_{K_s}$. This is the second input value and it is a dimensionless measure of dispersion of a probability distribution.

The natural logarithm is $lnK_s$, then it can follow normal distribution (Gaussian) with a normalized PDF obtaining a mean $\mu_{lnK_s}$ and a variance ${\sigma^2}_{lnK_s}$ (Fenton & Griffiths, 1996) (Çalamak, 2014):

$$ {\sigma^2}_{lnK_s} = ln\left(1 + \frac{{\sigma^2}_{K_s}}{{\mu^2}_{K_s}}\right) $$

[3.1]

$$ \mu_{lnK_s} = ln(\mu_{K_s}) - \frac{1}{2}{\sigma^2}_{lnK_s} $$

[3.2]

Considering this log-normal distribution, random variables for the saturated hydraulic conductivity can determine (Çalamak, 2014):

$$ K_s = e^{(\mu_{lnK_s} + \sigma_{lnK_s} r')} $$

[3.3]

Where $r'$ is an independent random variable with a standard normal distribution obtained by the Box and Muller transformation (Box & Muller, 1958):

$$ r' = (-2lnU_1)^{1/2} sin2\pi U_2 $$

[3.4]

Suppose $U_1$ and $U_2$ are uniform random numbers over the interval [0,1]. The transformation also consist a of of cosine format of $r'$, creating twice as much random variables for more randomness with the same uniform random numbers but for this analysis one format is sufficient. The mathematical transformations resulting in the scatterplot as visualized in figure 3-3.

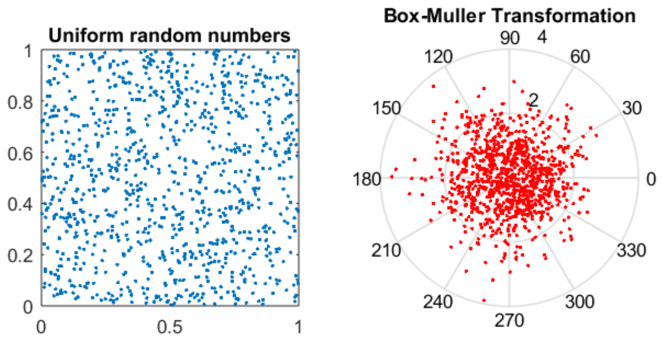


Figure 3-3 Uniform-normal transform by the Box-Muller method (Box & Muller, 1958)

This algorithm is written in C# language which code is run as an add-in function with the SEEP/W software. Two sub-functions are distinguished: one for generating variables for the hydraulic conductivity using the fitting parameters of Van Genuchten (1980). The same method is implemented for those variables. The other function computes the soil-water content using the Van Genuchten (1980) method. One part handles the generation of random variables for $K_s$ $[m \cdot sec^{-1}]$ and separately calls the sub-function for the computation of the water storage function (Appendix A-1 *Water storage function*) and hydraulic conductivity function (Appendix A-2 *Hydraulic conductivity function*). The C# code including the computation of the two soil property functions and the random variable generation can be found in Appendix E *The C# code*.

### 3.3 Monte Carlo Simulation

Monte Carlo experiments are a class of computational algorithms that rely on repeated random sampling. The objective is to use randomness to solve seepage problems that might be deterministically analyzed in principle. The uncertainties of soil properties can be obtained by observations on-site or laboratory measurements. However, a fully statistical approach can be investigated by a set of simulations using artificially random numbers from a known statistical distribution. Monte Carlo experiments can mainly be used for optimization goals or generating draws from a probability distribution. For example, investigating the location of the phreatic line may give more insights on how dike reinforcements should be executed and how costs of dike materials can be reduced while keeping the stability of the dike in mind. With Monte Carlo experiments those systems can be modeled close to reality i.e. it allows detailed description without using any simplifications or assumptions (Çalamak, 2014). This makes the method relatively simple and reliable. Though the computational calculations may be time-consuming but nowadays computer processors are speeding up which make the task easier to execute.

For the reasons mentioned above, this study adopted the Monte Carlo simulation technique. For different cases of dike compositions (e.g. core material, cover layers, etc.) but with the same geometry and boundary conditions (e.g. flood waveform, initial water tables, seepage potential lines, etc.), the transient seepage problems are solved using different random input variables. The one-at-a-time analysis is performed for the hydraulic conductivity parameter making use of the probability density functions. The outcomes of the simulations yield a set of locations with elevations $z_p$ $[m + \text{NAP}]$ of the phreatic line for different dike sections and a shading contour layer of the hydraulic head of the dike core. After that, the data-set is statistically analyzed consisting of frequency histogram, a fitted probability distribution function and, a box-plot.

The following steps were executed for the Monte Carlo simulation in this study:

1. Determination of a probability density function with a mean and COV for the hydraulic conductivity $K_s$ of different soil types. Those values will be entered in SEEP/W with respect to the dike material. The values are determined based on literature and the database of Sweco.
2. The dike of interest with its corresponding geometry, initial and boundary conditions (e.g. flood waveform), the materials are drawn and defined in SEEP/W.
3. $N$ number of copies are made of the original SEEP/W simulation file. This file must be solved for steady-state first, since transient analysis is built on steady-state results (Geo-Slope Int Ltd., 2013). This number corresponds with the number of Monte Carlo simulations, which can be determined using a student-t test. A (safe) starting point is to solve $500 - 1000$ SEEP/W simulation files for the determination of The files are copied using a batch file written in Windows Command Prompt (see Appendix F-1 *Generate copies*).
4. $N$ number of copies are solved for transient seepage using another prescribed batch file. When running the simulation in SEEP/W, the C# code works as an add-in and the code starts to generate random variables (see Appendix F-2 *Solve individual).*
5. $N$ number of SEEP/W simulation files are exported (only the phreatic line) as DXF file (Drawing eXchange Format) an extension for a graphic image typically used with AutoCAD softare. Extracting the phreatic line from SEEP/W is difficult. Therefore, AutoCAD is used for obtaining the coordinates of the phreatic line. This is done with AutoHotkey (AHK), an open-source scripting language for Microsoft Windows for automating representative tasks (Lawson, 2014). An extension named AutoScriptWriter enables to record the mouse- and key movements and automatically creates a script that can be run (see Appendix F-3 *Export DXF).*
6. $N$ number of DXF files are inserted with another AHK-script in AutoCAD (see Appendix F-4 *Insert DXF*).
7. $N$ number of phreatic lines are intersected with a section-location of interest in AutoCAD. The elevations $z_p$ are manually exported to an Excel file for statistical analysis. The total boundary, the spectrum of all phreatic lines that are calculated stochastically (i.e. all possible locations of the phreatic line) can be drawn in AutoCAD. By visualizing this spectrum of stochastic possibilities in combination with the deterministic location of the phreatic line, the intended user can derive the effect the COV of $K_s$ is on the location and development course of the phreatic line.
8. $N$ number of elevation coordinates are statistically analyzed in Excel, each Section containing a histrogram, a best fit probabilitiy density function (accepted or rejected) and a box-plot.

The above description of steps is used for both sensitivity analysis and further applications for problems that can be solved with a stochastic solution.

**STEP 1:**
Random variables of the hydraulic conductivity $K_s$ for the soil type of interest

**Method:**
- Generation of random numbers with pseudorandom generator (PRNG)
- Apply a transformation using the Box-Muller method
- Using the transformed random numbers for defining random probability density functions (PDFs) of $K_s$ with a mean and COV

**STEP 2:**
Definition of case dike in SEEP/W

**Method:**
- Draw geometry of the dike
- Define initial and boundary conditions (e.g. flood waveform, polder water level, potential seepage lines)
- Define input parameters per soil type (Appendix B)

**STEP 3:**
Number of simulations for transient seepage analyses and generation of copies of initial SEEP/W file

**Method:**
- Solve steady-state SEEP/W simulation with initial conditions
- Generate 500-1000 copies of steady-state SEEP/W simulation files using a Windows Command Prompt batch file (Appendix F-1)
- Solve 500-1000 steady-state SEEP/W simulation files using a Windows Command Prompt batch file (Appendix F-2)
- Export 500-1000 phreatic lines as DXF files using AHK code (Appendix F-3)
- Insert 500-1000 DXF files in AutoCAD (Appendix F-4)
- Extract coordinates of 500-1000 phreatic lines and convert to Excel
- Determine number of simulations for MCS using the Student-t test

**STEP 4:**
*N* number of transient SEEP/W simulations solved for Case number No.

**Method:**
- Generate *N* number of copies of transient SEEP/W simulations files, Case number No., using a Windows Command Prompt batch file (Appendix F-1)
- Solve *N* number of transient SEEP/W simulations files, Case number No., using a Windows Command Prompt batch file (Appendix F-2)

**STEP 5:**
*N* number of phreatic lines exported as DXF files

**Method:**
- Export *N* number of transient SEEP/W simulation files, Case number No., (only the phreatic line), to DXF files using a AHK-code (Appendix F-3)

**STEP 6:**
*N* number of phreatic lines as DXF file inserted in AutoCAD for Case number No.

**Method:**
- Insert *N* number of phreatic lines, Case number No., as DXF files in AutoCAD using a AHK-code (Appendix F-4)

**STEP 7:**
*N* number of elevation coordinates of phreatic lines converted to Excel and a total boundary zone of all phreatic lines for Case number No.

**Method:**
- Intersect *N* number of phreatic lines with the (8) Section locations using AutoCAD
- Export the coordinates of the intersection points as csv. files (Excel)
- Using the AutoCAD add-in 'TotalBoundary', a boundary can be drawn automatically.

**STEP 8:**
*N* number of elevation coordinates are statistically analyzed, containing a histogram, PDF and box-plot for each Section, Case number No.

**Method:**
- For each section, the *N* number of elevation coordinates of the phreatic line are statistically analyzed using data-tools in Excel (e.g. Data analyses, Solver)

## CHAPTER 4

## CASE TiWa

*This Chapter handles the case initiation with respect to STEP 2 and its validation procedure of the model. The case location in this study is the dike reinforcement project Tiel-Waardenburg (TiWa), the Waal river, the Netherlands at TG109 (see figure 4-1). Commissioned by Water Authority Rivierenland (WSRL), Sweco conducted a geotechnical substantiation for solutions with respect to macro stability and piping.*


Figure 4-1 case location project Tiel-Waardenburg TG109: Waal river at Varik and Heesselt (pictures: province Gelderland, The Netherlands, and Google Streetview).

The validation calculations in the report of Dike Reinforcement Tiel-Waardenburg (Van Middelkoop, et al., 2018) are elaborated for four locations along this dike trajectory. The results of these four locations are translated to the entire project area. One of these locations is TG109.

The choice for the case location TG109 is a pragmatic one since Sweco is involved in the project, data of dike geometry and geology were available. Also the soil characteristics of the subsurface obtained by the retrieval of soil site investigation, which enables to determine the input parameters (e.g. hydraulic conductivities, SWCC fitting parameters, et cetera). Besides, standpipe piezometers were monitored over more than 1.5 years for the use of validation. At last, the geometry and simplified geology were already set-up in SEEP/W (Van den Berg, 2019), which enables to validate the SEEP/W model (with C#-code add-in, Van Genuchten (1980) method, fitted soil input parameters) with the SEEP/W model of Van den Berg (2019) (with predefined soil input parameters (Sweco's material library in SEEP/W)) without changes in geometry, geology and boundary conditions.

Choosing location TG109 out of the four locations had also to do with the simplified homogeneous dike core (i.e. the other locations have multiple sand-layers inside the dike core), which was a starting point for the interpretation of the results and model testing, without dealing with relative complex phreatic lines due to different hydraulic soil properties in the dike core.

The results in this study are not normative for this location due to assumptions that are made (e.g. simplified geology, choice of $K_s$ and COV, wave type and waveform). The aim for validating TG109 is to explore the effects flood wave types have on the phreatic line and pore-water pressure in the aquifer and cover layers. However, the methodology used for executing the MCS can be applied to other dike locations using SEEP/W and the C# code for generating random variables.

## 4.1 Set-up SEEP/W model

The dike section including the surrounding subsurface is drawn in SEEP/W. The geometry and assigned geology for TG109 were already available in SEEP/W using the simulation file of  Van den Berg (2019). The geometry and boundary conditions of the dike section can be seen in figure 4-2.

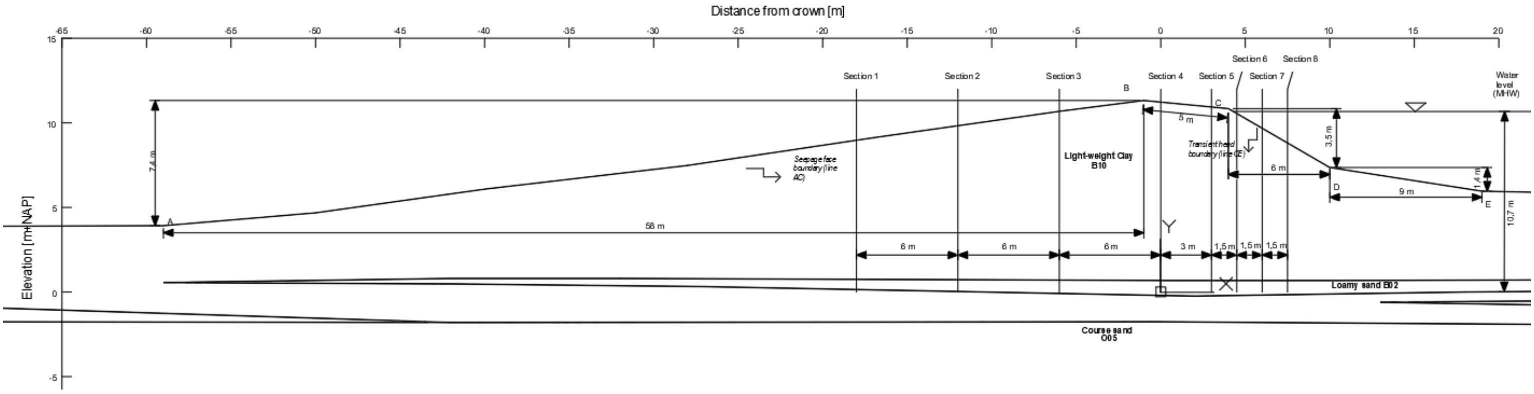


Figure 4-2 Dike section TG109 geometry, sections and boundary conditions considered for initial SEEP/W simulation [1].

The crown and downstream side are considered as seepage face boundary and the upstream side as the transient head boundary. The total width is 77 m and the height of the dike is $11.3m +$ NAP. The polder water level is set to $3.2m +$ NAP.

The soil compositions of the subsurface surround the executed cone penetration tests (CPTs) is supplemented with data of GeoTOP and REGES from DINOloket (Van den Berg, 2019). Therefore, the soil composition is schematized in relative detail surround the dike and more general at a greater distance from the dike (see figure 4-3).

[1] Figure 4-2 shows eight Sections located at $-18\ m, -12\ m, -6\ m, 0\ m, +3\ m, +4.5\ m, +6\ m$ and $+7.5\ m$ from crown. These sections are labeled as Section 1, Section 2, Section 3, Section 4, Section 5, Section 6, Section 7, Section 8, respectively from inner toe to outer toe. These Sections will be used as cross-sectional measure locations for the statistical analysis of the elevation coordinates of the phreatic lines in Chapter 5.

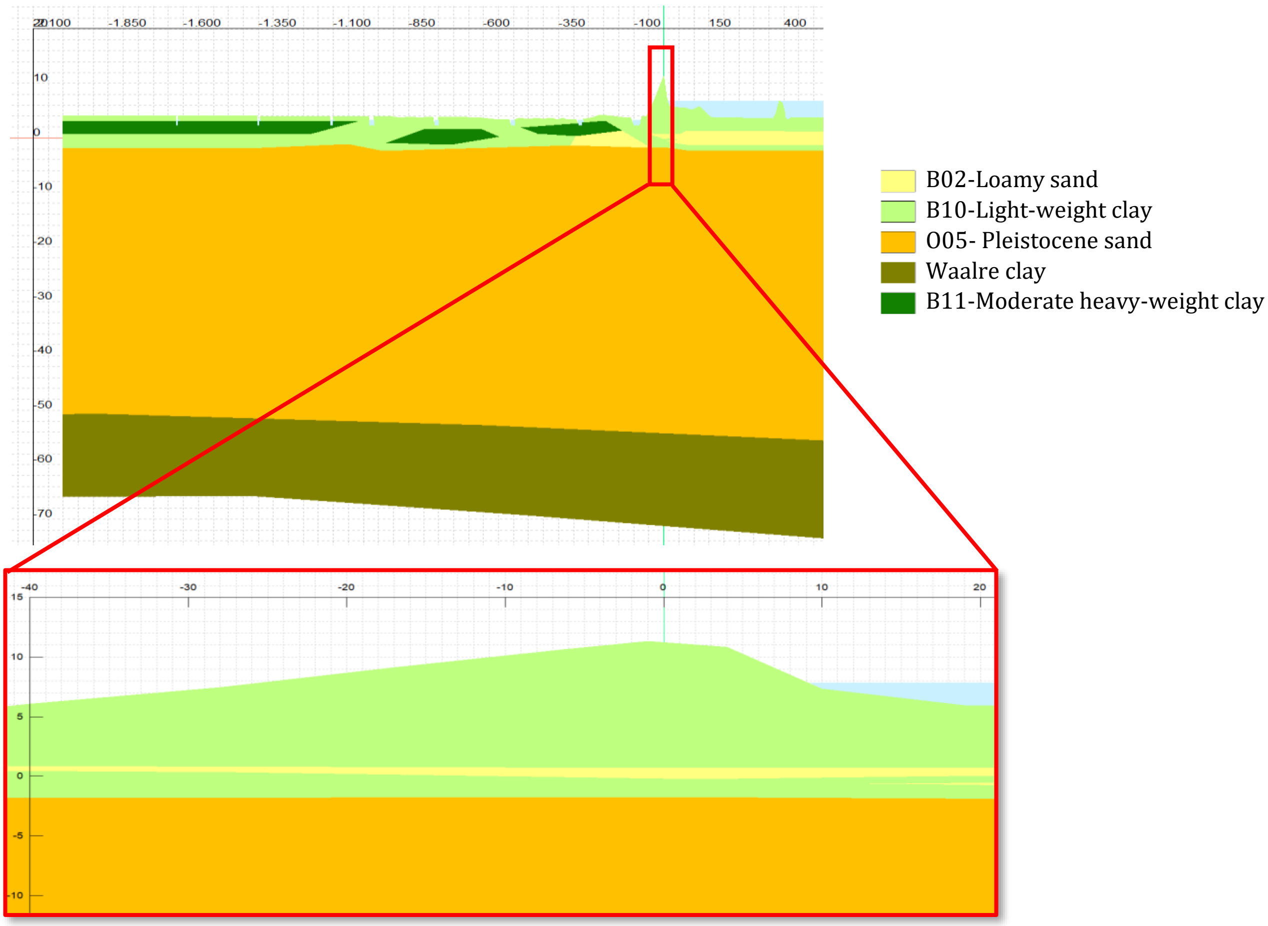


Figure 4-3 Dike profile TG109 in SEEP/W. Distances in meters. Dike crown at $0m$ x-axis and the N.A.P. reference point i.e. Normal Amsterdam water Level is at $0m$ y-axis. Image below is a close-up of the dike (Van den Berg, 2019).

By using measured data of the soil water content and pressure head, for different typical subsurface compositions (provided by Sweco), the parameters of the Van Genuchten (1980) method are estimated by the least square method (Yang & You, 2013):

$$minf = \sum_{i=1}^{N} (\theta_i - \theta(h_i, X))^2$$

[4.1]

Where, $\theta_i$ $[-]$ is the $i^{\text{th}}$ measured soil water content, $h_i$ $[m]$ is the $i^{\text{th}}$ measured pressure head corresponding to $\theta_i$, $\theta(h_i, X)$ is the calculated soil water content according to Eq. [2.2]. The parameter vector that needs to be optimized (i.e. minimized in this case) is $X(\theta_r, \theta_s, \alpha, \text{n})$. Herein is $N$ the number of measurements. This formula can be solved in Excel using the Solver add-in function. The parameter values of the hydraulic conductivity are obtained by laboratory research (executed by Fugro (Van Middelkoop, et al., 2018)). The resulting parameters for each soil texture are listed in table 4-1. According to Van den Berg (2019), Waalre clay is assumed to be saturated only.

For a more detailed description of the least square method and a quantification of the Van Genuchten (1980) model fit ( i.e. a statistical analysis where differences between estimated and measured values are considered using performance criterion), see Appendix B *Initiation of geohydrological soil parameters.*

| Texture | Parameters of the Van Genuchten (1980) model | | | | |
|---|---|---|---|---|---|
| | $\theta_r$ $[cm^3/cm^3]$ | $\theta_s$ $[cm^3/cm^3]$ | $\alpha$ $[kPa^{-1}]$ | n $[-]$ | $K_s$ $[m/s]$ |
| B02 – loamy sand | 0.019 | 0.430 | 0.237 | 1.536 | $1.157 \times 10^{-5}$ |
| B10 – light-weight clay | 0.005 | 0.420 | 0.123 | 1.219 | $1.354 \times 10^{-7}$ |
| B11 – moderate heavy-weight clay | 0.019 | 0.600 | 0.244 | 1.116 | $1.157 \times 10^{-8}$ |
| O05 – course sand | 0.010 | 0.320 | 0.613 | 2.046 | $4.630 \times 10^{-4}$ |

Table 4-1 Parameters of Van Genuchten (1980) model estimated with least square method using measured data of the soil water content and pressure head (Van den Berg, 2019).

The SEEP/W model is now ready to run for a steady-state seepage analyses since the geometry is drawn, all regions assigned a geological soil type with corresponding parameters of the Van Genuchten (1980) model. These characteristic soil parameters are input parameters for the C# code called by SEEP/W's soil property functions (i.e. water content function and hydraulic conductivity function). At last, the boundary conditions are added (i.e. seepage face, (transient) head and polder water level).

## 4.2 River water level

In this paragraph, the river water level is analyzed, since the steady-state SEEP/W model of TG109 needs to be validated for a representative water level (i.e. river water level at which the outer slope side of the dike is inundated).

The presence of wide foreshores is characteristic for dikes in the project area of Tiel-Waardenburg. Because of these relative wide and high-lying foreshores, the water level does not touch the dike for most of the year but remains in the river bed. River water does only touch the dike at periods of peak flows. Therefore, daily circumstances are not representative for estimating bulging effects.

The water level is measured between Tiel and Waardenburg. Standpipes at each dike pile were translated to their location alongside the Waal river to interpolate the water level linearly for location Heesselt (Van Middelkoop, et al., 2018). Based on these data it is decided which period is representative for the determination of the phreatic line in the dike body. Figure 4-4 represents the water level for the period 11 November 2016 till 16 February 2018. Some outliers can be observed. Those are the peak flows.

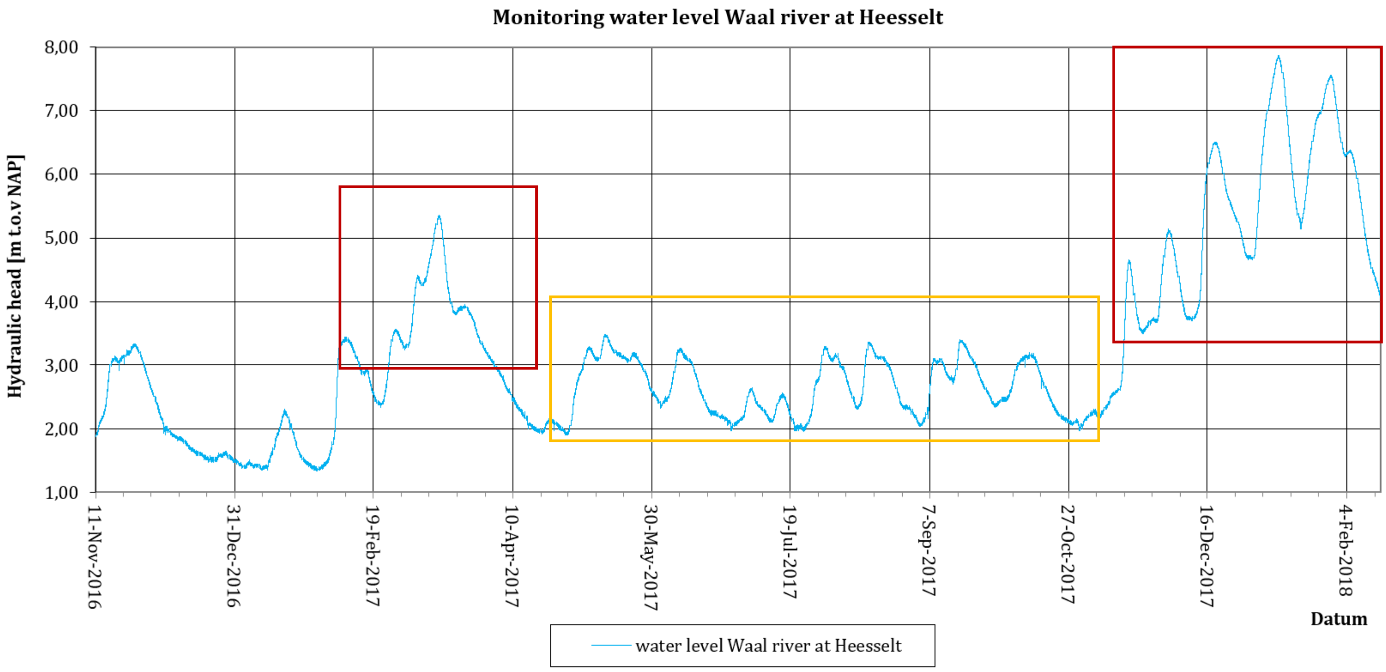


Figure 4-4 Interpolated water level Waal river at Heesselt (Van Middelkoop, et al., 2018); the average water level is highlighted in orange and peak flows are highlighted in red.

The average water level is highlighted with an orange box. In this period (15 April 2016 till 6 November 2017), the water level varied $2.0m$ + NAP to $3.2m$ + NAP. On average, the water level is approximately $2.6m$ + NAP. Figure 4-4 highlights also the flood waves i.e. periods of peak flow in red boxes The water levels in the red marked boxes are significantly higher than the average water level. In this case, the forelands will be inundated.

### 4.3 Analysis of standpipe measurements

At the height of dike piles, TG108 and TG109 three standpipes are placed. Figure 4-5 represents the standpipe measurements, the polder water levels, and interpolated water level. Some characteristics are described below (Van Middelkoop, et al., 2018) (Van den Berg, 2019):

- Surface level foreland $5.7m$ + NAP.
- Surface level hinterland $4.0m$ + NAP.
- Polder water level winter $3.2m$ + NAP.
- Polder water level summer $3.0m$ + NAP.
- The underside of the cover layer at crown $1.7m$ + NAP. Measuring point of the standpipes are just below the cover layer in the sand aquifer. TG109.+0.15_AB_BIT (hydraulic head inner toe $30m$ from crown). TG108.+0.93_PL_AL (hydraulic head inside the dike $80m$ from crown). TG109.+0.99_PL_AL (hydraulic head inside the dike $220m$ from crown)

As can be seen from figure 4-5, the hydraulic head responses on the outer water level. This is a non-linear relation i.e. the hydraulic head follows the rise of the water level at the Waal river. The measuring heads are on average $0.2 - 0.3m$ lower with respect to the outer water level under $4.0m$ + NAP and at higher levels on $0.3 - 1.5m$.

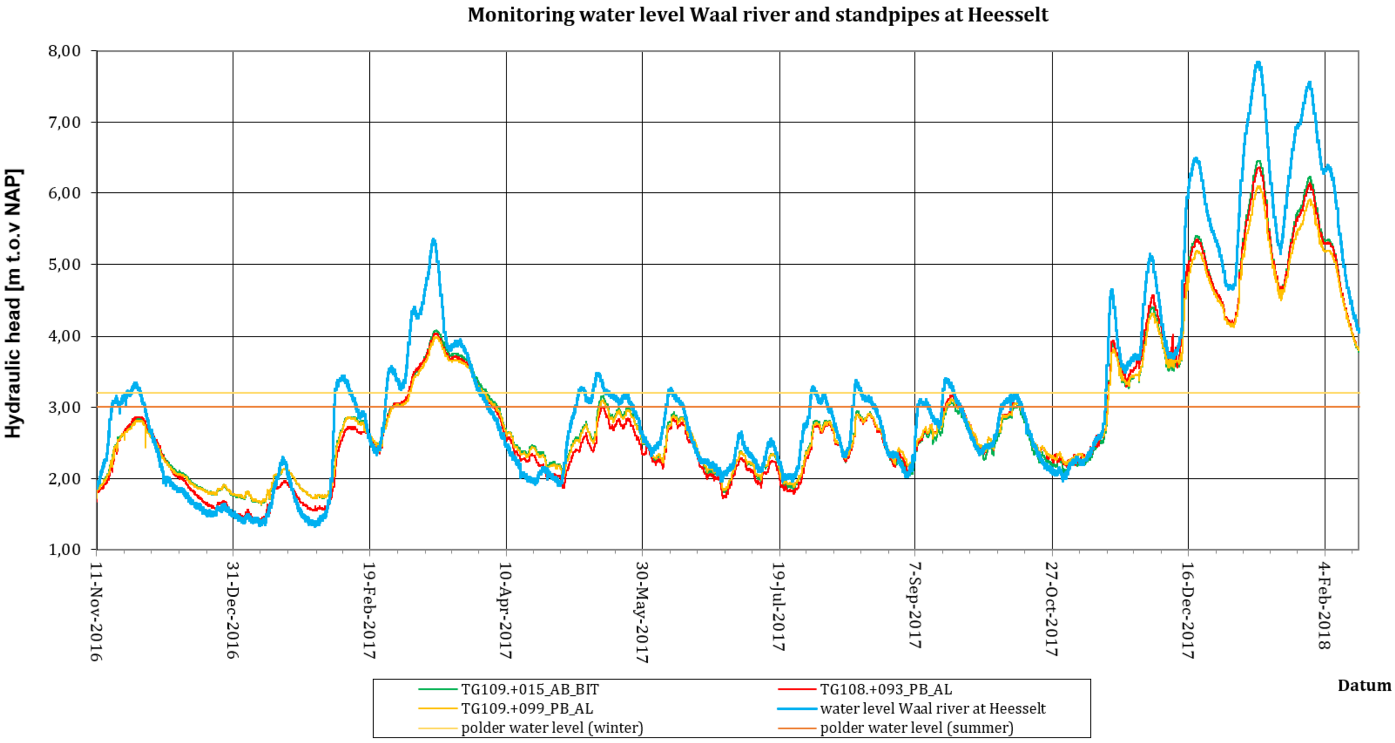


Figure 4-5 Interpolated water level Waal river and corresponding standpipe measurements at Heesselt (Van Middelkoop, et al., 2018); polder water levels are added.

### 4.3 Validation SEEP/W model

In this paragraph, the TG109 is validated for a steady-state seepage analysis in SEEP/W with hydraulic heads obtained by standpipe piezometers and validated with another model, the one set-up by Van den Berg (2019).

#### 4.3.1 Validation with standpipe measurements

The dike profile is validated stationary for the measured hydraulic heads during the peak flow period of January 2018 (see figure 4-4/4-5). The determination of input parameters for the SEEP/W simulation is described in Appendix B *Initiation of geohydrological soil parameters* of table B-1/4-1 were implemented via the C# code with the add-in function in SEEP/W. The calculated and measured hydraulic heads of the profile TG109 can be seen in figure 4-6. The hydraulic head in the cover layer varies with depth. Therefore, the hydraulic head at the underside, middle side, and topside of the cover layer is visualized. In this case, the hydraulic head at the underside of the cover layer is equal to the hydraulic head in the aquifer, and the hydraulic head at the topside of the cover layer is equal to the subsurface (Van den Berg, 2019).

The calculated values match well with the measured values in table 4-2. The hydraulic head at a distance of $80 - 250m$ inside the dike is calculated the best with a deviation of $10 - 15cm$. The hydraulic head at the inner toe of the dike has a higher deviation due to relative major differences in head around the dike e.g. over a distance of a few meters the changes in hydraulic heads are also tens centimeters.

| Location | Dike profile | Water level Waal river ($m$)<br><br>(top of peak flow (figure 4-4/4-5)) | Hydraulic head inner toe ($m$)<br><br>(30$m$ from crown) | Hydraulic head inside the dikes ($m$)<br><br>(-x$m$ from crown) |
|---|---|---|---|---|
| $TG109$ | Dike 1 | 7.85 | 6.50<br>TG109. +0.15_AB_BIT | 6.35(80$m$)<br>$TG108.+0.93\_PL\_AL$<br><br>6.10(220$m$)<br>$TG109.+0.99\_PL\_AL$ |

Table 4-2 Measured hydraulic head of standpipes during peak flow on 10 − 01 − 2018 (Van den Berg, 2019)

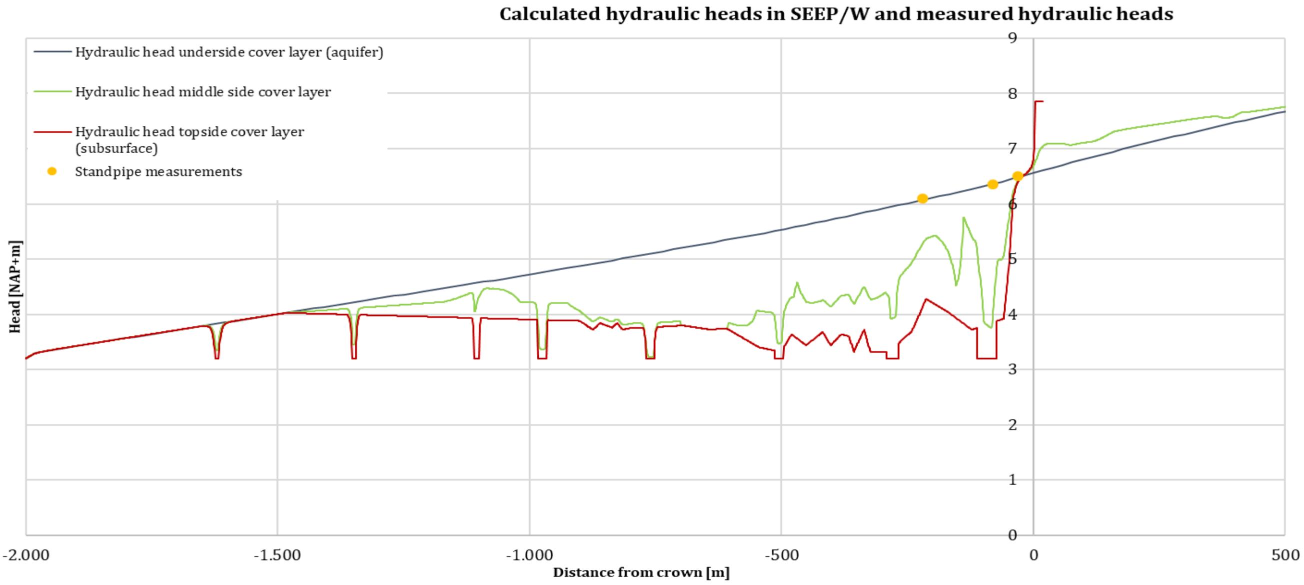


Figure 4-6 Calculated and measured hydraulic heads cover layer for dike profile TG109 during high tide period of January 2018. Left side of the crown is the inner dike area and on the right side the outer dike area.

Unfortunately, only three standpipe measurements are available and those that are usable were placed in the aquifer on relative great distance of the crown. If standpipe measurements were available nearby the crown in the dike core, the phreatic line could be validated better for historical peak flows.

### 4.3.2 Validation with another SEEP/W model

In this section the SEEP/W using the C# code for defining the soil property function is validated with the same SEEP/W of Van den Berg (2019) in which the property functions for the hydraulic conductivity and water storage are predefined in a library. The main reason why a new model is set-up is because of the random variable generator in the C# code which allows to perform the stochastic analyses.

In the report of Van den Berg (2019), the hydraulic heads are plotted similarly and validated with the same data of the standpipes. Both seem to be applicable for its intended purpose (operational validation) and fit the measured heads well. The simulation model of Van den Berg (2019) has been validated for the same measured heads. The differences between the two models are almost unobservable. Therefore, the root mean square error ($RMSE$) [Eq. B.2] and determination coefficient ($R^2$) [Eq. B.3] are calculated (see table 4-3). Small differences between two data-sets means a $RMSE$ close zero and a $R^2$close to one. Table 4-3 represents the comparison of both models with the measured hydraulic heads.

| **Statistical analysis** / **Location** | $\boldsymbol{R^2}$ | $\boldsymbol{RMSE/10^{-2}}$ |
|---|---|---|
| Hydraulic head topside cover layer (subsurface) | 0.999 | 0.326 |
| The hydraulic head middle cover layer | 0.996 | 5.624 |
| Hydraulic head underside cover layer (aquifer) | 0.999 | 0.003 |

Table 4-3 statistical analysis for simulation results SEEP/W model with calculated property functions with C#-code versus SEEP/W model with predefined soil property functions (Van den Berg, 2019).

| **Model** / **Measured hydraulic head ($m$)** | **SEEP/W model of TG109 with calculated soil property functions with C#-code (VG-method)** calculated hydraulic head ($m$) | **SEEP/W model of TG109 with predefined soil property functions (Sweco Library (VG-method)** (Van den Berg, 2019) calculated hydraulic head ($m$) |
|---|---|---|
| 6.50 TG109. +0.15_AB_BIT | 6.488 | 6.487 |
| 6.35 $TG108. +0.93\_PL\_AL$ | 6.360 | 6.360 |
| 6.10 $TG109. +0.99\_PL\_AL$ | 6.071 | 6.071 |
| **Statistical analysis** | | |
| $\boldsymbol{R^2}$ | 0998 | 0.998 |
| $\boldsymbol{RMSE/10^{-2}}$ | 1.920 | 1.930 |

Table 4-4 Statistical analysis for simulation results i.e. comparison with measured hydraulic heads (Van den Berg, 2019).

From table 4-3 it can be concluded that the model is relative similar to the model that is validated by Sweco for the same dike profile. The hydraulic head in the aquifer is almost linear over distance (see figure 4-3). The thickness of the aquifer is quite constant in contrast to the cover layer and the underside of the cover layer is approximately at the same depth (see figure 4.3). Small differences of geohydrological soil properties of sand do not lead to significant differences in outcome. However, that is not the case in the middle of the cover layer and the subsurface. Both locations change several meters in height over a distance which lead to irregular peaks in hydraulic head. The $RMSE$ for the hydraulic head in the middle of the cover layer is relative high compared to the head in the aquifer i.e. on average $5.6cm$. Locally, it can be tens of centimeters. This is also observed by Van den Berg (2019).

When comparing the two models with the measured hydraulic heads, the local differences are $1 - 3cm$ (see table 4-4). For the locations TG108. +0.93_PL_AL and TG109. +0.99_PL_AL, the calculated hydraulic head is the same for both models. Since there are only three standpipes available, it is difficult to statistically confirm if the model simulate reality well, but for those three measurements, it can be said that SEEP/W calculate the head in the aquifer quite good if a straight line is plotted through the three points.

Figure 4-7 is a hydraulic hysteresis of the standpipe measurements and interpolated outer water level at Heesselt (TG109). It shows the dependence of the state of the system on its history i.e. the hydraulic head may be observed for more than one possible water levels, depending on how the water level changed in the past. The line $y = x$ represents the linear relation where the outer water corresponds to the hydraulic head. However, due to the permeability of soil types, the water is delayed.

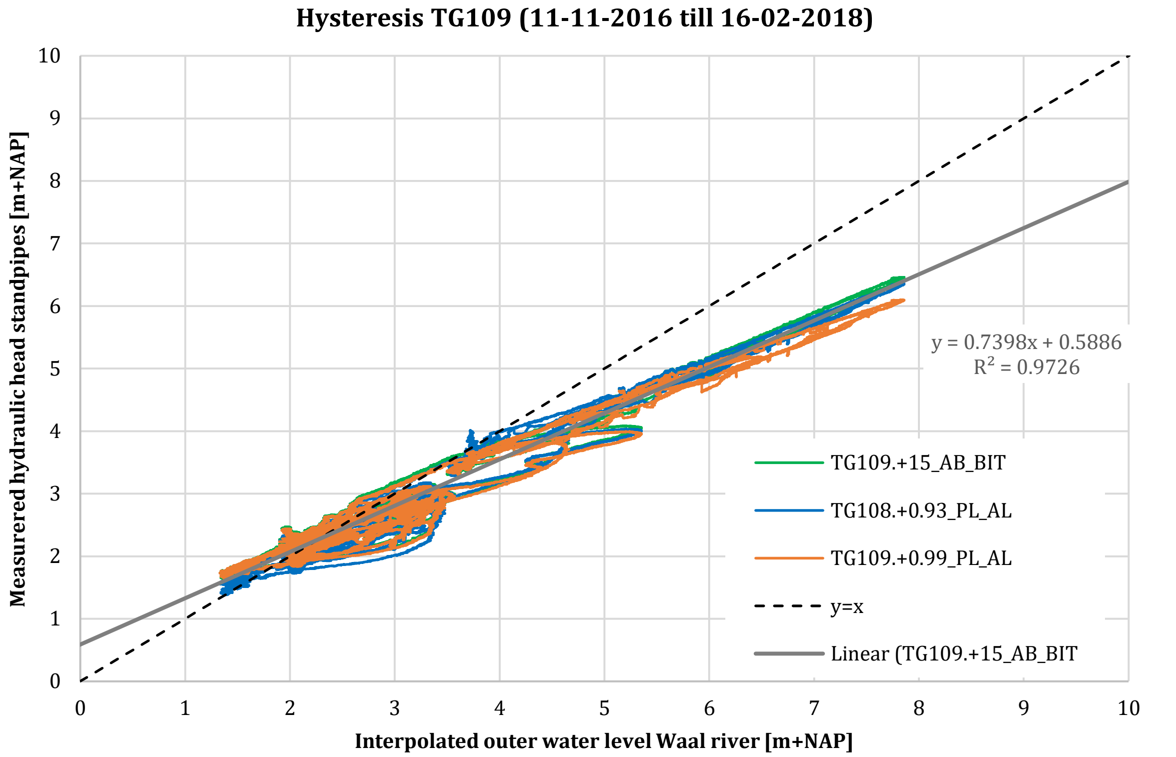


Figure 4-7 Hysteresis TG109

At frequent, prolonged water levels, the hydraulic head corresponds and is in line $(2 - 4\ [m + \text{NAP}])$. At higher values, the hydraulic head diverges. The reason is that those water levels are less frequent and are of short duration. Therefore, the groundwater level cannot come to an equilibrium. Certain loops can be observed clearly due to the peak flows i.e. the hydraulic head has a lower value when the flood wave rises and remains high when the flood wave descends. The curvature is determined by the dike material (e.g. for clay, the curvature is greater due to the response time, for sand the heads more correspond to the line $y = x$) but also the variation of data (e.g. if a fast rise-slow fall flood wave is signalized, the difference in head is greater for the same water level, then a relative great loop can be observed) since a hysteresis is time-depended i.e. different results are obtained from other periods.

If the hydraulic head is above the line $y = x$, the water level is lower. This is the case in dry periods. The polder water level is at 3.2 $[m + \text{NAP}]$. This point is on average the starting point for the deflection of the straight line.

Also, for TG109. +0.15_AB_BIT the linear trendline is plotted with its formula and $R^2$. If the pressure becomes too high, the cover layer will crack. When the hydraulic head for cracking is known, the water level at which this scenario occurs can be determined with the help of the extrapolated trendline.

Additionally, the location of the phreatic line is compared for the two models (see figure 4-8). Those lines are close together. In order to compare the locations, eight sections are chosen. At the inflow side, those sections are selected to have lower intervals since the phreatic line directly responses on outer water movements. More towards the dike toe, this effect weakens (see table 4-5). On this scale, the difference is close to zero.

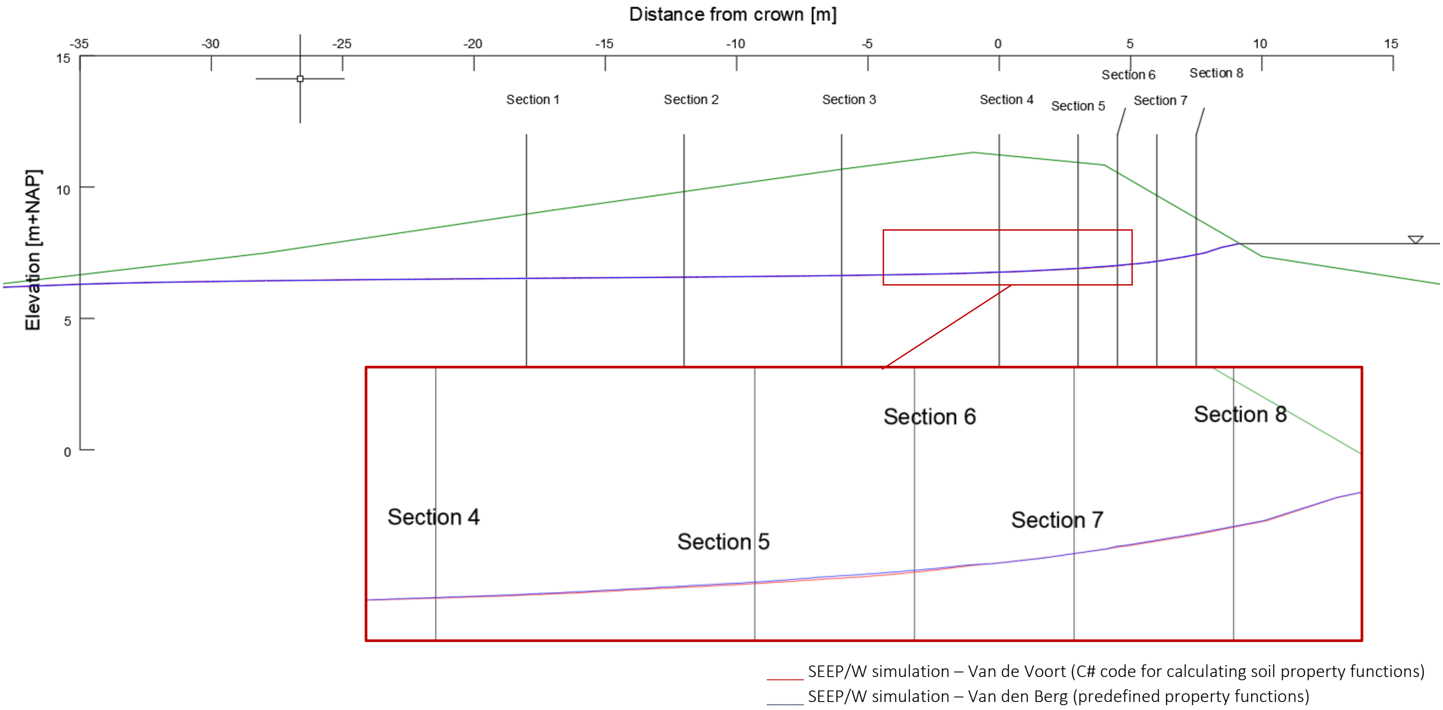


Figure 4-8 The phreatic line of deterministic seepage for TA109, the water level at 7.85 $[m + NAP]$ in January 2018. Small differences can be noticed for the two models where the input parameters are fixed (library of Sweco) or fitted by the GRG-algorithm and input parameters are calculated by an add-in (C#-script) (Van den Berg, 2019).

| **Location** | **Section 1** | **Section 2** | **Section 3** | **Section 4** | **Section 5** | **Section 6** | **Section 7** | **Section 8** |
|---|---|---|---|---|---|---|---|---|
| **Distance from crown** $[m]$ | $-18$ | $-12$ | $-6$ | 0 | 3 | 4.5 | 6 | 7.5 |
| Difference $(cm)$ | 0.00 | 0.12 | 0.24 | 0.56 | 1.41 | 0.94 | 0.03 | 0.76 |

Table 4-5 Section locations and differences in elevation of the phreatic line (Van den Berg, 2019).

### 4.4 Set-up Monte Carlo Simulation cases

On request of Sweco, two dike sections are used in the Monte Carlo Simulation which are common simplified dike section for Dutch river dikes compositions (see figure 4-9 and 4-10/4-11).

1. Dike 1: the original TG109 section with a dike core of light-weighted clay. The dike is shown with its geometry, sections and boundary conditions in figure 4-10 (=figure 4-2).
2. Dike 2: has the same geometry as TG109 but a loamy sand-core is drawn manually in the analyses with a cover layer of light-weighted clay with a thickness of $\pm$ 2.0 m. The dike is shown with its geometry, sections and boundary conditions in figure 4-11.

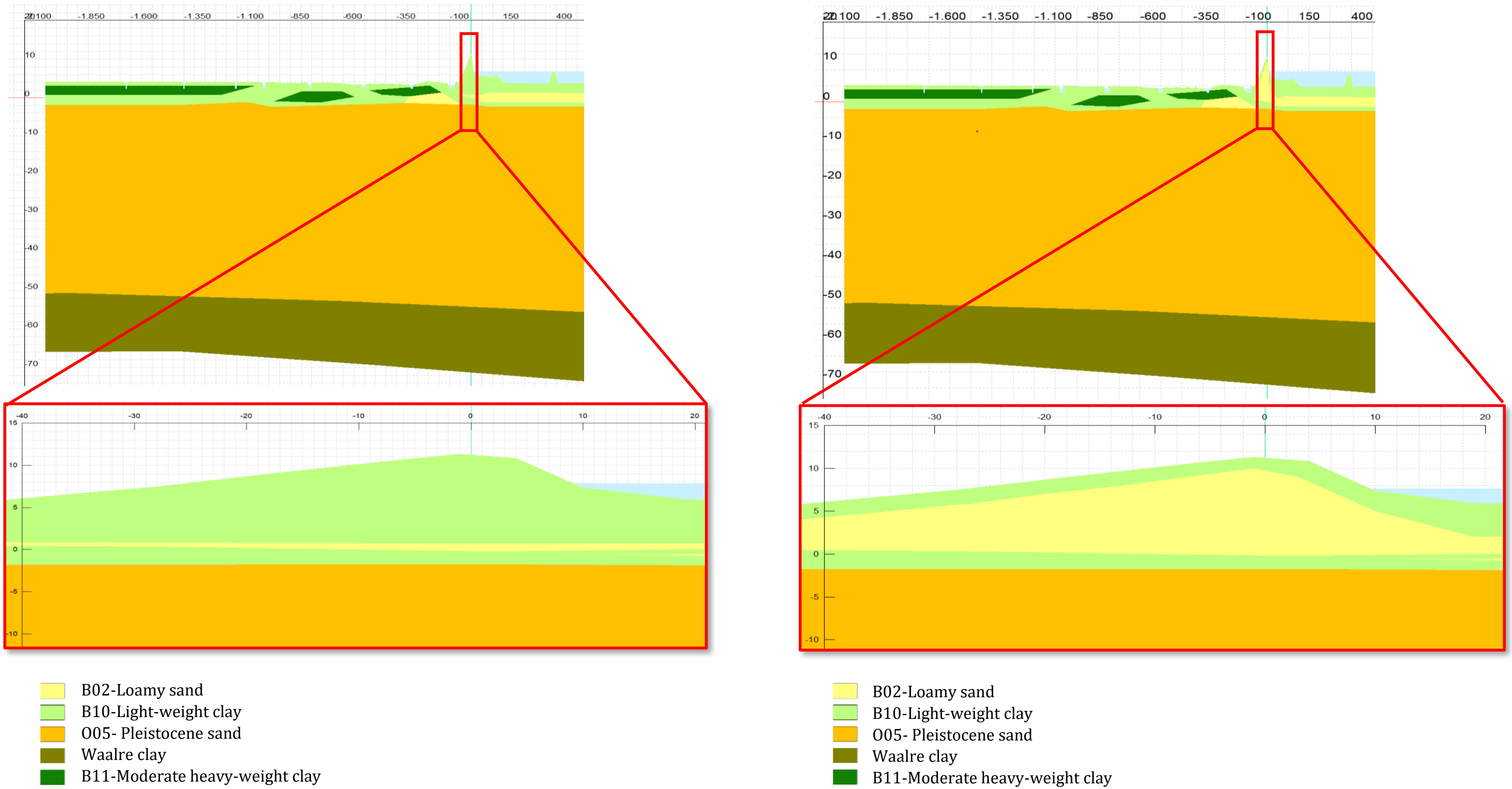


Figure 4-9 TG109 in SEEP/W. Left: original Dike with a light-weighted clay core (Case No. 1, 2 & 3). Right: Fictive Dike with a loamy-sand core and a layer of light-weighted clay on top (Case No. 4, 5, 6, 7, 8 & 9). Distances in meters. Dike crown at $0m$ x-axis and the N.A.P. reference point i.e. Normal Amsterdam water Level is at $0m$ y-axis. Image below is a close-up of the dike (Van den Berg, 2019).

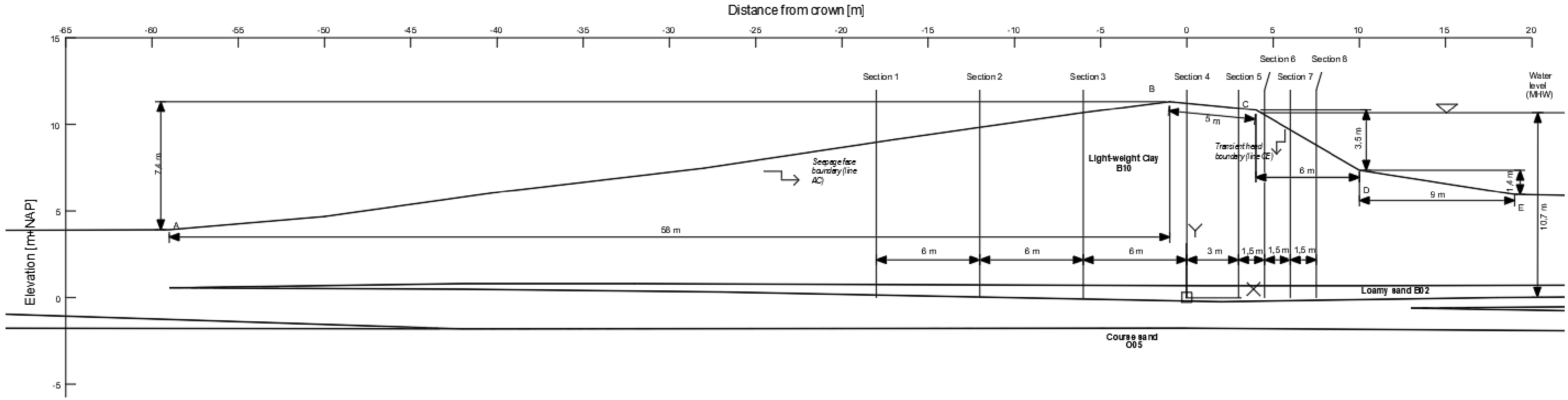


Figure 4-10 Dike 1: geometry, sections and boundary conditions considered for sensitivity analysis of transient seepage case number 1, 2 & 3.

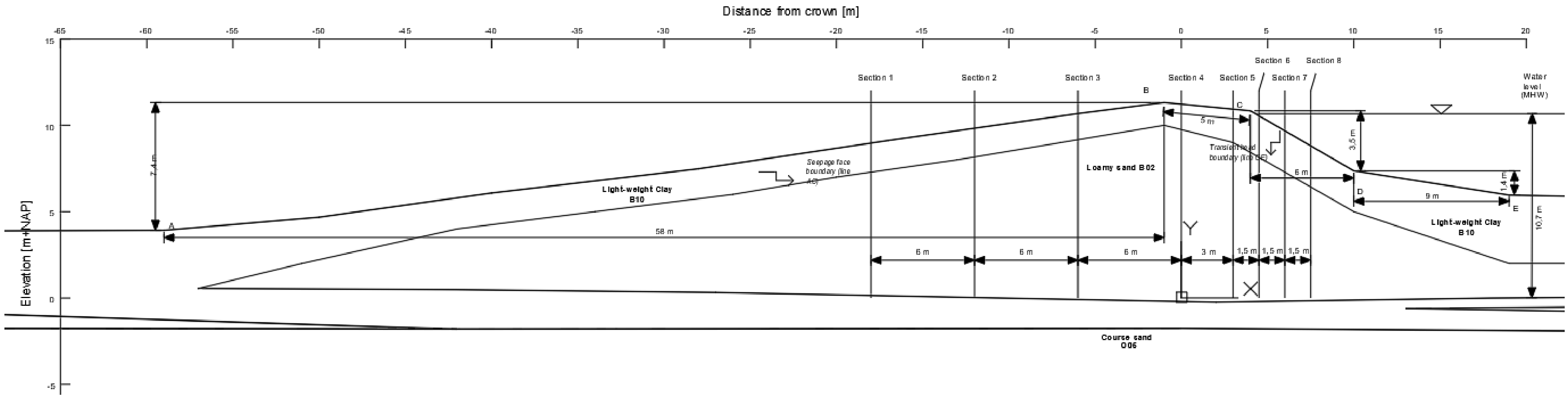


Figure 4-11 Dike 1: geometry, sections and boundary conditions considered for sensitivity analysis of transient seepage case number 4, 5, 6, 7, 8 & 9.

### 4.4.1 Defining flood wave scenarios

The two dike sections at TG109 are subjected to three different wave types:

1. fast rise – fast fall
2. average rise – average fall
3. slow rise – slow fall

These waves could be constructed with historical data and then the most frequent wave type can be used and simplified for analysis. Since the winter dike at TG109 is rarely exposed to water of the Waal river due to the summer dike (at $7.0m + \text{NAP}$) and relatively large extended foreland, historical hydraulic head measurements are also rarely available. For determining the location of the phreatic line and the hydraulic head in depth are then reliant on conservative estimates, al then not with help of groundwater flow calculations. For the purpose of assessing the macro stability of the outer slope during MHW, a method is given by the TAW (Barends, et al., 2004). This method does not require water pressure measurements and/or seepage calculations. It can be a first estimate of the water pressures. This method will be explained and compared with the results of the stochastic analysis in Chapter 6. For this reason, three waves are constructed with prescribed rules of thump for the simplification of peak flows (see figure 4-12) (van der Zaag, 2019). The peak is at $10.7\ m + \text{NAP}$ (MHW) (Van Middelkoop, et al., 2018). The waves are transformed to start day zero (see figure 4-13). In order to compare the effects of the wave types, all simulations are set to 55 days based on the long-term wave. Since the characteristic wave form stops at approximately $7{,}6\ m + \text{NAP}$, the last stage of the waves are set to $3{,}2\ m + \text{NAP}$ (polder water level winter) with an average fall (Van Middelkoop, et al., 2018). The reason is that the crown of the summer dike is at $7.0\ m + \text{NAP}$ and SEEP/W only can simulate seepage at a prescribed water level. In reality, the water that is enclosed in forelands will slowly infiltrate or drained by local land users after the peak flow. Therefore, in this study, it is assumed that the water drops to polder level instead of setting the water at an artificial level.

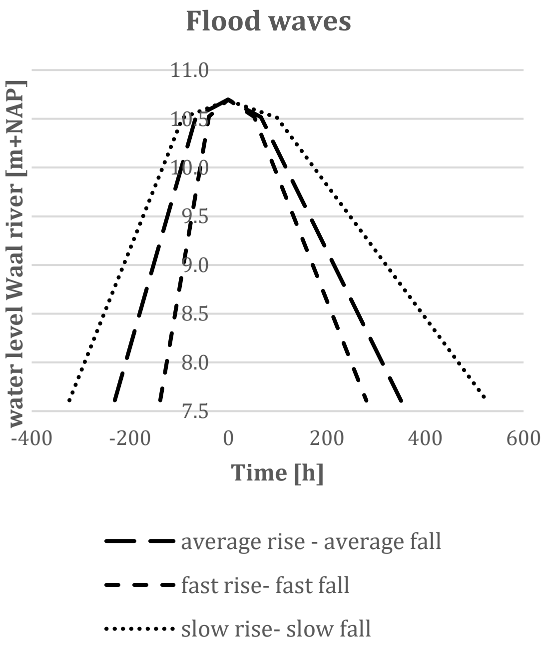


Figure 4-12 simplified flood waves with peak at $10.7\ m + \text{NAP}$ (van der Zaag, 2019).

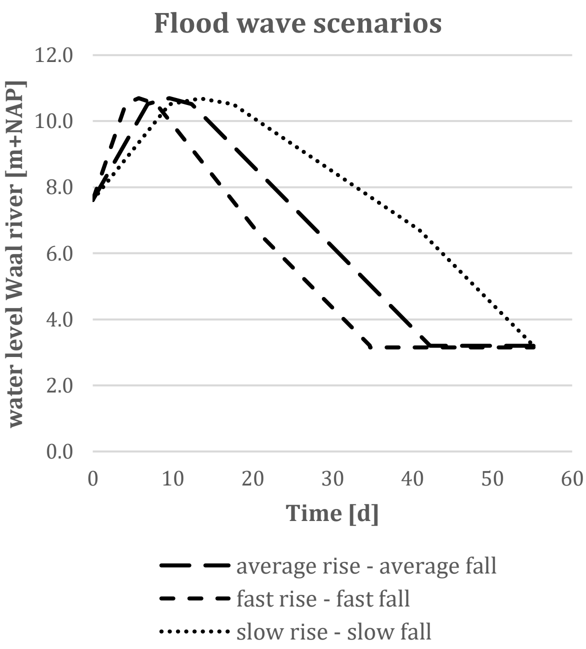


Figure 4-13 transformed flood wave scenarios with peak at $10.7\ m + \text{NAP}$. Duration: $t = 55$ days.

### 4.4.2 Monte Carlo Simulation cases

The Dike 1 & 2 are combined with the prescribed flood wave scenarios in the previous section. In total, nine different cases, each one investigating the variation effect of the hydraulic conductivity parameter on the location of the phreatic line and the differences in hydraulic head, are analyzed. The variation of the parameter depends on many soil properties i.e. grain size distribution, texture and water storage distribution, etc. By selecting coefficients of variation, it can be assumed that all possible degrees of variation are accounted for in the simulation. According to Çalamak (2014), the recommended coefficient of variation for the soil types is stated in the table below. Also, the cases considered for the analysis and their corresponding parameter statistics are shown in table 4-6. For example, for case 1 to 3 the hydraulic conductivity, $K_s$, is assumed to be random having a mean $0.0117\ m \cdot day^{-1}(1.354 \times 10^{-7}\ m \cdot s^{-1})$ and COV value of 1.35 while keeping the other parameters ( $\theta_r\ [-], \theta_s\ [-], \alpha\ [kPa^{-1},]$ n$[-]$) fixed at their mean values (see table B-1/4-1 in Appendix *Initiation geohydrological soil parameters).* Dike 2 is investigated for the random variable generation of the hydraulic conductivity for the clay cover layer (Case No. 1, 2 & 3) and the loamy sand core (Case No. 4, 5, 6, 7, 8 & 9) for the three prescribed flood wave scenarios.

| | | Case No. | Parameter | | Wavetype |
|---|---|---|---|---|---|
| | | | $\mu_{K_s}$ $[m/s]$ | COV | |
| Dike 1 (Light-weight clay) | | 1 | $1.354 \times 10^{-7}$ | 1.35 | fast rise – fast fall |
| | | 2 | $1.354 \times 10^{-7}$ | 1.35 | average rise – average fall |
| | | 3 | $1.354 \times 10^{-7}$ | 1.35 | slow rise – slow fall |
| Dike 2 | Light-weight clay | 4 | $1.354 \times 10^{-7}$ | 1.35 | fast rise – fast fall |
| | | 5 | $1.354 \times 10^{-7}$ | 1.35 | average rise – average fall |
| | | 6 | $1.354 \times 10^{-7}$ | 1.35 | slow rise – slow fall |
| | Loamy sand | 7 | $1.157 \times 10^{-5}$ | 0.04 | fast rise – fast fall |
| | | 8 | $1.157 \times 10^{-5}$ | 0.04 | average rise – average fall |
| | | 9 | $1.157 \times 10^{-5}$ | 0.04 | slow rise – slow fall |

Table 4-6 Cases considered for sensitivity analysis of transient seepage and corresponding statistical properties of soils. Reference coefficients of variation: (Çalamak, 2014) Reference hydraulic conductivity values: (Van Middelkoop, et al., 2018).

For each case, 250 transient seepage Monte Carlo Simulations are conducted stochastically. The determination of the number of simulations, using the Student-t test, can be found in Appendix C *Number of simulations*. In total, 2250 ($9 \times 250$) analyses are solved for wave types with a fast/average/slow rise and fast/average slow fall.

## CHAPTER 5

## RESULTS

*In this study, the sensitivity of the transient seepage is investigated with a series of analysis (i.e. different dike types and wave type scenarios) in which one selected parameter ($K$) is kept random varying while keeping the other hydraulic conductivity values of soil types at their mean value. This one-at-a-time sensitivity analysis enables to investigate the individual effect of each hydraulic conductivity parameter for different compositions of the dike core.*

### 5.1 Uncertainty based transient seepage analyses

For comparison purposes, the results of the MCS cases are statistically analyzed and visualized similarly. Therefore, a short description is given on how to interpret the results presentation.

Since the phreatic line is varying through the dike body for timestep $t$ $[days]$, the location of the phreatic line is statistically analyzed for sections located at $-18\ m, -12\ m, -6\ m, 0\ m, +3\ m, +4.5\ m, +6\ m$ and $+7.5\ m$ from crown, which enables to consider spatial variability. These sections are labeled as Section 1, Section 2, Section 3, Section 4, Section 5, Section 6, Section 7, Section 8, respectively from inner toe to outer toe (see figure 4-10 and 4-11). Also the phreatic lines are derived for three time steps of the total simulation duration: one around the peak ($t = 10\ days$), one from the intermediate state ($t = 30\ days$) and another from the final state ($t = 55\ days$), which corresponds to 19%, 55% and 100% fo the total simulation duration.

The results of the simulation are given in box-plots which enables to quickly compare the spatial variation of the phreatic line and also the comparison between wave types for a certain timestep. The statistical properties box-plots present are the median (line inside the box), first and third quartiles (lower and upper line in the box, respectively), and minimum and maximum (lower and upper extends, respectively). Box-plots also show the spread and symmetry of its distribution. It's known as a relatively simple visual method to interpret data (Williamson, et al., 1989). The location of the phreatic line for the deterministic hydraulic conductivity value is highlighted in blue in the box-plots and histograms if and only the deterministic output value is within the probability distribution of a section.

Besides the visual comparison, the properties of the phreatic line need to be defined in terms of statistical four moments i.e. mean, variance, kurtosis, and skewness. Also, the probability distribution type must be determined. These properties can be used when dealing with the uncertainty of the location of the phreatic line for a dike core composition and wave type. The application of these statistical properties is described in Chapter 6

To this end, the frequency histograms of the phreatic line are derived and probability distributions are fitted to the data set of each spatial section. For complexity reasons, the data sets are all fitted for the gamma distribution i.e. a two-parameter family of continuous probability distribution which is one of the commonly used functions engineering (e.g. describing cohesion and shear strength) to model continuous variables that have always skewed distributions. The probability density function in the shape-rate parametrization is:

$$f(x; \alpha', \beta) = \frac{\beta^{\alpha'} x^{\alpha' - 1} e^{-\beta z_p}}{\Gamma(\alpha')} \quad \text{for} \quad x > 0 \ \ \alpha', \beta > 0 \quad \text{with} \quad \alpha' = \frac{\mathrm{E[X]}}{\beta}, \qquad \beta = \frac{\mathrm{E[X]}}{Var(\mathrm{X})} \tag{5.1}$$

Where $\Gamma(\alpha')$ is the gamma distribution, $\alpha'$ the scale parameter and $\beta$ the rate parameter, E[X] the mean and $Var$(X) the variance of the data set.

The validity of the gamma distribution is verified using a common goodness of fit test: Chi-square test. The test compares the observed frequencies with the obtained ones from the probability distribution. The following formula is used (Ang & Tang, 1975):

$$X^2 = \sum_{i=1}^{k} \frac{(O_i - E_i)^2}{E_i}$$

[5.2]

Where, $k$ is the number of intervals (bins) used, $O_i$ $[-]$ the observed frequency and $E_i[-]$ the expected frequency for the tested probability function for interval number $i$. The hypothesis will be rejected if the Chi-square sum is greater than the critical value at the chosen significance level which is 5% in this study. The test results are used for estimating the location of the phreatic surface e.g. with 95% certainty [2].

The following part of this report contains the descriptive statistics including the range (minimum and maximum), the four moments i.e. mean, standard deviations, kurtosis, and skewness. These are listed in tables (see table 5-3, 5-4 & 5-5 / and also in Appendix D-1 *Results SEEP/W simulations* table D-1, D-2 & D-3). For each case, a box-plot is constructed having a fixed $y$ -axis per case in order to compare the results visually. Also, per section, a frequency histogram with corresponding gamma distribution plot is given. For sections with no phreatic lines or two-times crossing lines (i.e. two water tables at one section), the PDFs and corresponding skewness and kurtosis are not computed.

For example, Dike 1 Case 2 is shown in figure 5-1 with its results of the SEEP/W – color shading drawings (pressure head) and the stochastic spectrum of all 250 phreatic line locations compared to the deterministic phreatic line. Also, the histograms are and the corresponding box-plot of Dike 1 Case 2, timestep 30 days, are stated in table 5-2. The results of all cases considered for this sensitivity analyses of the hydraulic conductivity are given in Appendix D-1 *Results SEEP/W simulations.* An overview of the case scenarios and results presentation is given in table 5-1:

[2] In this study, also the rejected distributions are used for further application in Chapter 6. However, there is no 95% certainty for estimating the possible locations for the phreatic line.

| | | Case No. | Parameter | | Wavetype | Results |
|---|---|---|---|---|---|---|
| | | | $\mu_{K_s}$ $[m/s]$ | COV | | Appendix D-1 |
| Dike 1 (Light-weight clay) | | 1 | $1.354 \times 10^{-7}$ | 1.35 | fast rise – fast fall | Page 2’-21’ |
| | | 2 | $1.354 \times 10^{-7}$ | 1.35 | average rise – average fall | |
| | | 3 | $1.354 \times 10^{-7}$ | 1.35 | slow rise – slow fall | |
| Dike 2 | Light-weight clay | 4 | $1.354 \times 10^{-7}$ | 1.35 | fast rise – fast fall | Page 22’-41’ |
| | | 5 | $1.354 \times 10^{-7}$ | 1.35 | average rise – average fall | |
| | | 6 | $1.354 \times 10^{-7}$ | 1.35 | slow rise – slow fall | |
| | Loamy sand | 7 | $1.157 \times 10^{-5}$ | 0.04 | fast rise – fast fall | Page 42’-61’ |
| | | 8 | $1.157 \times 10^{-5}$ | 0.04 | average rise – average fall | |
| | | 9 | $1.157 \times 10^{-5}$ | 0.04 | slow rise – slow fall | |

Table 5-1 Cases considered for sensitivity analysis of transient seepage and corresponding statistical properties of soils. Reference coefficients of variation: (Çalamak, 2014) Reference hydraulic conductivity values: (Van Middelkoop, et al., 2018).

Before describing the results per Dike and Case, some similar patterns are observed for multiple cases:

- The descriptive statistics of tables 5-3, 5-4 & 5-5 showed that the probability distributions of the location of the phreatic line are always skewed negatively (i.e. skewed to the top) or positively (i.e. skewed to the downside). Also the distributions are platykurtic (i.e. kurtosis $< 0$) or leptokurtic (i.e. kurtosis $> 0$) in some degree. Most of the distributions are positively skewed. It can be said that there is no relation between skewness, kurtosis and time.
- The box-plots of figure 5-3, 5-4 & 5-5 showed that for all cases at timestep $t = 10\ days$ the phreatic line is approximately at the same height and significant higher at the outward slope side. This effect is significant stronger for Dike 1 (higher hydraulic conductivity).
- The box-plots of figure 5-3, 5-4 & 5-5 showed that for cases 1-6 the deterministic value is mostly inside one of the tales of the distribution and not inside the box from the first to the third quartile (i.e. equal to 50% of the distribution). At timestep $t = 10\ days$, the deterministic value is in the upper tale whereas the box is at a lower level. After $t = \pm 30\ days$ this observation is reversed i.e. the deterministic value starts to ‘move’ to the lower tale of the box-plot (see $t = 55\ days$) .
- From figure 5-1 can be obtained that the pressure head is related to the outer water level and decreases when the water level drops. However, figures 5-1 ($t = 55\ days$), D-14, D-16 D-18 (for example) show that a residual pressure head remains in the dike core even though the phreatic line drops. An underpressure occurs in the dike cover layers and aquifer whereas the dike core starts to behave as a pressure source i.e. the pressure head is kept in a local ‘bubble’ above the phreatic line at the outward slope side. The ‘bubble’ is much more extended towards the inner toe and has a higher local pressure head as the duration of the flood wave increases and thus the inflow time is higher.

**Example results presentation: Dike 1, Case 2** Figure 5-1 (left side: deterministic phreatic line and color shading pressure head. The interface of SEEP/W simulation. Right side: stochastic spectrum of possible locations of all 250 phreatic line (with random hydraulic conductivity value) compared to the deterministic phreatic line. Boundary spectrum (in yellow) created with AutoCAD).

$t = 10\ days$

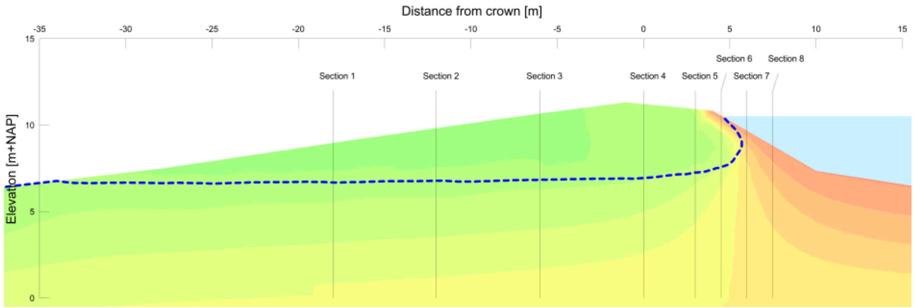


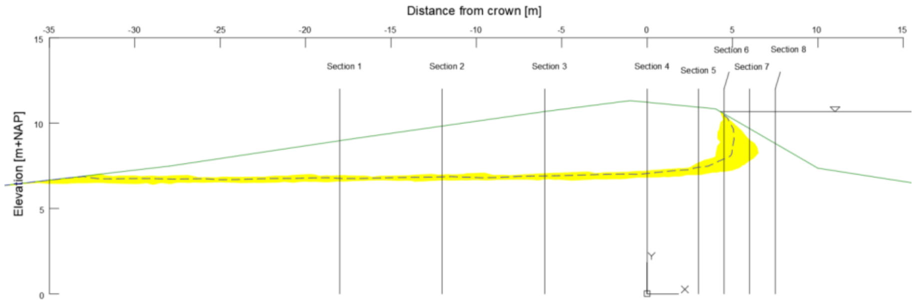


$t = 30\ days$

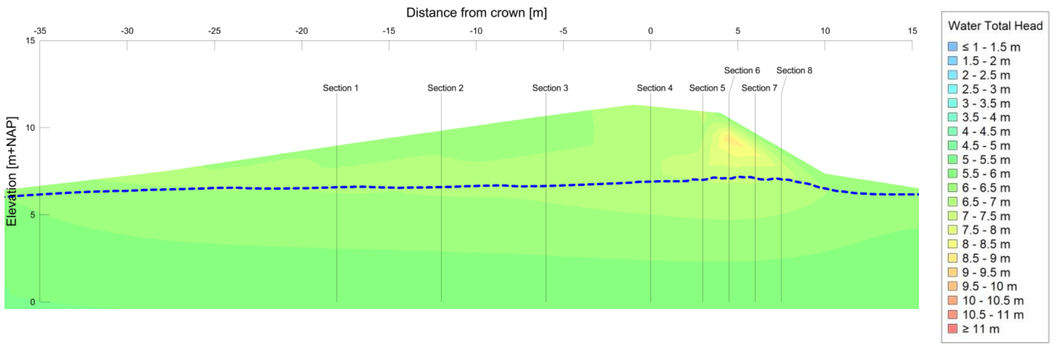


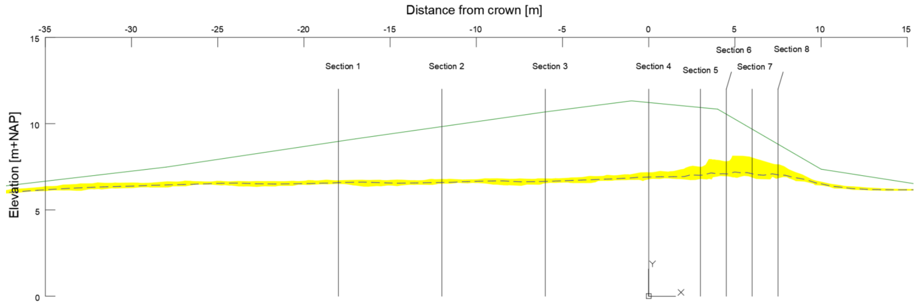


$t = 55\ days$

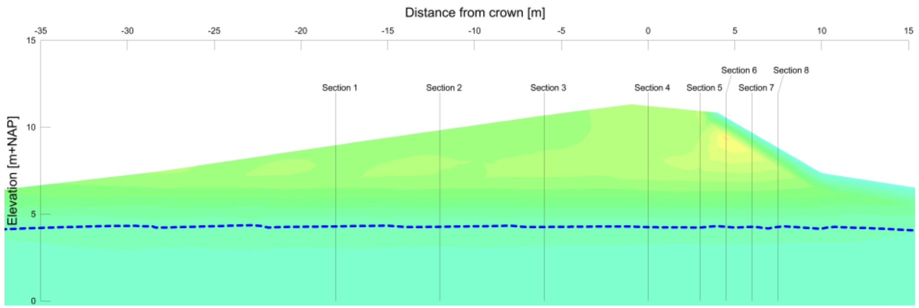


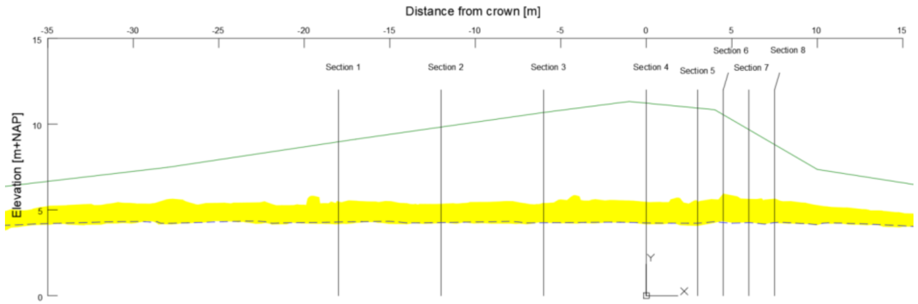

For the stochastic spectrum in figure 5-2, at the Sections of interest, an intersection is made in AutoCAD to retrieve the 250 elevation coordinates of the phreatic lines. These coordinates are statistically analyzed and visualized in histograms and box-plots (see table 5-1)

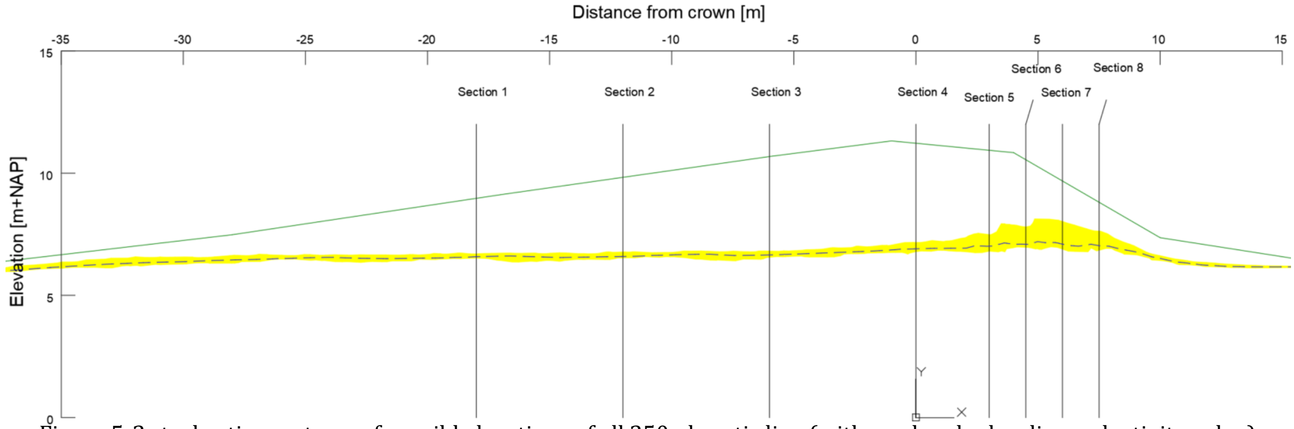


Figure 5-2 stochastic spectrum of possible locations of all 250 phreatic line (with random hydraulic conductivity value) compared to the deterministic phreatic line. Boundary spectrum (in yellow) created with AutoCAD).

| Section 1 | | Section 2 | | Section 3 | | Section 4 | |
|---|---|---|---|---|---|---|---|
| PDF type: | Gamma | PDF type: | Gamma | PDF type: | Gamma | PDF type: | Gamma |
| Decision: | Accept | Decision: | Accept | Decision: | Accept | Decision: | Reject |
| 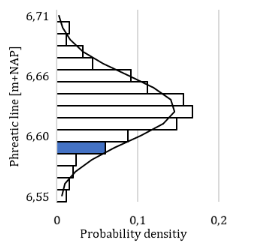 | | 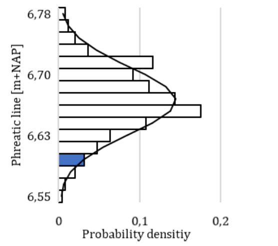 | | 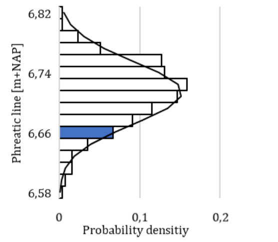 | | 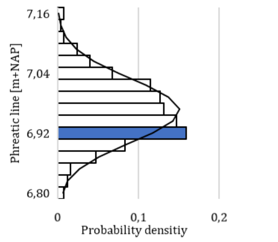 | |
| **Section 5** | | **Section 6** | | **Section 7** | | **Section 8** | |
| PDF type: | Gamma | PDF type: | Gamma | PDF type: | Gamma | PDF type: | Gamma |
| Decision: | Accept | Decision: | Reject | Decision: | Accept | Decision: | Accept |
| 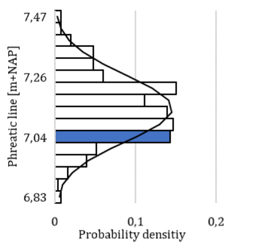 | | 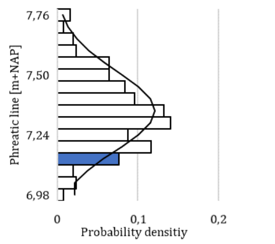 | | 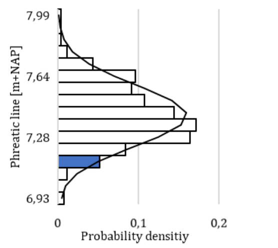 | | 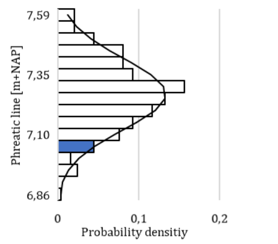 | |

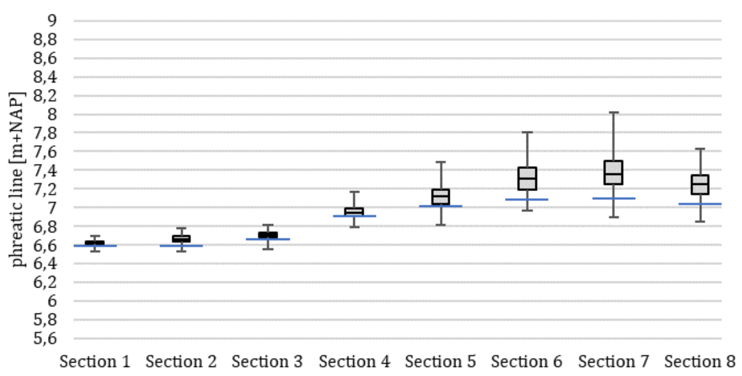


Table 5-2 Histograms of elevation coordinate of the phreatic lines. Deterministic value is highlighted in blue if it's within the probability density interval. Accept means that the gamma distribution function fits the distribution for at least 95%. Box-plots visualize the four statistical moments and the spatial comparison of the variation of the phreatic line along the dike.

### 5.1.1 Dike 1, Case 1-3

| Times | Case No. | Sect. | Max $(z)$ | Min $(z)$ | $\mu$ $(z)$ | $\sigma$ $(z)$ | Skewness | Kurtosis | Chi-square $(X^2)$ $\alpha' = 0.05$ |
|---|---|---|---|---|---|---|---|---|---|
| | | | $[m + NAP]$ | | | | | | Decision |
| $t = 10$ $days$ | 1 | 1 | 6.94 | 6.56 | 6.75 | 0.07 | 0.59 | 0.11 | Reject |
| | | 2 | 6.97 | 6.68 | 6.83 | 0.06 | -0.10 | -0.64 | Accept |
| | | 3 | 7.02 | 6.74 | 6.88 | 0.05 | 0.01 | -0.13 | Accept |
| | | 4 | 7.23 | 6.84 | 7.01 | 0.08 | 0.43 | -0.48 | Reject |
| | | 5 | 7.76 | 6.93 | 7.35 | 0.13 | 0.08 | 0.79 | Accept |
| | | 6 | 0.00 | 0.00 | 0.00 | 0.00 | - | - | - |
| | | 7 | 0.00 | 0.00 | 0.00 | 0.00 | - | - | - |
| | | 8 | 0.00 | 0.00 | 0.00 | 0.00 | - | - | - |
| $t = 10$ $days$ | 2 | 1 | 6.93 | 6.59 | 6.73 | 0.06 | 0.73 | 0.60 | Accept |
| | | 2 | 6.97 | 6.66 | 6.80 | 0.06 | 0.11 | -0.25 | Accept |
| | | 3 | 7.05 | 6.72 | 6.86 | 0.06 | 0.32 | -0.10 | Accept |
| | | 4 | 7.20 | 6.83 | 6.98 | 0.06 | 0.89 | 0.96 | Reject |
| | | 5 | 7.67 | 6.98 | 7.27 | 0.13 | -0.21 | -0.46 | Reject |
| | | 6 | 0.00 | 0.00 | 0.00 | 0.00 | - | - | - |
| | | 7 | 0.00 | 0.00 | 0.00 | 0.00 | - | - | - |
| | | 8 | 0.00 | 0.00 | 0.00 | 0.00 | - | - | - |
| $t = 10$ $days$ | 3 | 1 | 6.85 | 6.59 | 6.67 | 0.04 | 0.77 | 1.07 | Reject |
| | | 2 | 6.91 | 6.62 | 6.74 | 0.06 | 0.33 | -0.20 | Accept |
| | | 3 | 7.00 | 6.66 | 6.80 | 0.06 | 0.27 | 0.09 | Accept |
| | | 4 | 7.07 | 6.79 | 6.91 | 0.05 | 0.55 | 0.50 | Reject |
| | | 5 | 7.41 | 6.90 | 7.14 | 0.11 | 0.47 | -0.43 | Reject |
| | | 6 | 8.07 | 7.13 | 7.45 | 0.17 | 1.08 | 1.42 | Reject |
| | | 7 | 0.00 | 0.00 | 0.00 | 0.00 | - | - | - |
| | | 8 | 0.00 | 0.00 | 0.00 | 0.00 | - | - | - |
| $t = 30$ $days$ | 1 | 1 | 6.32 | 5.87 | 6.04 | 0.14 | -0.13 | -0.84 | Accept |
| | | 2 | 6.37 | 5.67 | 6.12 | 0.14 | -0.82 | 0.34 | Reject |
| | | 3 | 6.42 | 5.63 | 6.16 | 0.13 | -1.06 | 1.99 | Reject |
| | | 4 | 6.66 | 5.66 | 6.25 | 0.17 | 0.01 | 0.14 | Accept |
| | | 5 | 6.99 | 5.63 | 6.43 | 0.19 | -0.63 | 1.50 | Reject |
| | | 6 | 7.26 | 5.74 | 6.48 | 0.25 | -0.62 | 0.93 | Reject |
| | | 7 | 7.10 | 5.89 | 6.44 | 0.26 | -0.04 | -1.04 | Reject |
| | | 8 | 7.05 | 5.81 | 6.36 | 0.20 | 0.41 | 0.59 | Accept |
| $t = 30$ $days$ | 2 | 1 | 6.70 | 6.52 | 6.62 | 0.03 | -0.25 | 0.78 | Accept |
| | | 2 | 6.78 | 6.53 | 6.66 | 0.04 | -0.09 | 0.09 | Accept |
| | | 3 | 6.81 | 6.56 | 6.70 | 0.04 | -0.47 | 0.28 | Accept |
| | | 4 | 7.17 | 6.79 | 6.95 | 0.06 | 0.32 | 0.37 | Reject |
| | | 5 | 7.49 | 6.81 | 7.12 | 0.12 | 0.23 | 0.18 | Accept |
| | | 6 | 7.80 | 6.97 | 7.32 | 0.17 | 0.53 | 0.17 | Reject |
| | | 7 | 8.02 | 6.89 | 7.38 | 0.17 | 0.34 | 0.27 | Accept |
| | | 8 | 7.63 | 6.85 | 7.25 | 0.15 | 0.01 | -0.17 | Accept |
| $t = 30$ $days$ | 3 | 1 | 7.05 | 6.82 | 6.98 | 0.04 | -1.26 | 2.57 | Reject |
| | | 2 | 7.13 | 6.87 | 6.98 | 0.04 | 0.11 | 0.65 | Accept |
| | | 3 | 7.19 | 6.89 | 7.04 | 0.06 | 0.12 | -0.31 | Accept |
| | | 4 | 7.46 | 7.18 | 7.31 | 0.05 | 0.42 | 0.44 | Accept |
| | | 5 | 8.28 | 7.37 | 7.71 | 0.18 | 0.52 | -0.10 | Reject |
| | | 6 | 8.93 | 7.53 | 8.24 | 0.20 | 0.37 | 1.60 | Reject |
| | | 7 | 8.68 | 8.16 | 8.48 | 0.09 | -0.66 | 0.02 | Reject |
| | | 8 | 8.48 | 8.33 | 8.44 | 0.03 | -1.19 | 1.48 | Reject |
| $t = 55$ $days$ | 1 | 1 | 5.09 | 3.95 | 4.43 | 0.17 | 0.54 | 1.76 | Accept |
| | | 2 | 5.08 | 3.99 | 4.45 | 0.18 | 0.68 | 1.26 | Reject |
| | | 3 | 5.15 | 4.02 | 4.43 | 0.18 | 0.89 | 1.67 | Reject |
| | | 4 | 5.08 | 3.94 | 4.42 | 0.21 | 0.82 | 0.83 | Reject |
| | | 5 | 5.21 | 3.85 | 4.46 | 0.27 | 0.79 | 0.01 | Reject |
| | | 6 | 5.18 | 3.67 | 4.45 | 0.23 | 0.76 | 1.47 | Reject |
| | | 7 | 5.37 | 3.67 | 4.44 | 0.22 | 1.11 | 3.31 | Reject |
| | | 8 | 5.12 | 3.74 | 4.42 | 0.21 | 0.43 | 1.21 | Reject |
| $t = 55$ $days$ | 2 | 1 | 5.48 | 4.19 | 4.72 | 0.24 | 0.60 | -0.05 | Reject |
| | | 2 | 5.34 | 4.24 | 4.73 | 0.24 | 0.36 | -0.89 | Reject |
| | | 3 | 5.38 | 4.27 | 4.77 | 0.26 | 0.16 | -0.98 | Reject |
| | | 4 | 5.46 | 4.17 | 4.74 | 0.27 | 0.22 | -0.95 | Reject |
| | | 5 | 5.49 | 4.08 | 4.74 | 0.28 | 0.19 | -0.80 | Reject |
| | | 6 | 5.94 | 4.35 | 4.74 | 0.25 | 0.91 | 1.34 | Reject |
| | | 7 | 5.63 | 4.28 | 4.71 | 0.27 | 0.88 | 0.33 | Reject |
| | | 8 | 5.64 | 4.26 | 4.72 | 0.26 | 0.96 | 0.70 | Reject |
| $t = 55$ $days$ | 3 | 1 | 6.26 | 4.82 | 5.67 | 0.19 | -0.45 | 2.05 | Reject |
| | | 2 | 6.18 | 4.73 | 5.70 | 0.21 | -0.37 | 1.39 | Reject |
| | | 3 | 6.32 | 5.24 | 5.70 | 0.24 | 0.33 | -0.67 | Reject |
| | | 4 | 6.33 | 5.11 | 5.70 | 0.27 | 0.15 | -0.90 | Reject |
| | | 5 | 6.59 | 5.02 | 5.79 | 0.31 | 0.22 | -0.63 | Reject |
| | | 6 | 6.84 | 4.74 | 5.82 | 0.32 | 0.13 | 0.73 | Reject |
| | | 7 | 6.67 | 4.78 | 5.79 | 0.29 | 0.01 | 1.22 | Reject |
| | | 8 | 6.88 | 4.87 | 5.76 | 0.32 | -0.30 | 0.94 | Reject |

Table 5-3 The descriptive statistics of the phreatic line for Dike 1, Case 1 to Case 3.

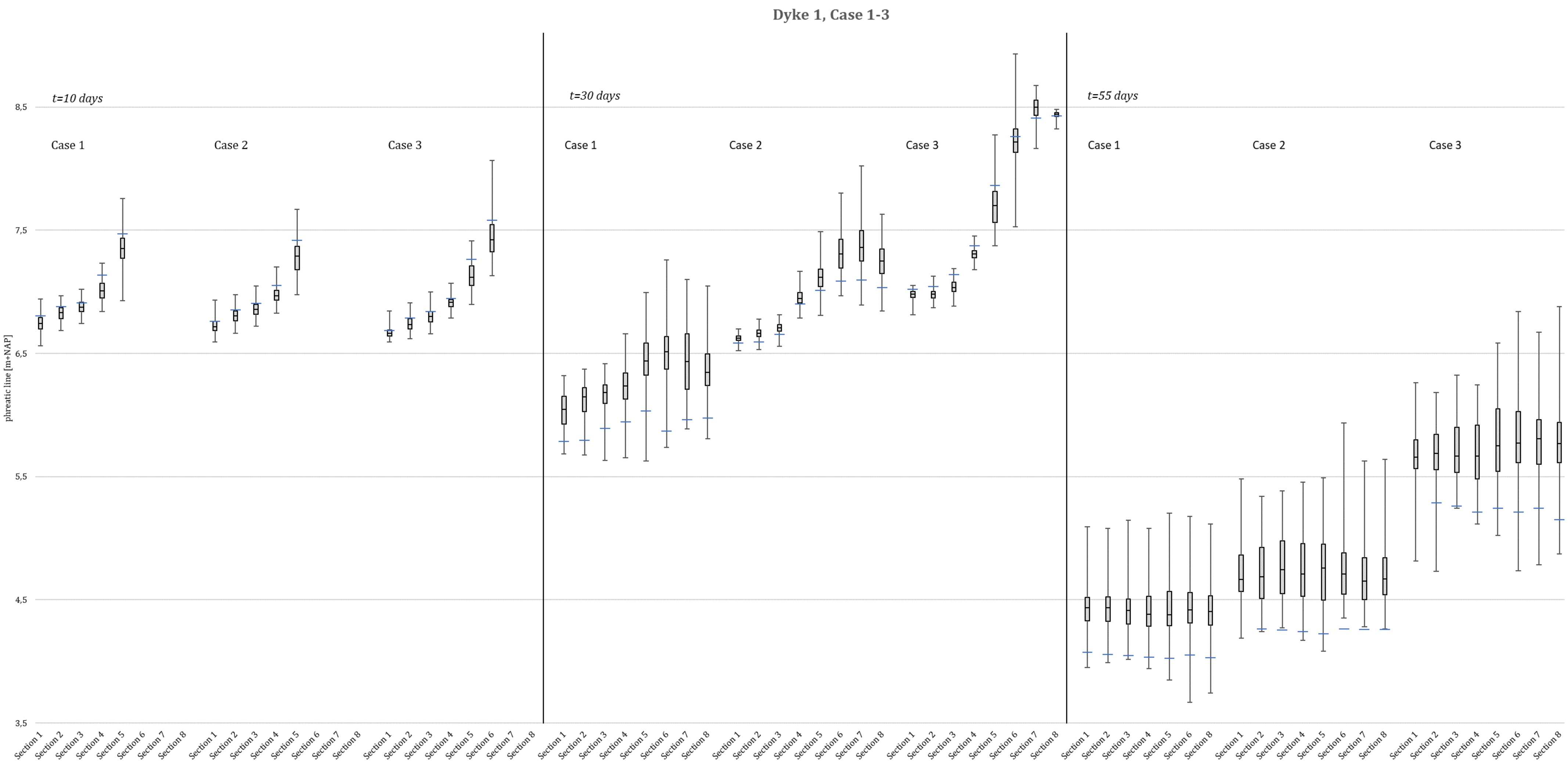


Figure 5-3 The box-plots of the phreatic line for Case 1 to Case 3

For dike type 1, case 1-3, the variation of hydraulic conductivity is found to have a crucial effect on transient seepage.

At $t = 10\,days$, figures D-2 – D-7, the phreatic line is approximately at the same height. The standard deviations are relatively small but are significant higher at the outward slope side of the dike where the water flows in.

At $t = 30\,days$, figures D-8 – D-13, the variation in case 1 is more spread out from the outward to inwarthe d slope. For case 1, the standard deviations at each location are overall higher than in case 2 and 3. The reason is that the outer water level is dropping faster than in Case 2 and 3, resulting in a relative quick response time of the pressure head in the aquifer. This leads to a decrease in pressure head alongside the aquifer under the phreatic line. Therefore, the phreatic line is dropping alongside the width of dike the at each Section. Since the outer water is dropping slower for the Case 2 and 3, the pressure head is also responding relatively slow, causing more local variation in the phreatic line towards the inflow side. Especially, Case 3 showed a local variation at Section 6 of $\Delta z_p = \pm 1.40m$. The phreatic line more towards the inflow side can respond on the dropping water level, but due to a relative high hydraulic conductivity, more inside the dike, the phreatic line cannot respond that quickly. This is causing a peak in the phreatic line (see Case 2 and 3). Therefore, the shape of the phreatic line is related to the duration of the flood wave and the peak of the phreatic line is significant higher (i.e. more bulged) when the duration of the flood wave increases.

At $t = 55\,days$, D-14 – D-19, the local variations is spread out but the peaks are less visible i.e. the phreatic line is almost flat. Even though the water has dropped to polder water level at $3.2m +$ NAP for all 3 cases, the difference between the phreatic lines of Case 1 and 3 is $\Delta z_p = \pm 1.30m$. The standard deviations between the cases do not differ much, but are relative high when comparing to previous timesteps. The local variation at Section 6 for case 3 is $\Delta z_p = \pm 2.10m$.

At the start of the simulation, the deterministic value is in the upper tale whereas the box is at a lower level. However, after $30\,days$, the stochastic simulation results are at higher levels, especially in case 1. At $t = 55\,days$ the center of gravity of the probability distributions are much higher and can differ $0.90 - 1.60m$ from the maximum. The chance these high phreatic lines occur is extremely small but cannot be excluded.

## 5.1.2 Dike 2, Case 4-6

| Times | Case No. | Sect. | Max $(z)$ | Min $(z)$ | $\mu$ $(z)$ | $\sigma$ $(z)$ | Skewness | Kurtosis | Chi-square $(X^2)$ $\alpha' = 0.05$ |
|---|---|---|---|---|---|---|---|---|---|
| | | | $[m + NAP]$ | | | | | | Decision |
| $t = 10$ $days$ | 4 | 1 | 7.35 | 6.97 | 7.22 | 0.07 | -0.67 | 0.07 | Reject |
| | | 2 | 7.43 | 7.03 | 7.23 | 0.07 | -0.20 | -0.03 | Accept |
| | | 3 | 7.48 | 7.12 | 7.30 | 0.07 | -0.14 | -0.27 | Accept |
| | | 4 | 7.60 | 7.27 | 7.44 | 0.07 | -0.18 | -0.39 | Accept |
| | | 5 | 7.69 | 7.35 | 7.52 | 0.07 | -0.13 | -0.35 | Accept |
| | | 6 | - | - | - | - | - | - | - |
| | | 7 | - | - | - | - | - | - | - |
| | | 8 | - | - | - | - | - | - | - |
| $t = 10$ $days$ | 5 | 1 | 7.34 | 6.92 | 7.18 | 0.08 | -0.16 | -0.24 | Accept |
| | | 2 | 7.36 | 6.95 | 7.17 | 0.07 | 0.22 | 0.31 | Accept |
| | | 3 | 7.43 | 7.04 | 7.24 | 0.06 | 0.35 | 0.26 | Accept |
| | | 4 | 7.60 | 7.20 | 7.40 | 0.07 | 0.20 | 0.15 | Accept |
| | | 5 | 7.71 | 7.28 | 7.50 | 0.07 | 0.18 | 0.25 | Accept |
| | | 6 | - | - | - | - | - | - | - |
| | | 7 | - | - | - | - | - | - | - |
| | | 8 | - | - | - | - | - | - | - |
| $t = 10$ $days$ | 6 | 1 | 7.24 | 6.82 | 7.02 | 0.07 | 0.35 | 0.21 | Accept |
| | | 2 | 7.17 | 6.85 | 7.01 | 0.06 | 0.30 | -0.02 | Accept |
| | | 3 | 7.23 | 6.95 | 7.09 | 0.05 | 0.34 | 0.00 | Reject |
| | | 4 | 7.42 | 7.09 | 7.23 | 0.06 | 0.53 | 0.32 | Accept |
| | | 5 | 7.53 | 7.18 | 7.32 | 0.06 | 0.53 | 0.16 | Accept |
| | | 6 | 7.60 | 7.24 | 7.38 | 0.07 | 0.46 | 0.20 | Accept |
| | | 7 | - | - | - | - | - | - | - |
| | | 8 | - | - | - | - | - | - | - |
| $t = 30$ $days$ | 4 | 1 | 6.17 | 5.82 | 6.01 | 0.07 | 0.02 | 0.01 | Accept |
| | | 2 | 6.26 | 5.86 | 6.08 | 0.07 | -0.18 | 0.11 | Accept |
| | | 3 | 6.27 | 5.83 | 6.09 | 0.08 | -0.39 | 0.16 | Accept |
| | | 4 | 6.22 | 5.77 | 6.04 | 0.08 | -0.46 | 0.31 | Reject |
| | | 5 | 6.19 | 5.73 | 5.99 | 0.08 | -0.47 | 0.46 | Accept |
| | | 6 | 6.17 | 5.68 | 5.96 | 0.09 | -0.61 | 0.57 | Accept |
| | | 7 | 6.12 | 5.65 | 5.91 | 0.08 | -0.50 | 0.59 | Reject |
| | | 8 | 6.08 | 5.60 | 5.87 | 0.09 | -0.58 | 0.70 | Reject |
| $t = 30$ $days$ | 5 | 1 | 6.76 | 6.54 | 6.66 | 0.04 | -0.27 | -0.05 | Accept |
| | | 2 | 6.87 | 6.67 | 6.77 | 0.04 | -0.12 | -0.26 | Accept |
| | | 3 | 6.93 | 6.69 | 6.80 | 0.04 | -0.09 | -0.08 | Accept |
| | | 4 | 6.93 | 6.63 | 6.79 | 0.05 | -0.32 | 0.23 | Accept |
| | | 5 | 6.90 | 6.58 | 6.75 | 0.05 | -0.34 | 0.16 | Accept |
| | | 6 | 6.88 | 6.56 | 6.73 | 0.05 | -0.44 | 0.31 | Reject |
| | | 7 | 6.85 | 6.53 | 6.70 | 0.05 | -0.43 | 0.32 | Accept |
| | | 8 | 7.16 | 6.53 | 6.87 | 0.12 | -0.11 | 0.04 | Accept |
| $t = 30$ $days$ | 6 | 1 | 7.52 | 7.25 | 7.36 | 0.05 | 0.48 | -0.06 | Reject |
| | | 2 | 7.61 | 7.36 | 7.48 | 0.04 | -0.11 | -0.10 | Accept |
| | | 3 | 7.70 | 7.44 | 7.56 | 0.04 | 0.01 | -0.10 | Accept |
| | | 4 | 7.76 | 7.49 | 7.60 | 0.04 | 0.20 | 0.01 | Accept |
| | | 5 | 7.77 | 7.51 | 7.62 | 0.04 | 0.21 | 0.01 | Accept |
| | | 6 | 7.77 | 7.51 | 7.62 | 0.04 | 0.23 | 0.08 | Accept |
| | | 7 | 8.60 | 7.59 | 7.96 | 0.21 | 1.10 | 0.75 | Reject |
| | | 8 | 8.85 | 7.78 | 8.24 | 0.13 | -0.72 | 0.36 | Reject |
| $t = 55$ $days$ | 4 | 1 | 4.85 | 4.19 | 4.52 | 0.12 | 0.16 | -0.08 | Accept |
| | | 2 | 4.88 | 4.18 | 4.53 | 0.13 | 0.09 | 0.00 | Accept |
| | | 3 | 4.86 | 4.13 | 4.49 | 0.12 | 0.05 | 0.11 | Accept |
| | | 4 | 4.80 | 4.06 | 4.43 | 0.12 | 0.03 | 0.08 | Accept |
| | | 5 | 4.77 | 4.03 | 4.39 | 0.13 | -0.04 | -0.01 | Accept |
| | | 6 | 4.76 | 4.01 | 4.37 | 0.12 | -0.05 | 0.08 | Accept |
| | | 7 | 4.73 | 4.00 | 4.35 | 0.12 | -0.09 | 0.10 | Accept |
| | | 8 | 4.71 | 3.97 | 4.33 | 0.13 | -0.11 | 0.10 | Accept |
| $t = 55$ $days$ | 5 | 1 | 5.15 | 4.44 | 4.81 | 0.12 | -0.33 | 0.29 | Accept |
| | | 2 | 5.52 | 4.46 | 4.82 | 0.13 | -0.19 | 0.11 | Accept |
| | | 3 | 5.14 | 4.42 | 4.78 | 0.14 | -0.11 | -0.08 | Accept |
| | | 4 | 5.10 | 4.30 | 4.71 | 0.15 | -0.21 | -0.03 | Reject |
| | | 5 | 5.06 | 4.24 | 4.67 | 0.15 | -0.24 | 0.05 | Accept |
| | | 6 | 5.04 | 4.22 | 4.65 | 0.15 | -0.27 | -0.03 | Accept |
| | | 7 | 5.02 | 4.19 | 4.62 | 0.15 | -0.26 | 0.01 | Accept |
| | | 8 | 4.98 | 4.15 | 4.59 | 0.15 | -0.32 | 0.06 | Accept |
| $t = 55$ $days$ | 6 | 1 | 5.82 | 5.30 | 5.60 | 0.09 | -0.42 | 0.09 | Accept |
| | | 2 | 5.86 | 5.34 | 5.66 | 0.10 | -0.58 | 0.19 | Reject |
| | | 3 | 5.86 | 5.30 | 5.63 | 0.11 | -0.69 | 0.53 | Reject |
| | | 4 | 5.81 | 5.15 | 5.55 | 0.12 | -0.68 | 0.49 | Reject |
| | | 5 | 5.76 | 5.10 | 5.49 | 0.12 | -0.55 | 0.31 | Reject |
| | | 6 | 5.72 | 5.08 | 5.46 | 0.12 | -0.57 | 0.35 | Reject |
| | | 7 | 5.69 | 5.04 | 5.42 | 0.12 | -0.54 | 0.19 | Reject |
| | | 8 | 5.64 | 4.98 | 5.38 | 0.13 | -0.51 | 0.05 | Reject |

Table 5-4 The descriptive statistics of the phreatic line for Dike 2, Case 4 to Case 6.

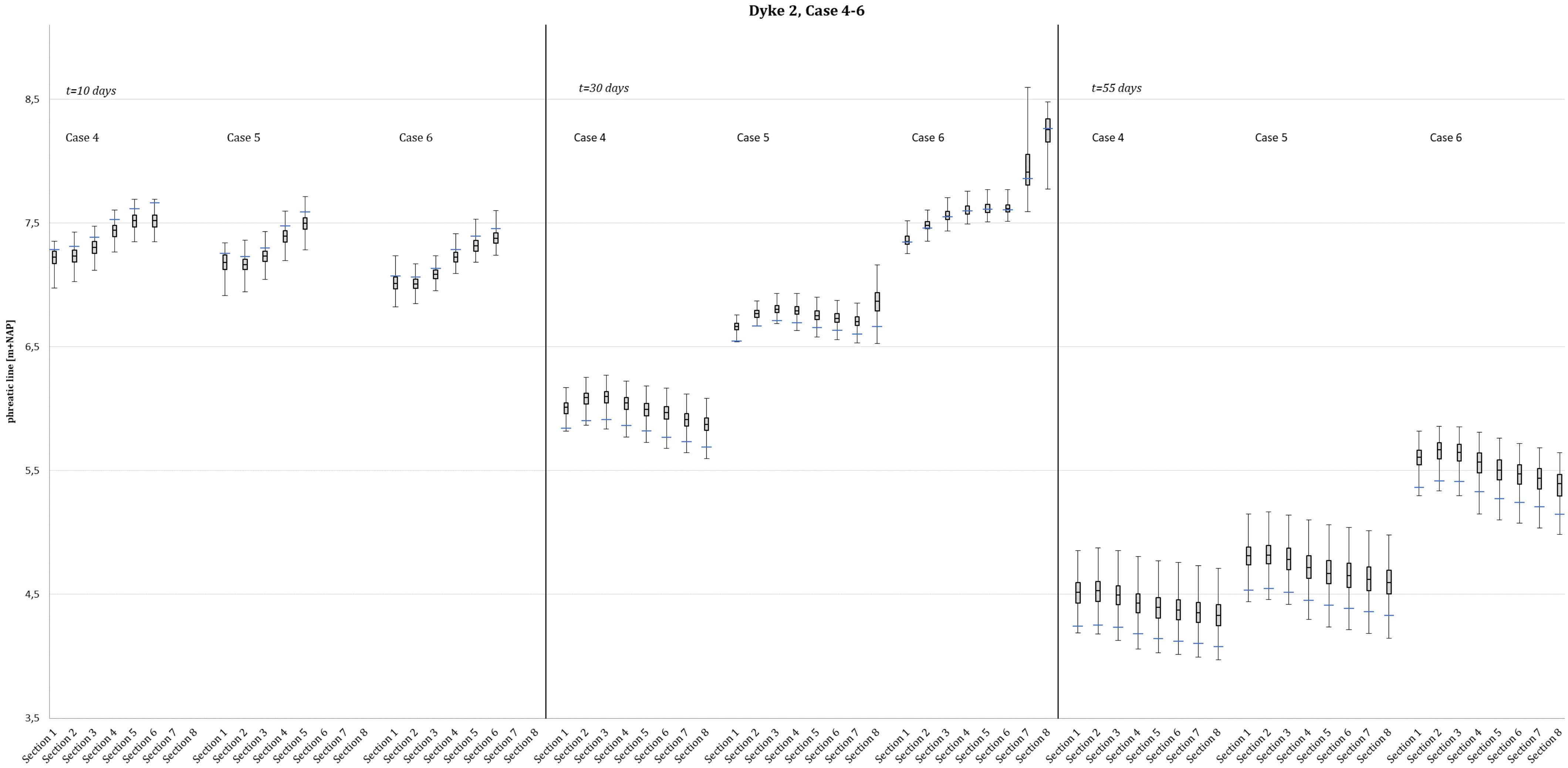


Figure 5-4 The box-plots of the phreatic line for Case 4 to Case 6

For dike type 2, case 4-6, the variation of hydraulic conductivity is found to have a significant effect on transient seepage. Hereby, the hydraulic conductivity of the light-weighted clay layer on top of the sand core is considered to be random.

At $t = 10\ days$, figures D-21 – D-26, the location of the phreatic line is significant higher at the outward slope side of the dike where the water flows in, but the variation is spread evenly throughout the dike core. Figures D-22, D-24 & D-26 show the variation of the phreatic line at the point of inflow but due to double intersections this, area cannot be analyzed statistically. The standard deviations are relatively small but do not converge towards to dike toe which is the case with a fully core out of light-weighted clay. Once the water flows into the sand core, the phreatic line does not fluctuate much i.e. the deviation does not decrease towards the dike toe. The variation effect caused by the randomness in the hydraulic conductivity of the clay layer is hardly reduced by the sand core alongside the width of the dike.

At $t = 30\ days$, figures D-27 - D-32, the variation in case 4 is more spread out from outward to inward slope. The standard deviations at each section are on average higher than in case 5 and case 6 (except Section 8, case 5; Section 7 & 8, case 6), which was also obtained in case 2 and case 3. In case 5 and 6 the variation is more local and towards the toe thi, effect decreases. Especially, case 6 showed also a local variation at Section 7 of $\Delta z_p = \pm 1.10m$ . The peak of the phreatic line that is slowly moving towards the dike toe due to the low permeability is less visible than in the cases 1-3. This weakened effect can be addressed by the higher hydraulic conductivity of sand, which results in less particle resistance and higher fluxes.

At $t = 55\ days$, figures D-33 – D-38, different to dike 1 is the fact that the variation for a slow falling wave (i.e. case 6) is relative lower than case 4 and 5. The clay layer causes more variation for relative fast rising/falling flood waves. Therefore, the hysteresis effect is stronger on long-the term. The center of gravity of the probability distributions are much higher (comparable with case 1-3) and can differ $0.45 - 0.65m$ from the maximum.

The ‘bubble’ has lower pressure head values than in the cases 1-3. This can be addressed to the soil type, where sand can release the pressure relative faster.

### 5.1.3 Dike 2, Case 7-9

| Times | Case No. | Sect. | Max ($z$) | Min ($z$) | $\mu$ ($z$) | $\sigma$ ($z$) | Skewness | Kurtosis | Chi-square ($X^2$) $\alpha' = 0.05$ |
|---|---|---|---|---|---|---|---|---|---|
| | | | $[m + NAP]$ | | | | | | Decision |
| $t = 10$ $days$ | 7 | 1 | 7.29 | 7.29 | 7.29 | 0.00 | 0.31 | -0.36 | Accept |
| | | 2 | 7.31 | 7.31 | 7.31 | 0.00 | 0.19 | 0.11 | Accept |
| | | 3 | 7.39 | 7.38 | 7.38 | 0.00 | 0.09 | -0.36 | Accept |
| | | 4 | 7.53 | 7.53 | 7.53 | 0.00 | 0.12 | -0.27 | Accept |
| | | 5 | 7.62 | 7.61 | 7.61 | 0.00 | 0.18 | 0.25 | Reject |
| | | 6 | 7.67 | 7.66 | 7.67 | 0.00 | 0.03 | 0.32 | Accept |
| | | 7 | - | - | - | - | - | - | - |
| | | 8 | - | - | - | - | - | - | - |
| $t = 10$ $days$ | 8 | 1 | 7.26 | 7.25 | 7.25 | 0.00 | -0.04 | -0.48 | Accept |
| | | 2 | 7.23 | 7.23 | 7.23 | 0.00 | -0.14 | -0.61 | Accept |
| | | 3 | 7.30 | 7.30 | 7.30 | 0.00 | -0.14 | 0.21 | Accept |
| | | 4 | 7.48 | 7.47 | 7.48 | 0.00 | 0.00 | 0.55 | Accept |
| | | 5 | 7.59 | 7.59 | 7.59 | 0.00 | -0.19 | -0.28 | Accept |
| | | 6 | 7.66 | 7.66 | 7.66 | 0.00 | 0.04 | -0.10 | Accept |
| | | 7 | - | - | - | - | - | - | - |
| | | 8 | - | - | - | - | - | - | - |
| $t = 10$ $days$ | 9 | 1 | 7.07 | 7.07 | 7.07 | 0.00 | -0.07 | -0.03 | Accept |
| | | 2 | 7.06 | 7.06 | 7.06 | 0.00 | 0.09 | -0.13 | Accept |
| | | 3 | 7.14 | 7.13 | 7.13 | 0.00 | -0.08 | -0.12 | Accept |
| | | 4 | 7.29 | 7.28 | 7.29 | 0.00 | -0.10 | -0.41 | Accept |
| | | 5 | 7.40 | 7.39 | 7.40 | 0.00 | 0.10 | 0.36 | Accept |
| | | 6 | 7.46 | 7.45 | 7.46 | 0.00 | -0.29 | 0.23 | Accept |
| | | 7 | - | - | - | - | - | - | - |
| | | 8 | - | - | - | - | - | - | - |
| $t = 30$ $days$ | 7 | 1 | 5.84 | 5.84 | 5.84 | 0.00 | -0.02 | -0.30 | Accept |
| | | 2 | 5.91 | 5.90 | 5.90 | 0.00 | -0.32 | -0.14 | Accept |
| | | 3 | 5.91 | 5.91 | 5.91 | 0.00 | -0.17 | -0.07 | Accept |
| | | 4 | 5.87 | 5.87 | 5.87 | 0.00 | -0.04 | -0.13 | Accept |
| | | 5 | 5.82 | 5.82 | 5.82 | 0.00 | -0.39 | 0.02 | Accept |
| | | 6 | 5.77 | 5.77 | 5.77 | 0.00 | -0.30 | 0.37 | Accept |
| | | 7 | 5.74 | 5.73 | 5.74 | 0.00 | -0.50 | 0.49 | Reject |
| | | 8 | 5.69 | 5.69 | 5.69 | 0.00 | -0.01 | -0.27 | Accept |
| $t = 30$ $days$ | 8 | 1 | 6.55 | 6.55 | 6.55 | 0.00 | -0.09 | 0.80 | Reject |
| | | 2 | 6.67 | 6.66 | 6.67 | 0.00 | 0.22 | 0.50 | Accept |
| | | 3 | 6.71 | 6.71 | 6.71 | 0.00 | -0.28 | -0.04 | Accept |
| | | 4 | 6.70 | 6.70 | 6.70 | 0.00 | 0.11 | -0.50 | Reject |
| | | 5 | 6.66 | 6.65 | 6.65 | 0.00 | 0.01 | -0.20 | Accept |
| | | 6 | 6.63 | 6.63 | 6.63 | 0.00 | -0.05 | -0.19 | Accept |
| | | 7 | 6.61 | 6.60 | 6.61 | 0.00 | 0.05 | 0.00 | Accept |
| | | 8 | 6.67 | 6.66 | 6.66 | 0.00 | 0.20 | -0.31 | Reject |
| $t = 30$ $days$ | 9 | 1 | 7.35 | 7.34 | 7.35 | 0.00 | -0.02 | -0.53 | Accept |
| | | 2 | 7.46 | 7.46 | 7.46 | 0.00 | 0.05 | -0.40 | Accept |
| | | 3 | 7.55 | 7.55 | 7.55 | 0.00 | -0.21 | -0.16 | Accept |
| | | 4 | 7.60 | 7.60 | 7.60 | 0.00 | -0.02 | -0.29 | Accept |
| | | 5 | 7.61 | 7.61 | 7.61 | 0.00 | -0.09 | -0.46 | Accept |
| | | 6 | 7.61 | 7.61 | 7.61 | 0.00 | 0.04 | -0.45 | Reject |
| | | 7 | 7.86 | 7.86 | 7.86 | 0.00 | -0.15 | -0.19 | Accept |
| | | 8 | 8.26 | 8.26 | 8.26 | 0.00 | -0.01 | -0.60 | Accept |
| $t = 55$ $days$ | 7 | 1 | 4.25 | 4.24 | 4.25 | 0.00 | -0.35 | -0.30 | Accept |
| | | 2 | 4.25 | 4.25 | 4.25 | 0.00 | -0.17 | -0.15 | Accept |
| | | 3 | 4.23 | 4.23 | 4.23 | 0.00 | -0.39 | -0.03 | Accept |
| | | 4 | 4.18 | 4.18 | 4.18 | 0.00 | -0.16 | 0.28 | Accept |
| | | 5 | 4.15 | 4.14 | 4.14 | 0.00 | -0.11 | -0.19 | Accept |
| | | 6 | 4.12 | 4.12 | 4.12 | 0.00 | -0.34 | -0.01 | Accept |
| | | 7 | 4.11 | 4.10 | 4.11 | 0.00 | -0.25 | 0.08 | Accept |
| | | 8 | 4.08 | 4.08 | 4.08 | 0.00 | -0.02 | 0.16 | Accept |
| $t = 55$ $days$ | 8 | 1 | 4.54 | 4.54 | 4.54 | 0.00 | -0.05 | -0.36 | Accept |
| | | 2 | 4.55 | 4.55 | 4.55 | 0.00 | -0.02 | -0.17 | Accept |
| | | 3 | 4.52 | 4.51 | 4.52 | 0.00 | 0.12 | -0.02 | Accept |
| | | 4 | 4.45 | 4.45 | 4.45 | 0.00 | 0.11 | -0.08 | Accept |
| | | 5 | 4.41 | 4.41 | 4.41 | 0.00 | -0.32 | -0.17 | Accept |
| | | 6 | 4.39 | 4.38 | 4.39 | 0.00 | -0.14 | 0.03 | Accept |
| | | 7 | 4.36 | 4.36 | 4.36 | 0.00 | -0.14 | -0.30 | Accept |
| | | 8 | 4.33 | 4.33 | 4.33 | 0.00 | -0.27 | -0.35 | Accept |
| $t = 55$ $days$ | 9 | 1 | 5.37 | 5.36 | 5.37 | 0.00 | 0.04 | 0.11 | Accept |
| | | 2 | 5.42 | 5.42 | 5.42 | 0.00 | 0.05 | 0.13 | Accept |
| | | 3 | 5.42 | 5.41 | 5.41 | 0.00 | -0.01 | -0.27 | Accept |
| | | 4 | 5.33 | 5.33 | 5.33 | 0.00 | 0.12 | -0.44 | Accept |
| | | 5 | 5.28 | 5.27 | 5.27 | 0.00 | 0.00 | 0.02 | Accept |
| | | 6 | 5.25 | 5.24 | 5.24 | 0.00 | 0.05 | -0.03 | Accept |
| | | 7 | 5.21 | 5.20 | 5.21 | 0.00 | 0.27 | 0.09 | Accept |
| | | 8 | 5.15 | 5.15 | 5.15 | 0.00 | 0.07 | -0.30 | Accept |

Table 5-5 The descriptive statistics of the phreatic line for Dike 2, Case 7 to Case 9.

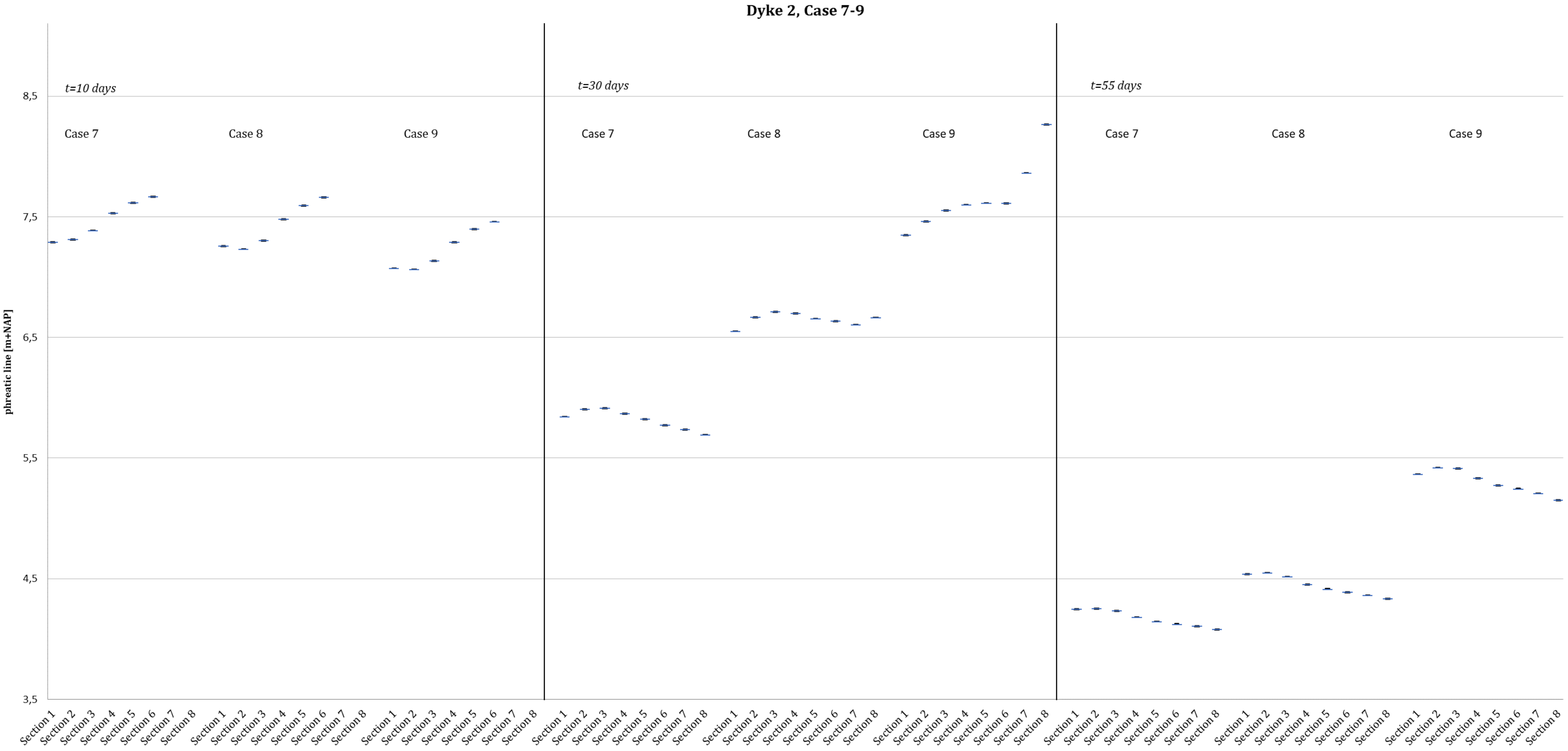


Figure 5-5 The box-plots of the phreatic line for Case 7 to Case 9

For dike type 2, case 7-9, the variation of hydraulic conductivity is found to have an extremely small effect on transient seepage. Hereby, the hydraulic conductivity of the sand core is considered to be random, but the uncertainty when determining the hydraulic conductivity of sand is not proportional towards clay/peat. The COV was considered to be 0.04 (while light-weighted clay was 1.35) (Çalamak, 2014).

For the cases 7-9, the standard deviations are extremely small and considered to be zero. Due to the deterministic hydraulic conductivity in the clay layer, the inflow path is almost the same. Once the water reaches the sand core, no significant fluctuations are caused. All phreatic lines are within $0.01m$ difference between the maximum and minimum elevation coordinate.

At $t = 30\ days$, figures D-46 – D-51, the shape of the phreatic line is related to the duration of the peak flow. And the peak of the phreatic line is slowly moving towards the dike toe. Local variation at section are extremely small.

At $t = 55\ days$, figures D-52 – D-57 the spatial differences for the sections showed a common pattern, the same pattern as in case 1-6 i.e. the phreatic line is becoming more flat. The difference between case 7 and 9 is $\Delta z_p = \pm 1.10m$ (i.e. the same as in case 4-6).

Different to the case 1-6, is that the deterministic value corresponds to the probability distribution. However, the scale at which the variations take place is extremely small and makes it less relevant.

Statistical analyses were performed but on this small scale a variation in the hydraulic conductivity does not lead to major errors in seepage analysis and therefore, for practical applications, the deterministic treatment of this parameter may be reasonable. However, for more accurate estimations of probabilistic behavior of the phreatic line, the hydraulic conductivity should be considered as stochastic variable.

# CHAPTER 6

# COMPARISON WITH METHOD WBI

*In this Chapter, a comparison is made for the method prescribed by WBI and an alternative method for the schematization of piezometric lines and the stochastic application of the phreatic line. The different schematizations are assessed for macro stability with the software D-Geo Stability. The Factor of Safety is compared for prescribed subcases.*

## 6.1 Introduction to method WBI

To ensure the flood safety of the dikes in the Netherlands, the government prescribes that the totality of the $3700km$ Dutch flood defense system is periodically assessed (Ministry I&M, 2017). In 2017 new flood safety standards were enacted in the Netherlands, including new assessment methods in a legal assessment framework called WBI2017 for the 2017-2023 assessment round (in Dutch: Wettelijk Beoordelings Instrumentarium). The WBI contains regulations that the administrator must use to perform an assessment. The manual also contains instructions for the amount of research, and the type of research that is required, in order to achieve good schematizations and how (field) data can be converted to correct calculation parameters.

For taking into account the non-stationary nature of a flood wave when locating the phreatic surface and the course of the phreatic line, WBI refers to the Technical Report Water Pressures at Dikes (TRWD) (Barends, et al., 2004). The TRWD adds and deepens the Technical Report Water-retaining Earth Structures (TRWG, 2001). It provides guidelines, warnings, and points for attention when determining the schematization of water pressures for the purpose of assessing the geotechnical stability of flood defenses.

Therefore, the TRWD provides guidelines for a step-by-step method for achieving safe schematizations. By safe is meant “conservative and optimized as efficiently as possible”. The following steps are considered (see figure 6-1):

1. Describing the soil structure and groundwater flow (aim: insights into the geohydrological system).
2. Determining the (non)-normative situation of the dike based on the effect of external loads on the pore-water pressure (aim: an overview of (non)-normative mechanisms and load combinations).
3. A quantitative elaboration of the schematization of pore-water pressure in the dike and associated verification tests (aim: safe schematization using a calculation model).

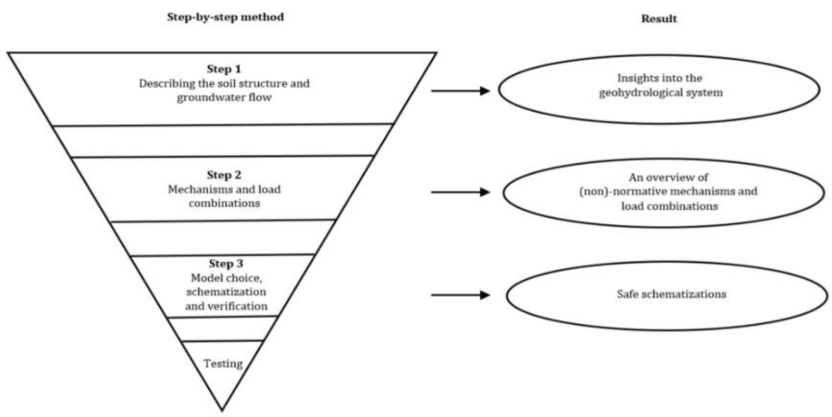


Figure 6-1 Step-by-step method for schematizing the phreatic line and pore-water pressures (Barends, et al., 2004)

In this research, step 2 differs from the standard initiation of normative mechanisms and load situations. The focus is on the variation of the outer water level and the effect on the course of the phreatic line over time and pressure head differences. Therefore, transient seepage analyses were performed for extremely high water (MHW) instead of steady-state analyses. Also, the situation is different since the parameters of hydraulic conductivity are random in order to determine the sensitivity on the development of the phreatic line.

The results of Chapter 5 showed the importance of uncertainty based analyses in research method which is also recommended by the TRWD: investigating the permeability of clay in the dike core is of importance for the location of the phreatic line. Further research makes sense if a (numerical) calculation is executed for the location determination of the phreatic line. By performing stochastic analyses (e.g. MCS) while considering the hydraulic conductivity as random variable, the heterogenic character of the soil type and the influence on the seepage system can be approached with more certainty.

### 6.2 Schematization of piezometric lines conform WBI

An important aspect when executing control or design calculations for macro stability is the schematization of the phreatic line during daily circumstances and the pressure head course in the subsurface. When assessing the outward macro stability, the critical situation is the relative fast water level drop after a peak flow (MHW).

Conform TRWD some basic assumption are prescribed for achieving a (safe) schematization:

- the location of the phreatic line in the dike core does not change after a rapid fall due to lagging. However, it more plausible to assume that the phreatic line at the outward slope side is falling slightly over a period of $10\,days$ for instance (Barends, et al., 2004). Therefore, TRWD prescribes a drop of the phreatic line of approximately $1m$ below the outward dike side considering the highest point of the phraetic line and $0.30m$ from the outer slope side. The phreatic line is dropping towards to inner slope side with another $0.5m$. The line's course is heading towards the dike toe towards surface level. Hereby, it is the case of a hefty fall of $4.5m$ of the outer water level (see figure 6-2). (If there's reason for doubt, in case the dike consist of exteremely permeable or low permeable material, another assumption of the location of the phraetic line can be made. Therefore, the TRWD recommends to perform a sensitivity analyses for the hydraulic properties of the dike material with respect to the phreatic line.);
- the water pressures in the aquifer and cover layers (i.e. compressible layers) are not lagging and react on the change of the outer water level.

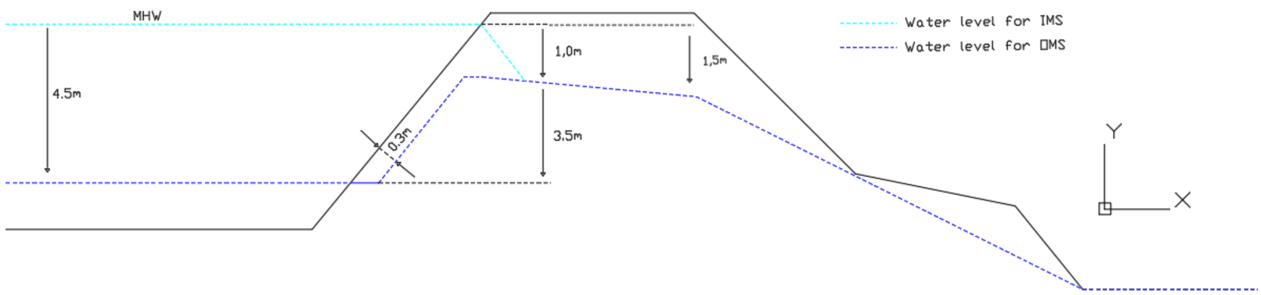


Figure 6-2 Schematization water levels for mechanism inward macro stability (IMS) and outward macro stability (OMS) (Van Middelkoop, et al., 2018).

The above schematization is normative for the assessment of macro stability of the inner and outer slope, where extremely high water (MHW) is critical for the assessment of inward macro stability and the absolute drop of $\Delta h = 4.5m$ (drop after MHW) is critical for the assessment of outward macro stability (see Chapter 2.2 *Macro stability and phreatic lines*).

For practical application, the TRWD distinguishes three piezometric level lines for water pressures that represent the pressure head per (soil) layer (see figure 6-3). These are:

- the phreatic water (PL1);
- the pressure head at the bottom side of the cover layer (PL2);
- and one for the pressure head in the aquifer (PL3), respectively.

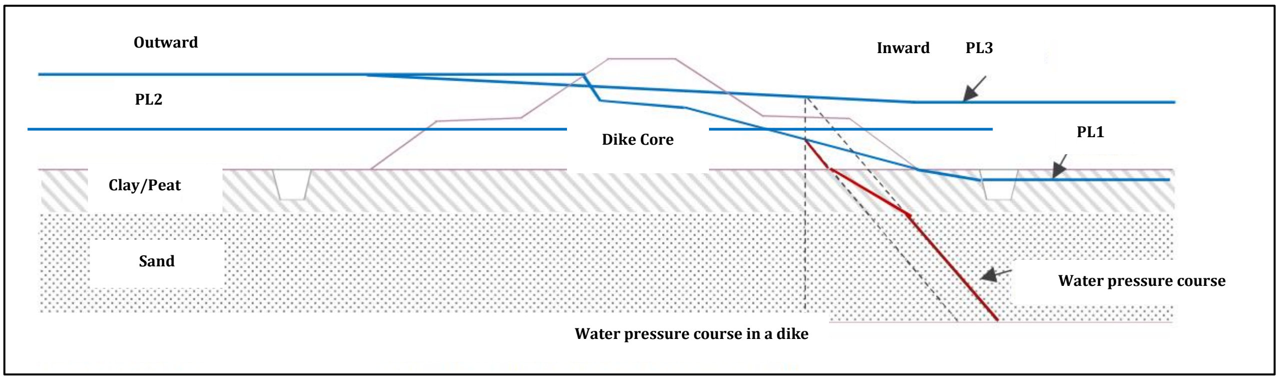


Figure 6-3 piezometric lines for the schematization of water pressure in a dike (Van Middelkoop, et al., 2018).

PL1: For the assessment of macro stability, the basic assumptions of TRWD can be adopted. Hereby, the water level is $3.5m$ within the dike (see figure 6-2 ). This is the schematization of the phreatic line for dike core materials with low permeability i.e. clay core.

PL2: The second piezometric line corresponds with the outer water level at daily circumstances and represents the pressure head at the bottom side of the cover layer e.g. if an enclosed sand layer lies between two low permeable cover layers.

PL3: The third piezometric line somehow corresponds with the actual outer water level and can be assumed to be a straight line. In reality, this line has a small angle and decreases towards the inward side of the dike. This line represents the water pressure in the aquifer.

### 6.3 Comparison of the schematization of piezometric lines

In this section, the prescribed method of the WBI for schematizing the three piezometric lines are compared with the stochastically simulated phreatic line (PL1) and the deterministically simulated pressure head in the aquifer (PL3). PL2 is kept at the same level since the lithology in the model of SEEP/W at TG109 is simplified i.e. an intersection graph of the pressure head in this layer would not be comparable with the model used for the assessment of macro stability.

For practical application, a simplified dike is chosen that was already set-up by Sweco at location TG107, project area of TiWa, also containing a clay core. By changing the PL-lines' location and the layer at which the piezometric line has an effect on, the conservative schematization method of WBI can be compared with the simulated piezometric lines in SEEP/W. The aim is to evaluate the factor of safety for outward macro stability with the software D-Geo Stability (Deltares, 2016). D-Geo Stability is a tool to analyze slope stability in two-dimensional geometry. In this case, the Uplift-Van model is used since the changes in editing PL-lines may result that some of the layers have a different piezometric level than the phreatic line. This might cause a portion of the layers to be lifted. Non-circular slide planes may come into effect (Deltares, 2016). Therefore, for this comparison, it is strongly advised to use the Uplift-Van method (see Appendix A-4 *Factor of Safety macro stability*).

### 6.3.1 Set-up D-Geo Stability cases

Nine cases are investigated for the assessment of outward macro stability in D-Geo Stability, respectively Dike 1, case 1-3 of the SEEP/W results at which the water level drops $4.5m$ (case of figure 6-2 ). Since the design water level for TG109 is defined to be at $10.7m +$ NAP (MHW), resulting in a drop level of $6.2m +$ NAP. For Case 1-3 this is at $t = 22\ days$, $t = 30\ days$ and $t = 43\ days$, respectively. The outer water level at daily circumstances is at $3.2m +$ NAP, which apparently corresponds with the polder level in the winter. The cases are given in table 6-1. , where:

**W**(BI) = piezometric lines schematized with the method prescribed by WBI
**A**(lternative) = piezometric lines schematized with simulation results SEEP/W

| | | **SEEP/W** | | | | **D-Geo Stability** | | |
|---|---|---|---|---|---|---|---|---|
| | Case No. | Parameter | | Wave type | Sub. No. | Parameter | | |
| | | $\mu_{K_s}$ | COV | | | PL1 | PL2 | PL3 |
| | | $[m/s]$ | | | | $[m +$ NAP$]$ | | |
| Dike 1 (Light-weight clay) | 1 | $1.354 \times 10^{-7}$ | 1.35 | fast rise – fast fall | 1 | W | W | A |
| | | | | | 2 | A | A | A |
| | | | | | 3 | A | W | A |
| | 2 | $1.354 \times 10^{-7}$ | 1.35 | average rise – average fall | 1 | W | W | A |
| | | | | | 2 | A | A | A |
| | | | | | 3 | A | W | A |
| | 3 | $1.354 \times 10^{-7}$ | 1.35 | slow rise – slow fall | 1 | W | W | A |
| | | | | | 2 | A | A | A |
| | | | | | 3 | A | W | A |

Table 6-1 Cases for the assessment of outward macro stability in D-Geo Stability.

For each case, three subcases are defined, where pressure head in the aquifer is obtained from the SEEP/W simulation. For the same outer water level, the duration of the peak flow does not lead to great differences in pressure head:

**Subcase 1**: schematization of PL1 based on prescribed method conform WBI (i.e. refers to TRWD), see figure 6-2 . the schematization of PL2 based on method conform WBI, see figure 6-4,  which is $3.2m +$ NAP.

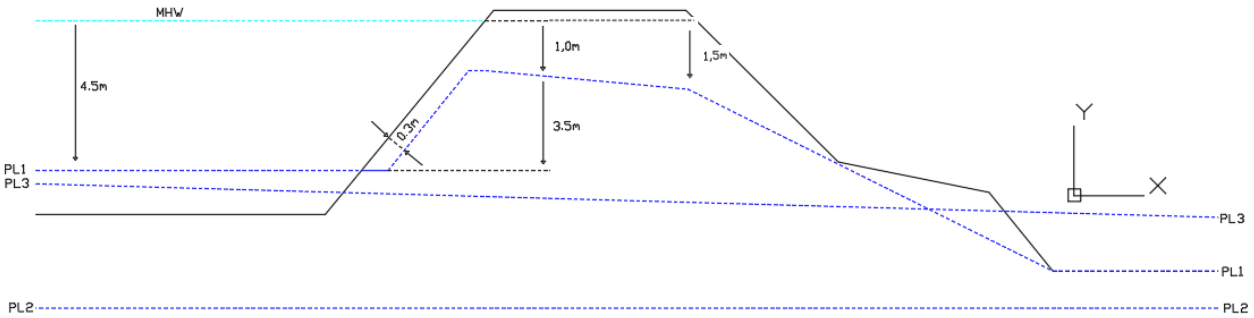


Figure 6-4 Subcase 1: PL-line schematization for the assessment of outward macro stability, a conservative method conform WBI.

**Subcase 2:** schematization of PL1 based on stochastic SEEP/W results, choosing the upper 95% boundary line, including the uncertainty of the dike core material. In Chapter 5 the probability distributions are plotted for the gamma distribution. Since the shape parameter $\alpha'$ and rate parameter $\beta$ of the gamma distribution are known of [Eq. 5.1], the cumulative probability distribution can be plotted. The exact 95% upper boundary line can be obtained by the least square method (Yang & You, 2013), see [Eq. 4.1]. The parameter vector $X$ needs to fit for a value of 0.95 of the cumulative probability, which is the elevation of the phreatic line $x$ in $f(x; \alpha', \beta)$ [Eq. 5.1 ] (see figure 6-5). This formula can be solved in Excel using the Solver add-in function (GRG-method (Lasdon, et al., 1973), the same algorithm used for fitting the soil property parameters, see Appendix B *Initiation of Geohydrological soil parameters*).

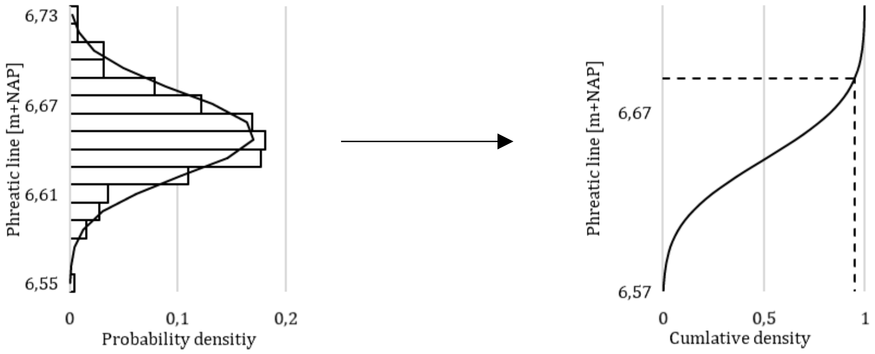


Figure 6-5 Right: Probability density function (Gamma) for the location of the phreatic line. Left: Cumulative density function of the phreatic line with the 95% boundary lines $z_{p;0.95} = 6.69m + \text{NAP}$ (example: Dike 1 Case 1, $t = 30\ days$, Section 2). Results of all cumulative density plots can be seen in Appendix D-2 *Results SEEP/W simulations (application).*

The phreatic line is only stochastically implemented for the eight sections and is made more piece-wise linear. For other locations, the deterministic values are used. This method could be adopted for a continuous phreatic line uncertainty based analyses but that requires more sections for statistical analyses. Besides, it can be doubted what level of detail is required for stability analyzes.

Results of Chapter 5 showed a residual pressure in thedike core which is caused by the height and duration of the peak flow. As soon as the peak drops, this pressure remains in the core and an underpressure occurs in the surrounding soil layers. Due to gravity, this 'bubble' slowly disappears due to small fluxes downwards the phreatic line. For soil parts above the phreatic line but where the residual pressure exists, PL2 is leading. In other words, the residual pressure is translated to a piezometric line 2 in order to account the excess pressure (see figure 6-6). The hypothesis is that the residual pressure results in a local decrease of the pore-pressure i.e. the cohesion and particle friction are lowered which can cause a slip surface (see Chapter 2.2 *Macro stability and phreatic lines*).

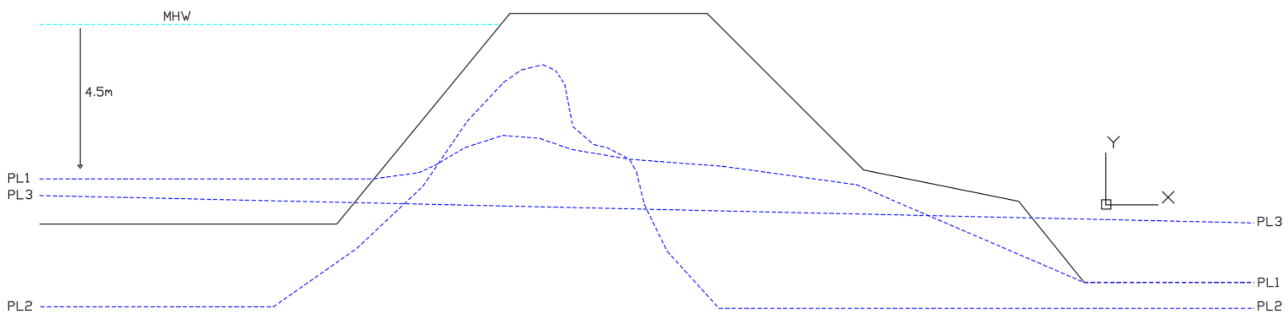

Figure 6-6 Subcase 2: PL-line schematization for the assessment of outward macro stability, an experimental method in which the PL1 (phreatic line) is at a more 'realistic' level, the one stochastically simulated in SEEP/W and PL2 represents the residual pressure head above the phreatic line.

**Subcase 3:** In order to compare the alternative method and the effect of schematizing the residual pressure with PL2, a case is set-up at which PL2 is kept at daily water level (method WBI), while schematizing the phreatic line based on stochastic SEEP/W results, see figure 6-7.

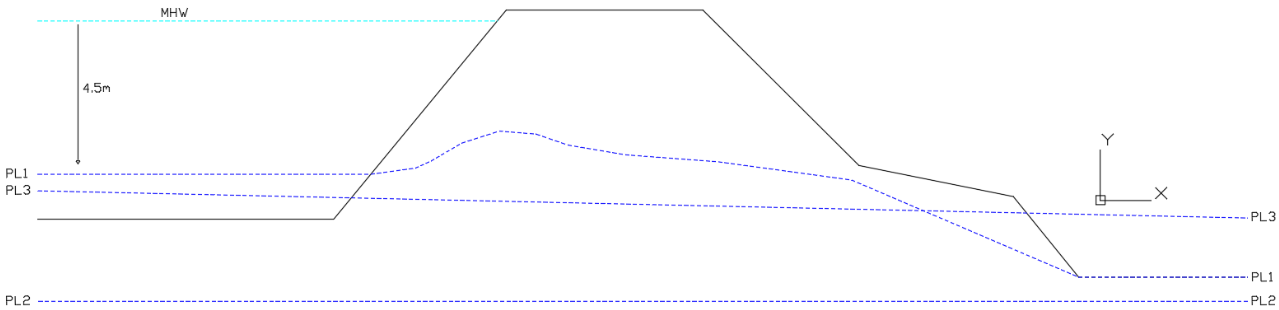


Figure 6-7 Subcase 3: PL-line schematization for the assessment of outward macro stability, the method conform WBI but with the more 'realistic' level of PL1 (phreatic line) which is stochastically simulated with SEEP/W

The simulation results of SEEP/W of Dike 1, Case 1-3 for the water level of $6.2m + \text{NAP}$, at $t = 22\ days$, $t = 30\ days$ and $t = 43\ days$, respectively, are given in the section below. Also the statistical, properties of the sections are stated in table 6-2 and the, histograms, probability density functions and cumulative density functions (i.e. including the computed values $z_{p;0.95}$ of the phreatic line per section in D-Geo Stability are given in Appendix D-2 *Results SEEP/W simulations (application)*

| Times | Case No. | Sect. | Max $(z)$ | Min $(z)$ | $\mu$ $(z)$ | $\sigma$ $(z)$ | Skewness | Kurtosis | $\alpha'$ $X \sim \Gamma(\alpha', \beta)$ | $\beta$ $X \sim \Gamma(\alpha', \beta)$ | Chi-square $(X^2)$ $\alpha' = 0.05$ |
|---|---|---|---|---|---|---|---|---|---|---|---|
| | | | $[m + NAP]$ | | | | | | | | Decision |
| $t = 22$ $days$ | 1 | 1 | 6.66 | 6.48 | 6.59 | 0.03 | -0.70 | 0.44 | 36910.4 | 0.00018 | Reject |
| | | 2 | 6.74 | 6.55 | 6.64 | 0.03 | 0.20 | 0.93 | 58079.3 | 0.00011 | Accept |
| | | 3 | 6.77 | 6.56 | 6.68 | 0.03 | -0.95 | 1.42 | 40802.8 | 0.00016 | Reject |
| | | 4 | 7.11 | 6.57 | 6.90 | 0.08 | -0.90 | 2.44 | 8429.87 | 0.00082 | Reject |
| | | 5 | 7.41 | 6.86 | 7.11 | 0.10 | 0.55 | 0.57 | 5477.47 | 0.00130 | Accept |
| | | 6 | 7.79 | 6.89 | 7.30 | 0.17 | 0.44 | 0.03 | 1948.62 | 0.00375 | Accept |
| | | 7 | 7.96 | 6.98 | 7.42 | 0.17 | 0.19 | -0.14 | 1979.22 | 0.00375 | Accept |
| | | 8 | 7.67 | 6.93 | 7.33 | 0.14 | 0.17 | -0.17 | 2653.06 | 0.00276 | Accept |
| $t = 30$ $days$ | 2 | 1 | 6.70 | 6.52 | 6.62 | 0.03 | -0.25 | 0.78 | 50663.6 | 0.00013 | Accept |
| | | 2 | 6.78 | 6.53 | 6.66 | 0.04 | -0.09 | 0.09 | 25349.3 | 0.00026 | Accept |
| | | 3 | 6.81 | 6.56 | 6.70 | 0.04 | -0.47 | 0.28 | 26142.6 | 0.00026 | Accept |
| | | 4 | 7.17 | 6.79 | 6.95 | 0.06 | 0.32 | 0.37 | 12388.7 | 0.00056 | Reject |
| | | 5 | 7.49 | 6.81 | 7.12 | 0.12 | 0.23 | 0.18 | 3744.82 | 0.00189 | Accept |
| | | 6 | 7.80 | 6.97 | 7.32 | 0.17 | 0.53 | 0.17 | 1811.24 | 0.00404 | Reject |
| | | 7 | 8.02 | 6.89 | 7.38 | 0.17 | 0.34 | 0.27 | 1787.14 | 0.00413 | Accept |
| | | 8 | 7.63 | 6.85 | 7.25 | 0.15 | 0.01 | -0.17 | 2480.31 | 0.00292 | Accept |
| $t = 43$ $days$ | 3 | 1 | 6.75 | 6.53 | 6.65 | 0.03 | -0.44 | 0.78 | 37233.3 | 0.00018 | Reject |
| | | 2 | 6.80 | 5.52 | 6.68 | 0.05 | -0.46 | 0.40 | 17336.5 | 0.00039 | Accept |
| | | 3 | 6.87 | 6.55 | 6.74 | 0.05 | -0.48 | 0.48 | 17683.5 | 0.00038 | Accept |
| | | 4 | 7.26 | 6.80 | 6.97 | 0.08 | 0.49 | 0.57 | 7410.77 | 0.00094 | Reject |
| | | 5 | 7.58 | 6.83 | 7.14 | 0.13 | 0.47 | 0.17 | 3022.67 | 0.00236 | Accept |
| | | 6 | 7.77 | 6.89 | 7.28 | 0.18 | 0.53 | -0.07 | 1655.06 | 0.00440 | Accept |
| | | 7 | 7.82 | 6.96 | 7.28 | 0.15 | 0.61 | 0.49 | 2234.16 | 0.00323 | Reject |
| | | 8 | 7.65 | 6.72 | 7.14 | 0.13 | 0.27 | 0.55 | 2810.41 | 0.00254 | Accept |

Table 6-2 Statistical results of SEEP/W (including the shape parameter $\alpha'$ and rate parameter $\beta$ of the gamma distribution $X \sim \Gamma(\alpha', \beta)$) considered cases for the assessment of outward macro stability in D-Geo Stability.

**Results presentation: Dike 1, Case 1-3** Figure 6-8 deterministic phreatic line and color shading pressure head. The interface of SEEP/W simulation.

Case 1: $t = 22\ days$, water level at $6.2m + \text{NAP}$

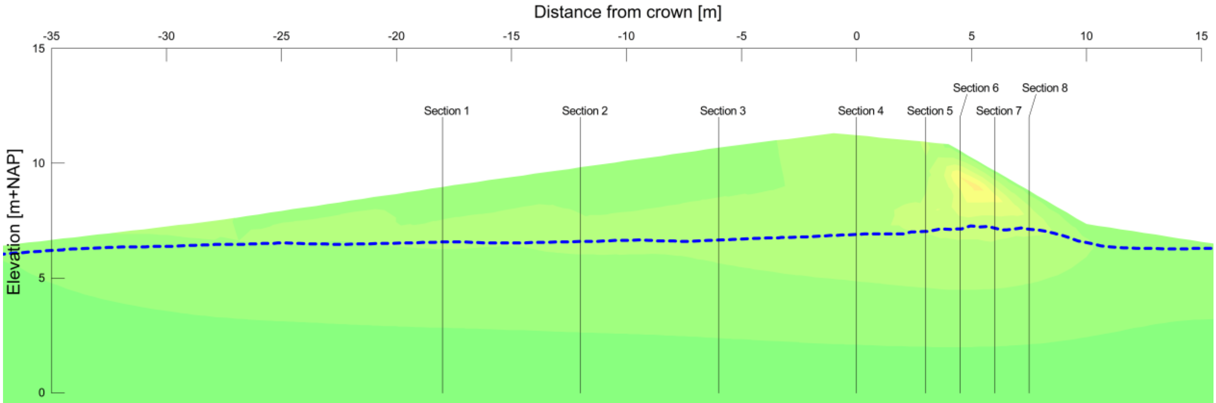


Case 2: $t = 30\ days$, water level at $6.2m + \text{NAP}$

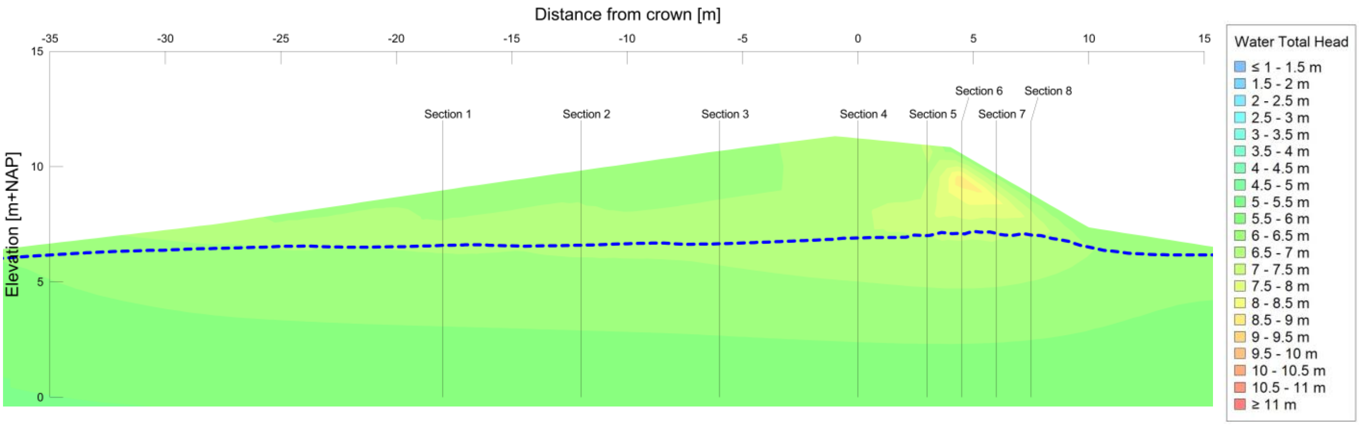


Case 3: $t = 43\ days$, water level at $6.2m + \text{NAP}$

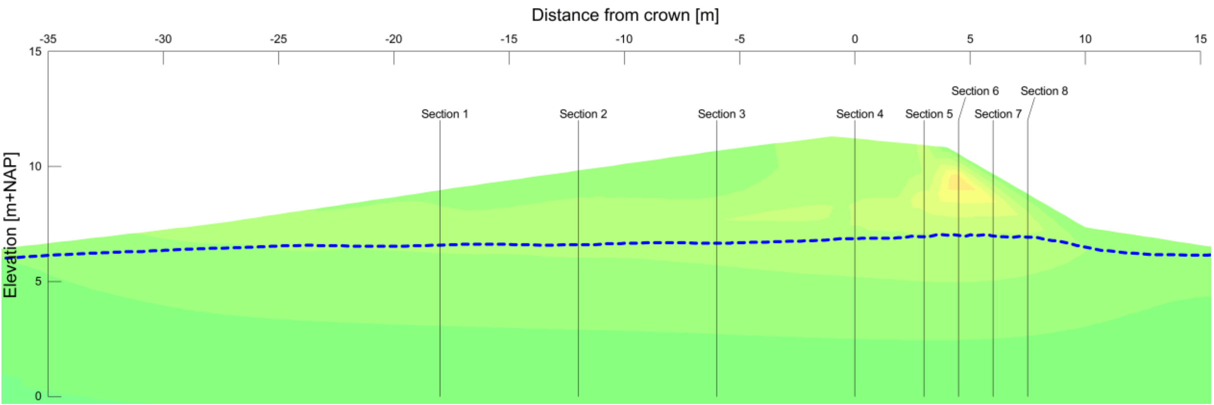


Table 6-2 shows that the phreatic lines are approximately at the same height for a fixed water level, despite the differences in duration of the flood wave. The difference between the maximum and minimum location is between $0.2 - 1.0m$ for all cases. Also, the standard deviation shows a similar pattern of variation from dike toe to the point of inflow. However, figure 6-8 shows a more extended pressure 'bubble' (yellow/green contour shading) towards the dike toe for Case 3. A longer duration of the flood wave, having a higher inflow time at the outer slope side, causes an increase of the local pressure head and more extended towards the dike toe. This was also observed in Chapter 5.

### 6.3.2 Results D-Geo Stability simulation

The results of the D-Geo Stability analyses per subcase are listed in the table below (table 6-3). The Factor of Safety $FoS$ $[-]$, the balance between the maximum resisting moment and driving moment (see Appendix A-4 *Macro stability and phreatic lines*) is compared for the conservative method prescribed by WBI (Sub. No. 1) with the alternative method using stochastic results of the phreatic line of SEEP/W simulations, using a more 'realistic' location of the phreatic line and analyze the excess pressure for dike core parts above the phreatic line by assigning the pressure head of PL2 (Sub. No.). Sub. No. 3 shows the effect of a more 'realistic' location of the phreatic line without considering the excess pressure.

**W**(BI) = piezometric lines schematized with the method prescribed by WBI
**A**(lternative) = piezometric lines schematized with simulation results SEEP/W

| | | **SEEP/W** | | | | **D-Geo Stability** | | | |
|---|---|---|---|---|---|---|---|---|---|
| | Case No. | Parameter | | Wave type | Sub. No. | Parameter | | | |
| | | $\mu_{K_s}$ | COV | | | PL1 | PL2 | PL3 | $FoS$ |
| | | $[m/s]$ | | | | $[m + \text{NAP}]$ | | | $[-]$ |
| Dike 1 (Light-weight clay) | 1 | $1.354 \times 10^{-7}$ | 1.35 | fast rise – fast fall | 1 | W | W | A | 1.02 |
| | | | | | 2 | A | A | A | 0.95 |
| | | | | | 3 | A | W | A | 1.08 |
| | 2 | $1.354 \times 10^{-7}$ | 1.35 | average rise – average fall | 1 | W | W | A | 1.02 |
| | | | | | 2 | A | A | A | 0.93 |
| | | | | | 3 | A | W | A | 1.08 |
| | 3 | $1.354 \times 10^{-7}$ | 1.35 | slow rise – slow fall | 1 | W | W | A | 1.02 |
| | | | | | 2 | A | A | A | 0.98 |
| | | | | | 3 | A | W | A | 1.09 |

Table 6-3 Cases for the assessment of outward macro stability in D-Geo Stability and calculated Factor of Safety $FoS$ $[-]$.

The results of the D-Geo Stability simulations can be found in Appendix D-3 *Results D-Geo Stability simulations.* The slip zones (Example figure 6-9) with corresponding $FoS$ $[-]$ are given including the schematization of the piezometric lines for the subcases

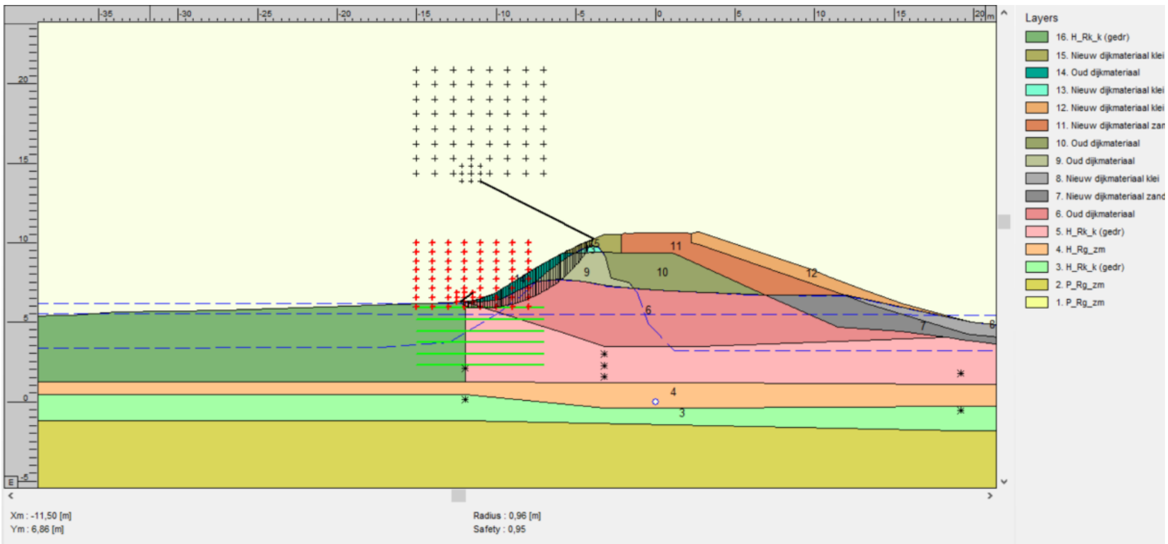


Figure 6-9 Example interface software D-Geo Stability Dike 1, Case 1, Sub No. 2, $t = 22\ days, FoS = 0.95$



SWECO UNIVERSITY OF TWENTE.

The Factor of Safety $FoS$ $[-]$ for the subcases follow a similar pattern for the three different flood wave types of Dike 1:

- For Sub. No. 1, the slightly changes of the piezometric line 3 do not lead to a different Factor of Safety. Since the conservative schematization of the phreatic line (PL1) is fixed despite the duration of the flood wave (also PL2 is fixed to polder water level), the computed Factor of Safety, $FoS = 1.02$, is equal for all three cases. Therefore, the differences in durthe ation of the flood waves do not lead to significant differences in computed Factor of Safeties.
- For Sub. No. 2, the Factor of Safety is significantly smaller compared to the schematization of the WBI and differ $\Delta FoS = \pm 0.04 - 0.09$. The differences between the flood wave types can be adressed to the fact that the 95% boundary line of the cumulative density function for case 1 and 2 is higher (see Appendix D-2 *Results SEEP/W simulations (application))* at the outward slope side (Section 5-8), resulting in a higher input value for the phraetic line in D-Geo Stability. A higher computed phraetic line, results in a higher water pressure which causes a decrease of the effective stress. This is a loss in balance and therefore the calculated Factor of Safety is lower for Case 1 and 2 compared to Case 3.
- For Sub. No. 3, the piezometric line 2 is fixed at polder water level and only the phreatic line significant changing per case. The Factor of Safety is significantly higher than Sub. No. 1 $\Delta FoS = \pm 0.06 - 0.07$ and Sub. No. 2 $\Delta FoS = \pm 0.11 - 0.15$. The phreatic line may be on a more 'realistic' level but the excess pressure is not taken into account which may lead to incorrect approval for the assessment of macro stability.

# CONCLUSION

This chapter presents the most important findings of this study, focusing on answering to the two main research questions:

1. What is the effect of flood waves on the development of the phreatic line in dike bodies?

2. To what extent does the development of the flood wave, and waveform, affect the hydraulic heads in the aquifers and the cover layers and how does this affect the stability of the dike?

Note that the conclusions as presented below are based only on the test cases used in this study for SEEP/W and D-Geo Stability as specified in Section 4.4.2 and 6.3.2, respectively. These cases all have a simplified subsoil composition and relatively high foreshores. Besides, the conclusions are based on the calculations executed in this research. Due to their limitations and assumptions, it is uncertain if the conclusions can be applied in general applications. However, this study proved that the uncertainty based analysis technique of transient seepage, adopted by the study of Çalamak (2014), can be applied to large-scale non-fictive seepage models with the software SEEP/W.

The main findings and contributions of the study to the field can be summarized as follows:

- The influence core materials have on the location and temporal development of the phreatic line in earth dike bodies can be addressed to two hydraulic soil properties: the volumetric water content and the hydraulic conductivity.
    - The volumetric water content is mostly influenced by the size distribution of particles in the soil. For uniformly distributed soil types and/or large particle size, water can be released more easily under small negative pore-water pressure.
    - The hydraulic conductivity is mostly influenced by the quantity of water that is moving through a cross-sectional area between the particles. The ability of a soil to conduct water depends on the amount of water that is available in the soil, which is represented by the volumetric water content. Therefore, movement of the phreatic line can be addressed to the value of hydraulic conductivity.

    Dike core materials with a relatively high hydraulic conductivity can drain water more easily under small negative pressure than materials with a relatively low hydraulic conductivity, resulting in a quicker response on the outer water level and development alongside the dike core of the phreatic line.

  Therefore, the temporal development of the phreatic line was stochastically analyzed by randomly variating the hydraulic conductivity of the dike core material. This one-at-time sensitivity analysis was performed for different types of dikes compositions and flood wave scenarios, using the Monte Carlo simulation technique, which enabled to perform uncertainty based transient seepage analyses. The uncertainties can be addressed to the heterogeneity of the soil or insufficient geotechnical site explorations, for instance. This has led to the following results

- The variation of hydraulic conductivity of fine-grained materials was found to have a significant effect on the location of the phreatic line, that may deviate from the position of the phreatic line when assuming homogeneous materials with average material properties. The deviations of the phreatic line become greater on the long-term. However, hydraulic conductivity variation of course-grained materials are found to be less significant since they generally have low variability. The deviations alongside the phreatic line are greater for dike materials with a high hydraulic conductivity at the start of the wave rise. For dike materials with low hydraulic conductivity, the deviations are more local towards the outer slope of the dike where the water flows in. On long-term, the deviations are spreading out along the phreatic line for all materials. The stochastic analyses showed that the center of gravity of phreatic lines is overestimated as the flood wave is rising and underestimated as the flood wave is falling by the deterministic value.

- The deviations of the phreatic line show no significant differences between a short-term flood wave and a long-term flood wave. However, on the long-term, the absolute location of the phreatic line can differ significantly as the duration of the flood wave increases.
- As the duration of the flood wave increases, the pressure head built up in the dike core is significantly higher. As soon as the flood wave is dropping, the phreatic line follows, resulting in a relative flat phreatic line alongside the dike core. Also, the pressure head in the aquifer and cover layer is dropping. However, residual pressure in the dike core remains at the outer slope side which is caused by the height and duration of the flood wave. An underpressure occurs in the surrounding soil layers and small fluxes downwards the phreatic line occur.
- An increase in pore-water pressure causes a decrease in effective stress and a decrease in shear strength, which leads to deformations and eventually sliding of the soil. Therefore, the residual pressure can cause dike instability.
- Finally, the schematizations of piezometric lines are compared with the conservative method of WBI. By schematizing the phreatic line at a more realistic level and addressing a piezometric line for the residual pressure above the phreatic line, the dike is assessed to be more instable for outward macro stability than without dealing with the residual pressure. Also, this method showed significant differences with the WBI method for the Factor of Safety.

All in all, this study showed more insight which piezometric lines are influencing soil layers in dike compositions and how stochastic analysis (i.e. the uncertainty quantification) of the phreatic line can be used for schematization of these piezometric lines when assessing macro stability, instead of making conservative choices in schematization or for parameter values.

To answer the research question the above showed that the effect flood waves have on dike bodies is not only dependent on the location of the phreatic line which may cause a reduction in effective stress (and therefore dike instability), but that also a residual pressure above the phreatic line emerges, that is influencing the dike stability. Also, the pressure head in the aquifer and cover layers do not lag significantly as the flood wave passes by.

## DISCUSSION

The present study showed that the randomness of hydraulic conductivity is strongly suggested to be considered in seepage modeling. Some exceptional cases may occur if the COV of the hydraulic conductivity is smaller than 0.05. In both geotechnical engineering (Jones, et al., 2002) and hydraulic engineering (Johnson, 1996) applications, such variations are considered as a very small degree. Therefore, it is reasonable to adopt deterministic models and keep the hydraulic conductivity constant for those cases (i.e. Dike 2, Case 7-9 in this study).

The COV of the hydraulic conductivity considered is adopted by the study of Çalamak (2014), since unambiguous quantification of the variation per soil types are hard to find in literature. Therefore, the significant differences in location of the phreatic line for the Cases 1-3 can be doubted and the following stability assessment are nog normative for this case location. This study shows the effects and described a stochastic analyzing method that can be used for other locations and further research.

For practical application, the probability distributions are all fitted for the gamma function, while maybe other density functions will not be rejected by the goodness of fit tests, such as the generalized extreme value (GEV) and three parameter log-normal (LN-3P), according to Çalamak (2014). It is recommended to fit the data with software in order to find the corresponding density function, for instance when using the cumulative distributions for safety assessment. In this study, the rejected cumulative density functions were also used for the assessment analyses. For further research, other density functions are suitable or maybe more Monte Carlo simulations result accepted function by the goodness of fit tests.

The findings of the research have clearly demonstrated the uncertainty effects of soil parameters, variation degree of the phreatic line and possible probability density distributions used to describe the phreatic surface. The findings of the sensitivity analyses may provide tools for geotechnical engineers conducting schematization guidance and recommendations which parameter to treat as deterministic and which as stochastic. However, for application in this research some simplifications are made:

The choice for the case location TiWa was rather pragmatic than a thoughtful one. As described in Chapter 4, this location was already implemented in SEEP/W by Sweco and measurements of standpipe piezometers were available for the validation process. The first tendency was to use historical data for the determination of frequent flood wave types at this location. However, the foreshores at TG109 were relatively high, resulting in extremely small peak flows, which could not be seen as critical for the determination of the phreatic line and sensitivity analyses. Therefore, fictive flood waves were created with its peak at extremely high water. These water levels are normative for the assessment of macro stability. However, the model set-up in SEEP/W for TG109 could not be validated properly for peak flows (only the one in January 2018).

Also, the simulation time of the SEEP/W has been found to be very long. The Monte Carlo Simulation is time-consuming. In this study, more than 2500 simulations were performed (20 minutes each, which is almost 35 days non-stop runtime). For the investigation of the local phreatic line, a smaller simulation area of TG109 may be sufficient in order to lower the runtime.

The converted phreatic lines could be exported easily to AutoCAD for data extraction. The statistical analyses performed on these data sets can be adopted. However, there is no simple method for converting the color shading contour lines of pressure head. Therefore, the coordinates of piezometric line 2 are inserted manually in D-Geo Stability. It can also be doubted what area parts should be assigned to piezometric line 2. In some cases, the residual pressure head is not only concentrated at the outward slope side but is extended towards the dike toe. This is not always a continuous contour line representing the local residual pressure head, but sometimes the contour lines form circular shapes at different locations above the phreatic line. For further research, it is highly recommended to find a proper method.

This study showed the application of stability assessment for outward dike stability. The schematization of the normative phreatic line was also given for inward dike stability but is not assessed due to the different dike used in D-Geo Stability. TG107 was used and simplified in order to investigate the differences between the piezometric schematization methods. However, TG109 has located nearby a road. That is the reason for the flat inner slope. Therefore, inward macro stability may not occur at this location. Also computing the phreatic lines for TG107, in D-Geo Stability, would not have done properly since the phreatic line is slightly dropping over a relatively long distance (the coordinates of the phreatic line are therefore not matching at all).

Finally, the results on variation degree of the hydraulic conductivity, the different flood wave scenarios and its effect on the piezometric lines give awareness to professionals working on the subject that each seepage problem in dikes is unique.

## REFERENCES


Ang, A. H.-S. & Tang, W., 1975. Probability Concepts in Engineering Planning and Design Vol 1: Basic Principles. *John Wiley & Sons.*

Arshad, I. & Babar, M., 2014. Comparison of SEEP/W simulations with field observations for seepage analysis through an earthen dam (case study: Hub Dam - Pakistan). *International Journal of Research,* pp. 57-70.

Barends, F. et al., 2004. *Technisch Rapport Waterspanningen bij dijken,* s.l.: Dienst Weg- en Waterbouwkunde van Rijkswaterstaat (DWW).

Box, G. & Muller, M., 1958. A Note on the Generation of Random Normal Deviates. *The annals of Mathematical Statistics,* Issue 29(2), pp. 610-611.

Çalamak, M., 2014. *Uncertainty based analysis of seepage through earth-fill dams,* Ankara: Middle East Technical Unisersity.

Calle, E., Halter, W. & Niemeijer, H., 2011. Schematiseringsfactor maakt keuzes in geotechniek beter zichtbaar. *Geotechniek,* juli.pp. 30-34.

Carsel, R. & Parrish, R., 1988. *Developing joint probability distributions of soil water retention characteristics,* s.l.: Water Resour. Res..

Deltares, 2016. *D-Geo Stability: Slope Stability software for soft soil engineering, user manual,* Delft: Deltares.

Elkateb, T., Chalaturnyk, R. & Robertson, P., 2003. An overview of soil heterogeneity: quantification and implications on geotechnical field problems.. *Canadian Geotechnical Journal,* Issue 40(1), pp. 1-15.

ENW, 2009. *Technisch Rapport: Actuele sterkte van dijken,* s.l.: s.n.

ENW, 2012. *Technische Rapport Grondmechanisch Schematiseren bij Dijken,* 's-Hertogenbosch: s.n.

Fenton, G. & Griffiths, D., 1996. Statistics of Free Surface Flow Through a Stochastic Earth Dam. *Journal of Geotechnical Engineering,* pp. 1-23.

Foster, M., Fell, R. & Spannagle, M., 2000. The Statistics of embankment dam failures and accidents. *Canadian Geotechnical Journal,* Issue 37(5), pp. 1000-1024.

Fredlund, D. & Rahardjo, H., 1993. Soil Mechanics for Unsaturated Soil. *John Wiley & Sons*, p. 560.

Fredlund, D. & Xing, A., 1994. Equations for the soil-water characteristic curve. *Canadion Geotechnical Journal*, Issue 31, pp. 521-532.

Fredlund, M., 2005. *SoilVision-A Knowledge Based Database System for Saturated/Unsaturated Soil Properties.* Saskatchewan: SoilVision Systems Ltd..

Freeze, R. & Cherry, J., 1979. *Hydraulic Conductivity and permeability for various geological materials.* [Art].

Gallage, C., Kodikara, J. & Uchimura, T., 2013. Laboratory measurement of hydrualic conductivity functions of two unsaturated sandy soils during drying and wetting processes. *The Japanese Geotechnical Society*, pp. 417-430.

Geo-Slope Int Ltd., 2013. *Seepage Modeling with SEEP/W,* Calgary: Geo-Slope International Ltd..

Husein Malkawi, A., Hassan, W. & Abdulla, F., 2000. Uncertainity and realiabity analysis applied to slope stability. *Structural Safety,* Issue 22(2), pp. 161-187.

Jamal, 2017. *Principle of effective stresses.* [Art].

Johnson, P., 1996. Uncertainty of Hydraulic Parameters. *Journal of Hydraulic Engineering,* 1996(122(2)), pp. 112-114.

Jones, A., Kramer, S. & Arduino, P., 2002. *Estimation of Uncertainty in Geotechnical Properties for Performanced-Based Earthquake Engineering,* Berkeley: s.n.

Lasdon, L., Fox, R. & Ratner, M., 1973. *Nonlinear Optimization Using the Generalized Reduced Gradient Method,* Springfield: National Technical Information Service; U.S. Department of Commerce.

Lawson, I., 2014. Indianapolis: AutoHotkey Foundation LCC.

Li, W., Lu, Z. & Zhang, D., 2009. Stochastic analysis of unstaturated flow with probabilistic collacation method. *Water Resources Research,* W08425(45(8)).

Lu, N. & Likos, W., 2004. *Unsaturated Soil Mechanics,* New Jersey: John Wiley & Sons, Inc..

Matlan, S., Mukhlisin, M. & Taha, M., 2014. *Performance Evaluation of Four-Parameter Models of the Soil-Water Characteristic Curve,* s.l.: The Scientific World Journal.

Ministry I&M, 2017. *Wettelijk Beoordelings Instrumentarium: Schematiseringshandleiding macrostabiliteit,* The Netherlands: s.n.

Montfoort, M. v., 2018. *Safety assessment method for macro-stability of dikes with high foreshores,* Delft: TU Delft.

Papagianakis, A. & Fredlund, D., 1984. A steady state model for flow in saturated-unsaturated soils. *Canadian Geotechnical Journal,* Issue 21(3), pp. 419-430.

Richards, L., 1931. Capillary conduction of liquids through porous mediums. *Journal of Applied Physics,* Issue 1(5), pp. 318-333.

Sako, K. & Kitamura, R., 2006. A Practical Numerical Model for Seepage Behavior of Unsaturated Soil. *SOILS AND FOUNDATIONS,* Issue 46(5), pp. 595-604.

Salih, A., 2016. *Weighted Residual Methods,* Thiruvananthapuram: Department of Aerospace Engineering, Indian Institute of Space Science and Technology.

Sullivan, L., 2006. *Estimation from samples,* s.l.: s.n.

't Hart, R., De Bruijn, H. & De Vries, G., 2016. *Fenomenologische beschrijving Faalmechanismen WTI. Technical report,* Delft: Deltares.

TAW, 1985. *Leidraad voor het ontwerpen van rivierdijken,* s.l.: s.n.

TAW, 2004. *Technisch Rapport Waterspanningen bij Dijken,* Delft: Technische Adviescommissie voor de Waterkeringen (TAW).

Thieu, N., Fredlund, M., Fredlund, D. & Hung, V., 2001. Seepage Modeling in a Saturated/Unsaturated Soil System. *International Conference on Management of the Land and Water Resources (MLWR)*, pp. 1-8.

Van den Berg, H., 2019. *SeepW modellering dijkprofielen, Revisie, Proj. nummer: 363913,* Eindhoven: Sweco .

van der Zaag, R., 2019. Enschede: University of Twente.

Van Genuchten, M., 1980. *A Closed-form Equation for Predicting the Hydraulic Conductivity of Unsaturated Soils.,* s.l.: Soil Science Society of America Journal.

Van Genuchten, M., Leij, F. & Yates, S., 1991. *The RETC Code for Quantifying the Hydraulic Functions of Unsaturated Soils,* California: U.S. Salinity Laboratory; U.S. Department of Argiculture, Argricultural Research Service Rvierside.

Van Middelkoop, I. M., Steenbergen, J., Bisschop, C. & Broersma, L., 2018. *Dijkversterking Tiel-Waardenburg,* De Bilt: Sweco Nederland B.V..

Williamson, D., Parker, R. & Kendrick, J., 1989. *The Box Plot: A Simple Visual Method to Interpret data,* s.l.: Annals of Internal Medicine.

Yang, X. & You, X., 2013. Estimating Parameters of Van Genuchten Model for Soil Water Retention Curve by Intelligent Algorithms. *Applied Mathematics & Information Sciences*, Issue 7 (5), pp. 1977-1983

## APPENDICES

## APPENDIX A: MODEL EQUATIONS

*Appendix A describes and derives the model equations used in this study based on literature.*

### A-1 Water storage function

The function of the SWCC can be formulated with saturated and residual values. In reality, $S$ $[-]$ in Eq. [2.1] never reaches 0 or 1 i.e. these are idealized for engineering use. Therefore, a dimensionless value is defined by Van Genuchten called the normalized water content $\Theta$ $[-]$, also known as the effective saturation $S_e[-]$ (Van Genuchten, 1980):

$$S_e = \Theta = \frac{\theta - \theta_r}{\theta_s - \theta_r}$$

[A.1]

Van Genuchten (1980) derived a closed form equation consisting of three curve-fitting parameters $\alpha$, n and m for the estimation of the SWCC:

$$\Theta = \frac{1}{[1 + (\alpha h)^{\mathrm{n}}]^{\mathrm{m}}}$$

[A.2]

Where $h$ is the pressure head, which can be taken as kPa and m (SI unit system). Parameter $\alpha$ is related to the inverse of air-entry value and is therefore related to the largest pore size of the soil (Lu & Likos, 2004). It must take as the same unit as the pressure head (i.e. $kPa^{-1}$ or $m^{-1}$). Parameter $n$ is related to the pore size distribution of the soil, and $m$ is related to the assymetry of the model (Matlan, et al., 2014). This equation is frequently used because it gives more flexibility to describe the continuous development of unsaturated soil hydraulic properties over a wide range of pressure head (i.e. both high suction and low suction range) (Fredlund & Xing, 1994). However, there are many mathematical equations proposed in the literature for presenting the SWCC. SEEP/W has built three methods built in the model which fit the SWCC to the best, namely Brooks and Corey (1971), Fredlund & Xing (1994) and Van Genuchten (1980), see figure A-1. In this study, Van Genuchten (1980) is adopted to estimate unsaturated soil hydraulic properties.

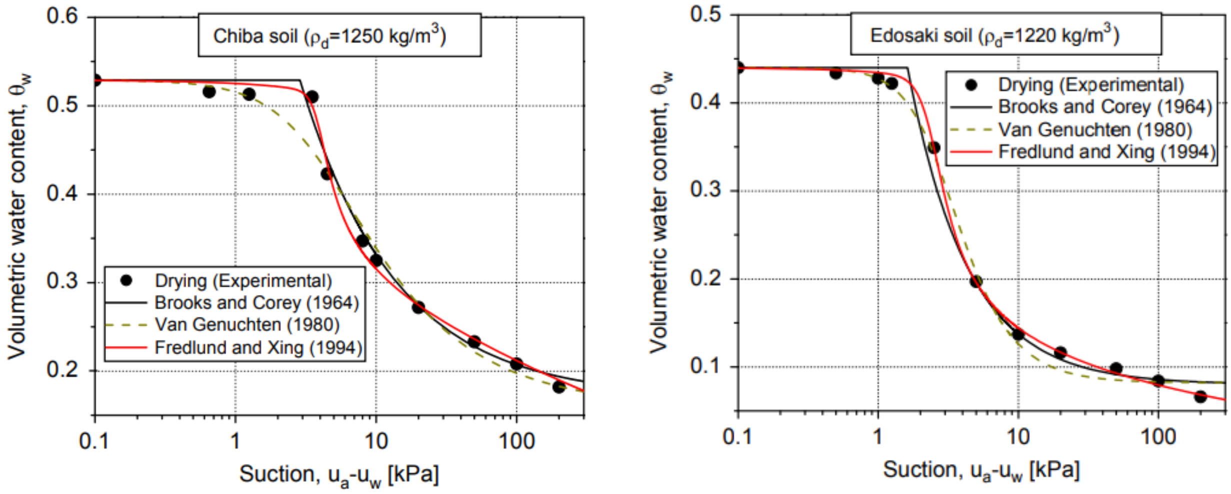


Figure A-1 Example fitting of drying soil-water characteristic data for three frequently used methods (Gallage, et al., 2013)

According to Van Genuchten (1980), the relation between the parameter n and m is as follows:

$$\mathrm{m} = 1 - \frac{1}{\mathrm{n}}$$

[A.3]

Using Eq. [A.1] and Eq. [A.2], the water content can be defined:

$$\theta = \theta_r + \frac{\theta_s - \theta_r}{[1 + (\alpha h)^{\mathrm{n}}]^{\mathrm{m}}}$$

[A.4]

**A-2 Hydraulic conductivity function**

How the hydraulic conductivity function can be predicted from the soil water characteristic curve is explained below. Therefore, the relative hydraulic conductivity is used, $K_r$ $[m \cdot sec^{-1}]$, which is the normalized form (i.e. like the method used to estimate the water content $\Theta$ $[-]$) of unsaturated hydraulic conductivity divided by the saturated hydraulic conductivity (Van Genuchten, 1980):

$$K_r = \frac{K}{K_s}$$

[A.5]

Herein, $K$ $[m \cdot sec^{-1}]$ is the hydraulic conductivity and $K_s$ $[m \cdot sec^{-1}]$ is the saturated hydraulic conductivity of a soil. The relation between the relative hydraulic conductivity and water content is proposed by Mualem (1976) with the following equation:

$$K_r = \Theta^{1/2} \left[ \frac{\int_0^{\Theta} \frac{1}{h(x)} d(x)}{\int_0^{1} \frac{1}{h(x)} d(x)} \right]^2$$

[A.6]

A closed form was derived by Van Genuchten (1980) for the relative hydraulic conductivity using Eq. [A.2], Eq. [A.3] and Eq. [A.6] with some restrictions, also known as the Mualem-Van Genuchten (MVG) hydraulic conductivity function:

$$K_r(\Theta) = \Theta^{1/2}\left[1 - (1 - \Theta^{1/\mathrm{m}})^{\mathrm{m}}\right]^2$$

[A.7]

The relative hydraulic conductivity can be expressed in terms of pressure head when Eq. [A.2] is substituted into Eq. [A.7]:

$$K_r(h) = \frac{\{1 - (\alpha h)^{\mathrm{n}-1}[1 + (\alpha h)^{\mathrm{n}}]^{-\mathrm{m}}\}^2}{[1 + (\alpha h)^{\mathrm{n}}]^{\mathrm{m}/2}}$$

[A.8]

For which the hydraulic conductivity can be computed using Eq. [A.5]:

$$K(h) = \begin{cases} K_s K_r(h) & (h < 0) \\ K_s & (h \geq 0) \end{cases}$$

[A.9]

**A-3 Hydraulic model for seepage analysis**

The partial differential equation governing the flow for the seepage through a two-dimensional medium can be expressed assuming that flow follows Darcy's law regardless of the degree of saturation of the soil (Richards, 1931) (Papagianakis & Fredlund, 1984) used for modeling of SEEP/W program (Arshad & Babar, 2014):

$$\frac{\partial}{\partial x}\left(K_x \frac{\partial H}{\partial x}\right) + \frac{\partial}{\partial y}\left(K_y \frac{\partial H}{\partial y}\right) + Q' = \frac{\partial \theta}{\partial t}$$

[A.10]

Where $H$ $[m]$ is the total head i.e. pressure head $h$ $[m]$ plus elevation head $z$ $[m]$, $K_x$ $[m \cdot sec^{-1}]$ and $K_y$ $[m \cdot sec^{-1}]$ are the hydraulic conductivities in $x$ and $y$, respectively, $Q'$ $[m^2 \cdot sec^{-1}]$ is the boundary flux, $\theta$ $[-]$ the volumetric water content, and $t$ $[sec]$ is the time. The equation states that the rate of change of the soil storage (i.e. the volumetric water content) with respect to time is equal to the summation of the change of flow in $x$ and $y$ directions and applied external flux (Çalamak, 2014). Both property functions are integrated in this partial differential equation for seepage problems i.e. hydraulic conductivity function and water storage function.

In the case of stead-state conditions, the net flow quantity from an element of the soil must be equal to zero i.e. there is no change in the storage of the soil. Therefore, the partial differential equation Eq. [A.10] can be written as follows:

$$\frac{\partial}{\partial x}\left(K_x \frac{\partial H}{\partial x}\right) + \frac{\partial}{\partial y}\left(K_y \frac{\partial H}{\partial y}\right) + Q' = 0$$

[A.11]

According to Fredlund and Morgenstern (1976), changes in volumetric water content of Eq. [A.10] are derived by soil properties and applied stresses. Therefore, the change can be described in terms of change in the pore-water pressure of a soil:

$$\partial\theta = m_w \partial u_w$$

[1.12]

Herein, $u_w$ $[kPa]$ is the pore-water pressure and $m_w$ $[-]$ is the slope of the water content curve. The relation is visualized in figure 2-4. Using terms of the total head and elevation head, Eq. [A.12] can be expressed as follows:

$$\partial\theta = m_w \gamma_w \partial(H - z)$$

[A.13]

Where $\gamma_w$ $[kN \cdot m^{-3}]$ is the specific weight of water. It states that if the elevation head $z$ $[m]$ is constant, the derivative will be zero with respect to time. If so, Eq. [A.10] can be reformulated (Geo-Slope Int Ltd., 2013):

$$\frac{\partial}{\partial x}\left(K_x \frac{\partial H}{\partial x}\right) + \frac{\partial}{\partial y}\left(K_y \frac{\partial H}{\partial y}\right) + Q' = m_w \gamma_w \frac{\partial H}{\partial t}$$

[A.14]

This partial differential equation can be solved for seepage analysis using the Finite Element Method (FEM). The method divides the problem domain, which is bounded, into small sections called elements. For each individual element, the equation is solved and connected to characterize the behavior of the domain. In order to do so, Eq. [A.14] must be integrated into function space.

Most commonly, Galerkin's weighted residual method is used to obtain the FE-form of the original equation (Çalamak, 2014). The weighted residual method consists of two major steps. First of all, an approximate solution is assumed based on the behavior of the dependent variables. The assumed solution is substituted in the equation but the solution does not satisfy the equation and hence results in an error i.e. a residual (Salih, 2016). The residual is then vanish over the entire solution domain. This will produce a system of algebraic equations. The second step is to solve this system of equations. For example, when iterating the hydraulic conductivity of an element, the pore-water pressure of its nodes is used to compute a solution. For the next iteration, the results of the hydraulic conductivity are used to compute the pore-water pressure. The procedure repeats until convergence is reached. The boundary values for convergence can be set to the level of acceptance in the seepage analysis (Çalamak, 2014).

The Galerkin's approach forms an integral for the residual of all nodes using weight functions and the residual is set to zero (Çalamak, 2014). Applying the Galerkin method to Eq. [A.14], the FE for two-dimensional seepage equation can be derived (Geo-Slope Int Ltd., 2013):

$$\tau \int_A ([B]^T [C][B]) dA \{H\} + \tau \int_A (\lambda < N >^T < N >) dA \{H\}, t = q\tau \int_L (< N >^T) dL$$

[A.15]

Where,

$[B]$ = gradient matrix,

$[C]$ = element hydraulic conductivity matrix,

$\{H\}$ = vector of nodal heads,

$< N >$ = vector of interpolating function,

$q$ = unit flux across the edge of an element,

$\tau$ = thickness of an element,

$t$ = time,

$\lambda$ = storage term for transient seepage equals to $m_w \gamma_w$,

$A$ = designation for summation over the area of an element

$L$ = designation for summation over the edge of an element

Since the analysis is axisymmetric, the thickness of an element $\tau$ is equal to the circumferential dinstance $2\pi$ radian times a different radius $R$. Since the radius is not constant in the mesh-analysis as is the case of the thickness $\tau$, consequently must $R$ be included as a variable inside the integral. Additionally, the analysis in SEEP/W is formulated for one radian (Geo-Slope Int Ltd., 2013). The FE-equation is as follows:

$$\int_A ([B]^T [C][B]R) dA \{H\} + \int_A (\lambda < N >^T < N > R) dA \{H\}, t = q \int_L (< N >^T R) dL$$

[A.16]

For the FE transient seepage analysis, the abbreviated form of Eq. [A.16] is (Geo-Slope Int Ltd., 2013):

$$[K]\{H\} + [M]\{H\}, t = \{Q\}$$

[A.17]

Herein, $[K]$ is the characteristic matrix of the element, $[M]$ the element mass matrix, the vector $\{H\}$ for the nodal heads of the analysis, and $\{Q\}$ the applied flux vector. The flux is the rate of water discharged by a cross-sectional area of the porous medium.

For an FE steady-state seepage analysis, the head remains the same and does not depend on time, so the term $\{H\}, t$ is left out, which leads to the abbreviated FE-form of Eq. [A.11], Darcy's Law :

$$[K]\{H\} = \{Q\}$$

[A.18]

**A-4 Factor of Safety macro stability**

Stability calculations of dikes can be assessed using the Limit Equilibrium Method (LEM). LEM compares the loads to the maximum mobilizable resistance for moment and force equilibria (Montfoort, 2018). The method tries a lot of different slop surface and finds the critical one i.e. the slip surface that leads to the least stability.

For comparing macro-stability cases, the factor of safety is introduced which can be calculated as follow:

$$FoS = \frac{M_r}{M_a}$$

[A.19]

Where $M_r$ $[kNm]$ is the maximum resisting moment and $M_a$ $[kNm]$ the driving moment. The $FoS$ $[-]$ must be at least 1.0 or higher in most cases for safety approval (ENW, 2009). Figure A-2 shows a soil balance along a circular slip plane in schematized form. The maximum resisting moment is compared to the driving moment. The driving moment is calculated with the following formula (TAW, 1985):

$$M_a = aQ$$

[A.20]

And the maximum resisting moment is calculated as follow:

$$M_r = \sum \tau_m \,\Delta sr = \int_{-\theta 2}^{+\theta 1} \tau_m \, r^2 d\theta'$$

[A.21]

Where, $\tau_m$ $[kN \cdot m^{-2}]$ is the maximum shear stress, $\theta'$ the angles and $r$ $[m]$ the radius of the circular slip plane.

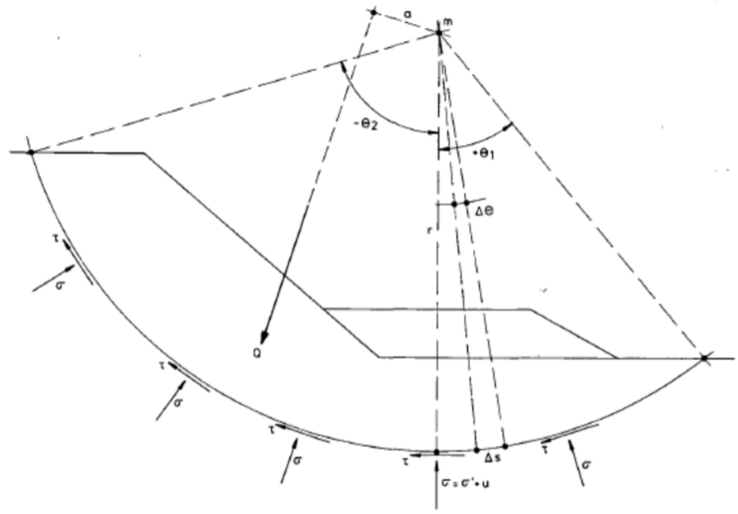

Figure A-2 Basic schematization of the soil balance (inner slope) for the mechanism macro-stability (TAW, 1985).

The mostly used LEM models, each with slip surface shapes based on their assumptions, are Bishop, Uplift-Van, and Spencer. For more specifications and differences between the models see Montfoort (2018). In this study, D-Geo stability uses the Uplift-Van method, which is suitable for addressing different piezometric lines to soil layers which can cause non-circular shapes, also the case in uplift conditions. Non-circular planes are not well represented by the Bishop model. The model of Spencer can simulate completely different shapes. However, there is little experience with the Spencer model and the calculations take more time than the other two models (Montfoort, 2018)

## APPENDIX B: INITIATION OF GEOHYDROLOGICAL SOIL PARAMETERS

Using measured data of the soil water content and pressure head, for different typical Dutch subsurface compositions (provided by Sweco), the parameters of the van Genuchten method can be estimated for Eq. [A.4] by the least square method (Yang & You, 2013):

$$minf = \sum_{i=1}^{N} (\theta_i - \theta(h_i, X))^2$$

[B.1]

Where, $\theta_i$ is the $i^{\text{th}}$ measured soil water content, $h_i$ is the $i^{\text{th}}$ measured pressure head corresponding to $\theta_i$, $\theta(h_i, X)$ is the calculated soil water content according to Eq. [A.4]. The parameter vector that needs to be optimized (i.e. minimized in this case) is $X(\theta_r, \theta_s, \alpha, \text{n})$. Herein is $N$ the number of measurements. This formula can be solved in Excel using the Solver add-in function. The Excel-Solver uses the Generalized Reduced Gradient (GRG) method i.e. an algorithm for solving non-linear data-points initiated by Lasdon, Fox and Ratner (Lasdon, et al., 1973). In order to quantify how well the Van Genuchten (1980) model fits the data, the differences between estimated and measured values must be considered using the following performance criterion (Yang & You, 2013). The optimal value for root mean square error ($RMSE$) is zero and for the determination coefficient ($R^2$), 1.

$$RMSE = \left[\frac{1}{n}\left(\sum_{i=1}^{N} P_i - M_i\right)^2\right]^{1/2}$$

[B.2]

$$R^2 = 1 - \frac{\sum_{i=1}^{N}(M_i - P_i)^2}{\sum_{i=1}^{N}(M_i - \overline{M})^2}$$

[B.3]

Where, $n$ corresponds to $N$, the number of measurements, $P_i$ the predicted values conform the van Genuchten (1980) model and $M_i$ the measured values of the $i^{\text{th}}$ measured data, $\overline{M}$ the mean value of the measured data.

Table B-1 showed the $R^2$ and $RMSE$ values in the determination of the Van Genuchten (1980) model by GRG-method and their characteristic soil property parameters for the soil layers considered in this case-study. The $R^2$ is close to 1 and the $RMSE$ is extremely small, close to 0.This indicates a good fit.

| Texture | Parameters of the Van Genuchten (1980) model | | | | | Statistical analysis | |
|---|---|---|---|---|---|---|---|
| | $\theta_r$ $[cm^3/cm^3]$ | $\theta_s$ $[cm^3/cm^3]$ | $\alpha$ $[kPa^{-1}]$ | n | $K_s$ $[m/s]$ | $R^2$ | $RMSE/10^{-2}$ |
| B02 – loamy sand | 0.019 | 0.430 | 0.237 | 1.536 | $1.157 \times 10^{-5}$ | 0.999 | 0.109 |
| B10 – light-weight clay | 0.005 | 0.420 | 0.123 | 1.219 | $1.354 \times 10^{-7}$ | 0.999 | 0.050 |
| B11 – moderate heavy-weight clay | 0.019 | 0.600 | 0.244 | 1.116 | $1.157 \times 10^{-8}$ | 0.999 | 0.098 |
| O05 – course sand | 0.010 | 0.320 | 0.613 | 2.046 | $4.630 \times 10^{-4}$ | 0.999 | 0.199 |

Table B-1 Parameters of Van Genuchten (1980) model obtained from GRG-algorithm and statistical analysis for simulation results (Van den Berg, 2019).

## APPENDIX C: NUMBER OF SIMULATIONS

The determination of the number of replications will be handled by calculating the margin of error after each simulation. A confidence interval is made of the mean $z$ – coordinate of the phreatic line for a fixed location. The margin of error is the critical value multiplied with the standard error (Sullivan, 2006). The critical value is a cut-off value that tells how far from the sample mean data can vary and remain confident. Therefore, the typical $t$ – value is computed. Since the standard deviation is unknown, a two-tailed $t$ – test is executed for a 95% level of confidence.

The standard error is the standard deviation divided by the sample size. At a certain point, the margin of error will be smaller due to an increasing number of simulations. Hereby, the confidence interval becomes smaller than the threshold (i.e. significance level of $\alpha = 5\%$) relative to the mean. The formula is as follows (Sullivan, 2006):

$$ME = t \cdot \frac{\sqrt{\frac{S}{n}}}{\bar{x}}$$

[C.1]

Where $t$ is the calculated $t$ – value for a 95% level of confidence and degrees of freedom which is $df = n - 1$. The variance of the sampe size $n$ is $S$, and $\bar{X}$ is the mean value of the Key Performace Indicator (KPI) which is the $z$ – coordinate of the phreatic line.

The number of replications is acceptable if $ME \leq 0.05$. Figure C-1 shows the graph of the margin of error as the number of simulations increases for a steady-state seepage simulation at TG109 with a water level of 7.85 $[m + \text{NAP}]$. After 222 simulations, the margin of error was small enough. In order to exclude uncertainty, for each application at least 250 Monte Carlo simulations are conducted.

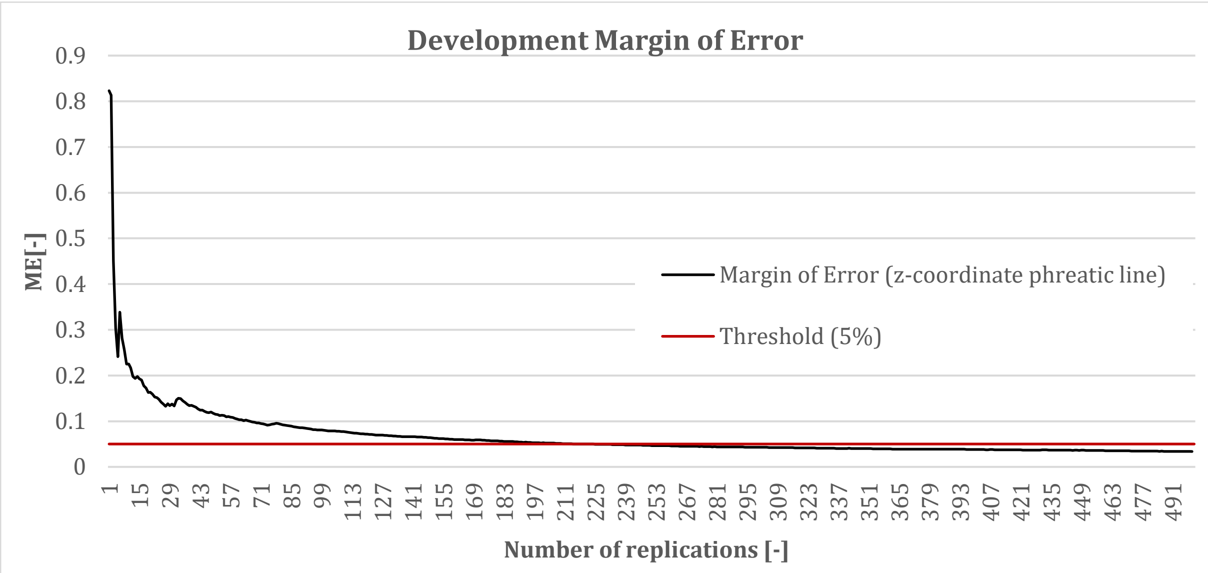


Figure C-1 Development margin of error $z$ – coordinate of the phreatic line with respect to the number of replications.

## APPENDIX D: SIMULATION RESULTS

*The results of the investigated cases of the simulations SEEP/W and D-Geo Stability are listed in an additional appendix due to its length.*

### D-1 Results SEEP/W simulations

Dike 1, Case 1-3, page 2'-21'

Dike 2, Case 4-6, page 22'-41'

Dike 2, Case 7-9, page 42'-61'

### D-2 Results SEEP/W simulation (application)

Dike 1, Case 1-3 page 62'-68'

### D-3 Results D-Geo Stability simulations

Dike 1, Case 1-3 page 69'-71'

## APPENDIX E: THE C# CODE

*The C# code used for the application of Van Genuchten (1980) method and random variable generation for hydraulic conductivity (and also for Van Genuchten fitting parameters α and n) are given in this section:*

```
// There are two general functions that get used within other functions.
// These are not called directly by the solvers. They are used in the
// other functions below.
using System;
using Gsi;

    public class My_General_Functions
    {
        static void Main(string[] args)
        {}
            // This is a C# random number generation function
            // It is used in other functions within this file.
            public static Random autoRand = new Random();
            //This first function takes a pressure and returns the Van_G K value
            // given the hard wired a,n,m and Ksat values.
            // It is a general function here because the same code is used
            // twice below and it is not necessary repeating it both times
            // if it is made public to all other function in this file.
            // Notice that it does NOT have a Calculate() method in it. It will not
            // show up in Define View. It will just be available to other function
in this file.
            public static double Van_G_K_Unsat( double pressure, double fa, double
fn, double fm, double fKsat )
            {
                // returned K value
                double fKx;

                // temporary variables
                double fTemp1, fTemp2, fTemp3, fTemp4, fTemp5, fTemp6;

                if(pressure < 0.0) // if in the unsaturated side of the function
                {
                double fSuction = Math.Abs (pressure);
                fTemp1 = fSuction*fa;
                fTemp2 = (Math.Pow((1.0 + Math.Pow(fTemp1, fn)), (fm/2)));
                fTemp3 = Math.Pow(fTemp1, (fn-1));
                fTemp4 = (1.0 + Math.Pow(fTemp1, fn));
                fTemp5 = Math.Pow(fTemp4, -fm);
                fTemp6 = Math.Pow((1.0 - fTemp3 * fTemp5), 2.0);
                fKx = fKsat * (fTemp6/fTemp2);
                }
                else // use the user input Ksat if pwp are zero or positive
                fKx = fKsat;
                return fKx;
            }
```

```
            // This is the second general function in this file. It is called by
other functions
            // below that do have a Calculate() method in them.
            public static double Van_G_VWC( double pressure, double fa, double fn,
double fm,
            double fPorosity, double fResidualWC )
            {
                double fWC, suction; // returned K value
                double fTemp1, fTemp2; // temporary variables

                if(pressure < 0.0) // if in the unsaturated side of the function
                {
                    suction = Math.Abs (pressure);
                    fTemp1 = suction*fa;
                    fTemp2 = Math.Pow( 1.0 / (1.0 + Math.Pow(fTemp1, fn) ) , fm );
                    fWC = fResidualWC + (fPorosity-fResidualWC) * fTemp2;
                }

                else // use the user input porosity if pwp are zero or positive
                    fWC = fPorosity;

            return fWC;
            }
        } // end of general functions in this file

    // The following function generates random hydraulic conductivity variables
    // using random van Genuchten "a" parameter and van Genuchten "n" parameter.

    public class Random_Van_G_K_Unsat : Gsi.Function
    {

        public double muK; //mean of the hydraulic conductivity
        public double COVK; //coefficient of variation of hydraulic conductivity
        public double malpha; // mean of the van G "a" parameter in units of
1/pressure
        public double COValpha; //coefficient of variation of van G "a"parameter
        public double mn; // mean of the van G "n" parameter
        public double COVn; //coefficient of variation of the van G "n" parameter
        double u1, u2, u3, u4, u5, u6;

        public Random_Van_G_K_Unsat()
        {

        u1 = My_General_Functions.autoRand.NextDouble();
        u2 = My_General_Functions.autoRand.NextDouble();
        u3 = My_General_Functions.autoRand.NextDouble();
        u4 = My_General_Functions.autoRand.NextDouble();
        u5 = My_General_Functions.autoRand.NextDouble();
        u6 = My_General_Functions.autoRand.NextDouble();
```

```
        }

        public double Calculate( double pressure )
        {

            double sigmaa, sigmalna, r1, alpha, sigman, sigmalnn, r2, n, m, sigmaK,
sigmalnK, r3;

    // Generation of random variables of van Gencuhten "a" parameter

            sigmaa = COValpha * malpha;
            sigmalna = Math.Sqrt(Math.Log(1 + Math.Pow((sigmaa / malpha), 2)));
            r1 = Math.Sqrt(-2.0 * Math.Log(u1)) * Math.Sin(2.0 * Math.PI * u2);
            alpha = Math.Log(malpha) - 0.5 * Math.Pow(sigmalna, 2) + sigmalna * r1;
            alpha = Math.Exp(alpha);

        // Generation of random variables of van Gencuhten "n" parameter

            sigman = COVn * mn;
            sigmalnn = Math.Sqrt(Math.Log(1 + Math.Pow((sigman / mn), 2)));

        loop:
            r2 = Math.Sqrt(-2.0 * Math.Log(u3)) * Math.Sin(2.0 * Math.PI * u4);
            n = Math.Log(mn) - 0.5 * Math.Pow(sigmalnn, 2) + sigmalnn * r2;
            n = Math.Exp(n);
            if (n < 1.0)
            {
                u3 = My_General_Functions.autoRand.NextDouble();
                u4 = My_General_Functions.autoRand.NextDouble();
                goto loop;
            }
            m = 1 - (1 / n);

    // Calculation of random hydraulic conductivity

            double fKx = My_General_Functions.Van_G_K_Unsat(pressure, alpha, n, m,
muK);
            if (pressure < 0.0)
            {
                return fKx;
            }
            else

            fKx = Math.Log(fKx);

            sigmaK = COVK * muK;
            sigmalnK = Math.Sqrt(Math.Log(1 + Math.Pow((sigmaK / muK), 2)));

            r3 = Math.Sqrt(-2.0 * Math.Log(u5)) * Math.Sin(2.0 * Math.PI * u6);
```

```
            fKx = fKx - 0.5 * Math.Pow(sigmalnK, 2) +sigmalnK * r3;

            return Math.Exp(fKx);

        }
}

    // The following function is used to compute volumetric water content of the
    // soil using random van Genuchten "a" parameter and van Genuchten "n"
    // parameter

    public class Van_Genuchten_VWC : Gsi.Function
    {
        public double Porosity; //Saturated water content
        public double Residual_WC; //Residual water content
        public double malpha; // mean of the van G "a" parameter in units of
1/pressure
        public double COValpha; //coefficient of variation of van G "a" parameter
        public double mn; // mean of the van G "n" parameter
        public double COVn; //coefficient of variation of the van G "n" parameter
        double u1, u2, u3, u4;

        public Van_Genuchten_VWC()
        {

        u1 = My_General_Functions.autoRand.NextDouble();
        u2 = My_General_Functions.autoRand.NextDouble();
        u3 = My_General_Functions.autoRand.NextDouble();
        u4 = My_General_Functions.autoRand.NextDouble();

        }

            public double Calculate( double pressure )
            {
            double sigmaa, sigmalna, r1, alpha, sigman, sigmalnn, r2, n, m;

    // Generation of random variables of van Gencuhten "a" parameter for water
content function

        sigmaa = COValpha * malpha;
        sigmalna = Math.Sqrt(Math.Log(1 + Math.Pow((sigmaa / malpha), 2)));
        r1 = Math.Sqrt(-2.0 * Math.Log(u1)) * Math.Sin(2.0 * Math.PI * u2);
        alpha = Math.Log(malpha) - 0.5 * Math.Pow(sigmalna, 2) + sigmalna * r1;
        alpha = Math.Exp(alpha);

    // Generation of random variables of van Gencuhten "n" parameter for water
content function

        sigman = COVn * mn;
```

```
        sigmalnn = Math.Sqrt(Math.Log(1 + Math.Pow((sigman / mn), 2)));

    loop:
        r2 = Math.Sqrt(-2.0 * Math.Log(u3)) * Math.Sin(2.0 * Math.PI * u4);
        n = Math.Log(mn) - 0.5 * Math.Pow(sigmalnn, 2) + sigmalnn * r2;
        n = Math.Exp(n);
        if (n < 1.0)
        {
            u3 = My_General_Functions.autoRand.NextDouble();
            u4 = My_General_Functions.autoRand.NextDouble();
        goto loop;
        }
        m = 1 - (1 / n);

        double fWC = My_General_Functions.Van_G_VWC(pressure, alpha, n, m, 
Porosity, Residual_WC);

        return fWC;
    }
}
```

## APPENDIX F: SUPPLEMENTARY CODES

*This Appendix contains the most important supplementary codes for performing the Monte Carlo simulations*

### F-1 Generate copies

*A sample code written in Windows command line. This code generates copies of SEEP/W simulation files:*

```
@echo on

for /L %%i IN (1,1,250) do call :docopy %%i

goto end

:docopy

set FN=%1

set FN=%FN:~-4%

copy "G:\Transient seepage\case_1\case_1.gsz" "G:\Transient seepage\case_1\case_1-%FN%.gsz"

:end
```

### F-2 Solve individual

*A sample code written in Windows command line. This code solves the generated copies of SEEP/W simulation files individually:*

```
for /L %%i IN (1,1,250) do call :dosolve %%i

goto end

:dosolve

set FN=%1

set FN=%FN:~-4%

"C:\Program Files (x86)\GEO-SLOPE\GeoStudio 9\Bin\GeoStudio.exe" "/solve:all" "G:\Transient seepage\case_1-%FN%.gsz"

:end
```

**F-3 Export DXF**

*A sample code is written in Windows open-source scripting language, set-up with AutoScriptWriter (extended with mouse coordinates), an application of AutoHotKey (AHK). This code exports the solved SEEP/W results for prescribed timestep:*

```
^q::
Loop, 250
{
	Next_Index := A_Index
Run, "G:\Transient seepage\case_1 -%Next_Index%.gsz"
Sleep, 3000
Send, {ENTER}
WinWait, case_1 -%Next_Index% - GeoStudio 2019 (SEEP/W Definition),
IfWinNotActive, case_1 -%Next_Index% - GeoStudio 2019 (SEEP/W Definition), , WinActivate, case_1 -%Next_Index% - GeoStudio 2019 (SEEP/W Definition),
WinWaitActive, case_1 -%Next_Index% - GeoStudio 2019 (SEEP/W Definition),
Sleep, 1000
Send, {ALTDOWN}{SPACE}x{ALTUP}
MouseClick, left,  137,  100
Sleep, 100
WinWait, case_1 -%Next_Index% - GeoStudio 2019 (SEEP/W Results),
IfWinNotActive, case_1 -%Next_Index% - GeoStudio 2019 (SEEP/W Results), , WinActivate, case_1 -%Next_Index% - GeoStudio 2019 (SEEP/W Results),
WinWaitActive, case_1 -%Next_Index% - GeoStudio 2019 (SEEP/W Results),
Sleep, 15000
MouseClick, left,  96,  41
Sleep, 100
MouseClick, left,  137,  285
Sleep, 100
WinWait, Preferences,
IfWinNotActive, Preferences, , WinActivate, Preferences,
WinWaitActive, Preferences,
MouseClick, left,  251,  309
```

```
Sleep, 100

MouseClick, left,  251,  358

Sleep, 100

MouseClick, left,  33,  308

Sleep, 100

MouseClick, left,  29,  180

Sleep, 100

MouseClick, left,  660,  639

Sleep, 100

WinWait, ccase_1 -%Next_Index%* - GeoStudio 2019 (SEEP/W Results),

IfWinNotActive, case_1 -%Next_Index%* - GeoStudio 2019 (SEEP/W Results), , WinActivate, case_1 -%Next_Index%* - GeoStudio 2019 (SEEP/W Results),

WinWaitActive, case_1 -%Next_Index%* - GeoStudio 2019 (SEEP/W Results),

MouseClick, left,  83,  673

Sleep, 100

MouseClick, left,  24,  47

Sleep, 100

MouseClick, left,  71,  229

Sleep, 100

WinWait, Export,

IfWinNotActive, Export, , WinActivate, Export,

WinWaitActive, Export,

MouseClick, left,  233,  365

Sleep, 100

Send, case{SHIFTDOWN}-{SHIFTUP}1{SHIFTDOWN}-{SHIFTUP} Next_Index%.dxf

MouseClick, left,  334,  388

Sleep, 100

MouseClick, left,  311,  510

Sleep, 100

Send, {ENTER}

WinWait, case_1 -%Next_Index%* - GeoStudio 2019 (SEEP/W Results),

IfWinNotActive, case_1 -%Next_Index%* - GeoStudio 2019 (SEEP/W Results), , WinActivate, case_1- %Next_Index%* - GeoStudio 2019 (SEEP/W Results),
```

```
WinWaitActive, case_1 -%Next_Index%* - GeoStudio 2019 (SEEP/W Results),
MouseClick, left,  1523,  17
Sleep, 100
Send, {RIGHT}{ENTER}
}
return
```

**F-4 Insert DXF**

*A sample code is written in Windows open-source scripting language, set-up with AutoScriptWriter (extended with mouse coordinates), an application of AutoHotKey (AHK). This code insert the DXF files in AutoCAD:*

```
^p::
Loop, 248
{
	Next_Index := A_Index+2

Send, i
WinWait, CAcDynInputWndControl,
IfWinNotActive, CAcDynInputWndControl, , WinActivate, CAcDynInputWndControl,
WinWaitActive, CAcDynInputWndControl,
Send, nsert{SPACE}
WinWait, Insert,
IfWinNotActive, Insert, , WinActivate, Insert,
WinWaitActive, Insert,
Send, {TAB}{ENTER}
WinWait, Select Drawing File,
IfWinNotActive, Select Drawing File, , WinActivate, Select Drawing File,
WinWaitActive, Select Drawing File,
Send,case{SHIFTDOWN}-{SHIFTUP}1{SHIFTDOWN}-
{SHIFTUP}%Next_Index%.dxf{ENTER}{TAB}{LEFT}{ENTER}
WinWait, Autodesk AutoCAD 2019 - [case_1.dwg],
```

```
IfWinNotActive, Autodesk AutoCAD 2019 - [case_1.dwg], , WinActivate, Autodesk AutoCAD 2019 - [case_1.dwg],

WinWaitActive, Autodesk AutoCAD 2019 - [case_1.dwg],

Send, 0

WinWait, CAcDynInputWndControl,

IfWinNotActive, CAcDynInputWndControl, , WinActivate, CAcDynInputWndControl,

WinWaitActive, CAcDynInputWndControl,

Send, ,

WinWait, Autodesk AutoCAD 2019 - [case_1.dwg],

IfWinNotActive, Autodesk AutoCAD 2019 - [case_1.dwg], , WinActivate, Autodesk AutoCAD 2019 - [case_1.dwg],

WinWaitActive, Autodesk AutoCAD 2019 - [case_1.dwg],

Send, 0{ENTER}

Sleep, 200

}

return
```